Methods for automatization of radiotherapy treatment planning

Méthodes pour l'automatisation de la planification de traitements en radiothérapie

Thèse de doctorat de l'université Paris-Saclay

École doctorale n° 573 Interfaces: matériaux, systèmes, usages
Spécialité de doctorat: Mathématiques Appliquées
Graduate School: Sciences de l'Ingénierie et des Systèmes
Référent: CentraleSupélec

Thèse préparée dans les unités de recherche **Radiothérapie** (Institut Régional du Cancer de Montpellier), **Advanced Research** (TheraPanacea), et **Mathématiques et Informatique pour la Complexité et les Systèmes** (Université Paris-Saclay, CentraleSupélec) , sous la direction de **Nikos Paragios**, Professeur, et le co-encadrement de **Paul-Henry Cournède**, Professeur

Thèse soutenue à Paris-Saclay, le 16 décembre 2024, par

Paul Raymond François DUBOIS

Composition du jury

Membres du jury avec voix délibérative

David AZRIA Professeur des universités - Praticien hospitalier, Faculté de Médecine de Montpellier-Nîmes	Président
Daniela THORWARTH Professeure des universités, Université de Tübingen	Rapporteur & Examinatrice
Vincent LEPETIT Professeur des universités, ENPC ParisTech	Rapporteur & Examinateur
Pascal FENOGLIETTO Docteur, Institut du Cancer de Montpellier	Examinateur

THESE DE DOCTORAT

NNT : 2024UPAST189

université PARIS-SACLAY

ÉCOLE DOCTORALE
Interfaces:
matériaux, systèmes, usages

Titre: Méthodes pour l'automatisation de la planification de traitements en radiothérapie

Mots clés: Cancer, Radiothérapie, Santé Digitale, Traitement Adaptatif, Intelligence Artificielle, Apprentissage Profond

Résumé:
La dosimétrie en radiothérapie est essentielle pour garantir la précision et la sécurité des traitements contre le cancer. La complexité et la variabilité de la planification des traitements nécessitent des méthodologies avancées pour l'automatisation et l'optimisation. Cette thèse présente des approches novatrices visant à automatiser le processus de dosimétrie en radiothérapie.

Cette thèse commence par le développement d'un moteur de dosimétrie et une évaluation approfondie des algorithmes d'optimisation open-source existants pour la planification des traitements. Ensuite, ce manuscrit analyse les relations entre différentes doses. Cette analyse conduit à la proposition d'un cadre novateur pour l'optimisation multi-objectif et la sélection robuste de plans à l'aide de la théorie des graphes.

Afin de réduire davantage le temps nécessaire pour la planification en radiothérapie, la thèse explore l'application de l'apprentissage par renforcement pour l'optimisation des doses. Le système proposé réalise la dosimétrie pour de nouveaux patients en exploitant les données de dose des patients traités dans le passé. Cette méthode entièrement automatisée peut s'adapter aux pratiques de différentes cliniques, réduisant ainsi le besoin d'ajustements manuels et facilitant son adoption en pratique.

De plus, la thèse examine l'utilisation de l'apprentissage profond pour la prédiction des doses, en proposant une série de modèles guidés par des Histogrammes Dose-Volume (DVH) cibles. Ce guidage orientation permet l'incorporation de directives lors de la génération de doses par les modèles. En outre, cette technique permet d'entraîner un seul modèle capable de s'adapter, plutôt qu'un modèle pour chaque clinique.

Les contributions de cette thèse présentent des avancées dans la dosimétrie en radiothérapie, ouvrant la voie au développement d'un système de planification de traitement entièrement automatisé, s'adaptant aux contraintes cliniques. Ces innovations pourraient améliorer les flux de travail cliniques, en réduisant l'intervention humaine à un minimum, rendant la radiothérapie plus efficiente.

Title: Methods for automatization of radiotherapy treatment planning

Keywords: Cancer, Radiotherapy, Digital Health, Adaptative Treatment, Artificial Intelligence, Deep Learning

Abstract:
Radiotherapy dosimetry is critical in ensuring the precision and safety of cancer treatments. The complexity and variability of treatment planning necessitate advanced methodologies for automation and optimization. This thesis introduces novel approaches aimed at automating the radiotherapy dosimetry process.

The research begins with developing a dosimetry engine, and comprehensively evaluating existing open-source optimization algorithms for treatment plannification. Then, this thesis analyzes the relationships between different treatment plans. This analysis leads to the proposal of a novel framework for multi-objective optimization and robust plan selection using graph theory.

To further reduce the time required for radiotherapy planning, the thesis explores the application of reinforcement learning for dose optimization. The proposed system performs dosimetry for new patients by leveraging dose data from past patients. This fully automated method can adapt to clinical dependencies, reducing the need for manual fine-tuning and easing its adoption in practice.

In addition, the thesis investigates the use of deep learning for dose prediction, proposing a series of models guided by target Dose Volume Histograms (DVH). This guidance facilitates the incorporation of guidelines into the deep-generated doses. Moreover, it allows a single model to be trained instead of one for each clinic.

The contributions of this thesis represent advancements in radiotherapy dosimetry, paving the way for the development of a fully automated, clinically dependent treatment planning system designed to operate with minimal human intervention. These innovations could enhance clinical workflows, making radiotherapy more efficient.

Acknowledgments

During those three years, I often felt alone, but I eventually realized that I could not name people who supported me, not because there were too few, but because there were so many. This section is dedicated to all those who directly or indirectly contributed to this manuscript.

I want to express my deepest gratitude to my PhD directors for their unwavering support and invaluable guidance throughout this journey.

To Nikos Paragios, thank you for the network and opportunities you have opened for me. Your insight and encouragement have broadened my horizons and enriched my academic experience.

To Pascal Fenoglietto, your guidance has been indispensable. Your thoughtful advice and attention to detail have steered me through the complexities of this work, and I sincerely appreciate your dedication to my progress.

To Paul-Henry Cournède, you have been more than a supervisor; you are a model of excellence in research and leadership. I am immensely grateful for inspiring me to reach new heights.

I would like to thank the TheraPanacea team, these numerous individuals who have contributed to my PhD journey in various ways:

To Alexandre Cafaro, for our exchanges on research. Sharing our experiences has been a source of motivation.

To Alexis Benichoux, for valuable insights into AI engineering practices.

To Alexis Bombezin-Domino, for sharing interesting facts e.g.: about military aviation.

To Amaury Leroy, for insightful discussions about PhD life and post-PhD life plans.

To Anne Walrafen, for sharing extensive knowledge about radiotherapy.

To Anothkanth Mahendran, for maintaining and updating specialized software, essential to my research.

To Audrey Duran, for maintaining nice colleague relationship despite the physical distance.

To Ayoub Oumani, for showing great skills on the soccer field during our 5v5 after-work matches.

To Baris Ungun, for fascinating discussions about unconventional scientific topics, like color theory.

To Basile Bertrand, for making ESTRO conference an enjoyable and memorable experience. Should I express my gratitude for sending me to ASTRO instead of attending yourself?

To Carlos Santos-Garcia, for being a true friend across multiple domains - from climbing to soccer, from AI discussions to board games.

To Catherine Martineau-Huynh, for showing genuine care for employees, and keeping us on our toes with unexpected questions.

To Claire Diaz, for bringing joy and enthusiasm to after-works and conferences.

To Clemence Gueguen, for the privilege of knowing you as both student and colleague. Many of us thank you for organizing memorable company events.

To Despina Ioannidou, for managing internal ~~gossips~~ communications with grace and discretion.

To Edouard Delasalles, for enlightening discussions about AI techniques.

To Elie Mangin, for leading me at the Centrale Night'N'Day race, and being a worthy baby-football opponent, and a great colleague.

To Ethan Corcos, for engaging scientific exchanges, and showing me cool figures.

To Eugenie Ullmann, for being a great colleague.

To Giorgi Benashvili, for resolving all my technical issues promptly and efficiently; you are a lightning bolt of efficiency.

To Gizem Temiz, for the gentle push toward abstract submissions, contributing to my academic growth.

To Jacob Buatti, for being an outstanding volleyball player and bringing athletic spirit to TheraPanacea.

To Jules Potel, for enriching scientific discussions.

To Lhassa Macke, for bringing energy and liveliness to the clinical room.

To Lisa Letournel, for sharing Catherine's front desk office, and maintaining a nice atmosphere.

To Lorenzo Colombo, for animating the clinical office room with complains, and successfully organizing the last company event.

To Louis Ducamp, for enlightening discussions about AI applications in healthcare.

To Léo Hardi, for patiently answering my database questions, no matter how basic they seemed.

To Mathilde Ravier, for meaningful conversations about company life and being a reliable running companion.

To Niels Pichon, for productive exchanges about development of AI tools.

To Norbert Bus, for an inspiring performance at Advent of Code.

To Olivier Teboul, for exemplary leadership of the scientific team.

To Quentin Spinat, for being an excellent climbing partner, providing much-needed breaks from work.

To Rafael Marini Silva, for providing invaluable guidance.

To Rafael Roblin, for engaging technology discussions and creative problem-solving during team building events.

To Rémi Vauclin, for stimulating scientific discussions.

To Sami Romdhani, for leading the AI team, and letting me participate to interesting meetings.

To Samia Achour, for expertize coordinating conferences, facilitating valuable networking.

To Sanmady Kandiban, for being a great colleague.

To Sofia Broome, for showing genuine interest in my work, and always having interesting questions.

To Sofiane Horache, for discussions on AI that helped shape my research.

To Sonia Martinot, for being an excellent DSBA co-teacher and sharing PhD life experiences.

To Tessa Kolb, for patiently guiding me through ASTRO demonstrations and enhancing my technical understanding.

To Thaís Roque, for bringing a bit of Oxford experience to TheraPanacea.

To Vincent Luc, for making SFPM conference a valuable experience.

I would like to extend my heartfelt gratitude to my colleagues and friends from the MICS laboratory, whose presence and support have enriched the past three years in countless ways:

To Aaron Mamann, for our endless and enriching life discussions that often provided unneeded breaks, but relieved from academic pressures.

To Antonin Della Noce, for our engaging discussions about mathematics that challenged my thinking.

To Brice Hannebicque, for our enlightening discussions about teaching strategies.

To Céline Hudelot, thank you for trusting me to be your teaching assistant for computer vision and for advertising my enigmas, which has contributed to making them part of our lab culture.

To Fabienne Brosse, for expertly managing the administrative aspects of the lab and (most notably) for organizing our summer and Christmas parties.

To Félicie Giraud-Sauveur, for being my desk mate and creating an enjoyable environment.

To Gabriel Claret, for his incredible devotion to the lab life.

To Guillaume Joslin, for helping out with the computing resources. I do **not** thank you for hacking my enigmas!

To Gurvan Hermange, whose perspectives on PhD experience have helped me better understand the academic ecosystem.

To Hakim Benkirane, for our discussions about the latest developments in AI.

To Imane Chraki, for her contribution to lab life and the fun times we shared at the autumn school in Porto.

To Inès Malleval, for creating a laboratory sportive life.

To Jun Zhu, whose exemplary work ethic has been truly inspiring. Thank you for always keeping me company during lunch!

To Konstantinos Florakis, for your endless enthusiasm for mathematical discussions.

To Laura Vuduc, for being a wonderful companion on our bus rides to CentraleSupélec, and for being an exceptional colleague throughout our PhD journey.

To Leo Filioux, for our enlightening discussions about teaching.

To Leo Milecky, for your sage advice on publication strategy and those memorable spike ball victories.

To Lily Monnier, for collaborating with me in teaching reinforcement learning, for being part of the autumn school in Porto team, and for our mutual encouragements during the PhD.

To Mahmoud Bentriou, for sharing your expertise on publication.

To Malek Ben Salah, for being a central member of the biomathematics team; I hear you will take over the annual BBQs.

To Manon Ramaroson, for volunteering to take over the enigmas for lab days, with Margherita.

To Margherita Bruno, for being a great member of the biomathematics team; I hear you will take over the engimas for lab days.

To Maria Vakalopoulou, for organizing the Biomath seminars, which have been an incredible source of inspiration and knowledge.

To Marin Scalbert, for your intermittent yet enjoyable appearances at the lab.

To Marine Tesson, for her support with high school internship. It is always a pleasure to work with you.

To Othmane Laousy, for his insights about reinforcement learning (among others).

To Quentin Blampey, for his contribution to the lab, and for challenging during the climbing after-works.

To Romain Lhotte, for consistently challenging my coding and pushing me to excel. Teaching courses together has been an invaluable learning experience.

To Stergios Christodoulidis, for allowing me to teach reinforcement learning. His involvement in the autumn school in Porto have greatly enriched my academic journey.

To Sylvain Lannuzel, for his perspectives on PhD life and willingness to share his experience.

To Vessna Lukic, for our varied life discussions. Your ability to balance research with life's other aspects is genuinely inspiring.

To Vincent Mousseau, for validating my "heures de formation"[1].

To Véronique Letort, thank you for providing teaching opportunities, and valuable advice.

To Wassila Ouerdane, for providing the opportunity to teach NLP.

To Yoann Pradat, for our stimulating discussions about science and the intricacies of academic publishing.

Beyond the walls of MICS and Therapanacea, I've been fortunate to share this doctoral journey with fellow PhD candidates and friends. I would like to express my gratitude to the following individuals for their friendship, support, and challenges:

To Aiden Manley, for being not just a flatmate but a true friend, making our shared living space a home during this academic journey.

To Amaury Ajasse, for being a great partner, both in sports and theater.

To Arthur Vervaet, for your unwavering friendship, for consistently pushing my limits at the climbing gym, and for our thoughtful discussions about career trajectories and aspirations.

To Axel Kerbec, for our stimulating mathematical discussions and for our mutual drive to challenge each other intellectually, pushing us both to grow and excel.

[1] even oenology was accepted

To Camille Béhar, for your friendship and for the humbling reminder that unlike my path in computer science, you will become a "real" medical doctor, bringing perspective to our different journeys in academia.

To Caroline Bouat, for maintaining our friendship through the years, and pursuing together a scientific PhD.

To Jeanne Redaud, for being an exceptional friend and confidante, sharing the unique challenges and triumphs of PhD life at L2S, making this journey feel less solitary.

To Landry Duguet, for our enduring friendship and the remarkable parallel journey we've shared in our scientific careers.

To Marie Girodengo, for sharing the unique experiences and concerns of PhD life, making this challenging journey more manageable.

To Pierre Houdouin, for our engaging climbing sessions that provided much-needed breaks from research, and for our meaningful discussions about PhD progress and milestones at L2S.

I've been fortunate to have friends outside academia whose insights, support, and contributions have enriched both this manuscript and my understanding of its broader impact.

To Axel Arno, for the hours we spent talking about mathematics, and creating/testing problems.

To Enea Sharxhi, for the countless hours spent mutually challenging each other with mathematical problems, often pushing the limits of our understanding and problem-solving abilities.

To Erwan Le Guennec, for sharing great climbing sessions.

To Julien Bruyninckx, for ensuring I maintained a balanced life beyond science while engaging in fascinating discussions about mathematics, quantum computing, and AI.

To Justin Cuzin, for our laughs and tears while teaching together.

To Louis Lhotte, for our engaging discussions about career, and being a great employee.

To Maxime Dufour, for forming an extraordinary hackathon team with Romain and Arthur, where our combined creativity led to innovative solutions and memorable coding adventures.

To Mélanie Kojaartinian, for her careful review and insightful feedback on the background chapter, contributing to its clarity and accessibility.

To Oscar Valdini, for our thoughtful discussions about career paths and possibilities.

To Roderick Rens, for being one of my longest-standing mathematician friend.

To Thomas Heyen-Dube, for sharing invaluable life wisdom and unwavering support.

Despite already having several doctors in our family tree, I somehow found myself trying to add another branch to this academic legacy. This journey would not have been possible without the unwavering support of my family, who have been my foundation throughout this adventure.

To my grandparents (Jean-Bernard, Marie-Paule, Maxime, Maguy), whose pride in their grandchildren's achievements has always been a source of motivation.

To my uncles (François, Philippe, Sylvain, Davi) and aunts (Anne, Vinciane), for showing genuine interest in my research even when I struggled to explain it in family-friendly terms.

To my cousins (Camille, Clément, Nathan, Louis, Victor, Jules, Mark, Mathilde, Adam, Jean, Matthis, Maryline, Julia, Hugo, Gabriel, Cécile, Lucie), for bringing laughter and perspective to our family gatherings.

To my parents (Pierre, Yollaine), who have supported every decision in my academic journey, never questioning my choice to pursue yet another family doctorate.

To my siblings (Marie, Emmanuel), who have masterfully balanced supporting my academic endeavors while keeping my ego in check through well-timed teasing.

Synthèse

Le cancer constitue l'une des principales causes de mortalité dans le monde, en particulier dans les pays les plus développés. Le cancer est caractérisé par la prolifération incontrôlée et anormales de cellules. Ces cellules cancéreuses envahissent les tissus voisins et peuvent se propager à d'autres parties du corps (un processus appelé métastase). Avec une incidence croissante liée au vieillissement de la population et aux facteurs environnementaux, le cancer représente un défi majeur pour la santé publique.

Pour lutter contre cette maladie, trois principales approches thérapeutiques sont utilisées: la chirurgie, la chimiothérapie et la radiothérapie. La chirurgie est le traitement de choix les cancers localisés, permettant une ablation physique des tumeurs. La chimiothérapie utilise des agents chimiques pour détruire les cellules cancéreuses, mais elle affecte aussi les cellules saines, entraînant des effets secondaires significatifs. La radiothérapie repose sur l'utilisation de rayonnements ionisants pour cibler et détruire les cellules tumorales, avec un impact plus ciblé que la chimiothérapie.

La dosimétrie en radiothérapie joue un rôle central dans la prise en charge des cancers, où l'objectif est de maximiser l'efficacité thérapeutique tout en minimisant les effets indésirables sur les tissus sains. La complexité croissante des techniques de planification et la variabilité des cas cliniques nécessitent des approches avancées pour automatiser et optimiser ces processus. Cette thèse explore plusieurs méthodologies innovantes pour améliorer la dosimétrie, avec pour ambition long terme de créer un système de planification entièrement automatisé et adaptable aux contraintes cliniques.

Dans un premier temps, la thèse présente le développement d'un moteur de dosimétrie performant, accompagné d'une évaluation exhaustive des algorithmes d'optimisation open-source existants. Ces travaux initiaux permettent d'identifier les limites et opportunités pour l'amélioration des systèmes actuels. Une analyse approfondie des relations entre différentes doses conduit à l'élaboration d'un cadre novateur pour l'optimisation multi-objectif et la sélection robuste de plans, basé sur les concepts de la théorie des graphes. Ce cadre simplifie la gestion des compromis entre objectifs cliniques concurrents, tout en garantissant la qualité et la sécurité des traitements.

Pour répondre au défi du temps de planification, la thèse se penche sur l'apprentissage par renforcement comme levier d'accélération. Le système proposé utilise les données historiques de patients pour optimiser les plans de nouveaux cas, apprenant à reproduire des stratégies efficaces et adaptées aux spécificités cliniques. Cette approche réduit considérablement le besoin d'ajustements manuels, rendant le processus plus rapide et plus homogène.

Par ailleurs, la thèse explore l'application de l'apprentissage profond pour prédire les distributions de dose, en s'appuyant sur des Histogrammes Dose-Volume (DVH) cibles. Ce guidage structuré permet non seulement d'incorporer les directives cliniques dans la prédiction, mais aussi de créer un modèle unique capable de s'adapter aux pratiques variées des cliniques. Cette innovation évite le besoin de développer un modèle spécifique pour chaque centre, facilitant l'adoption de la méthode dans des environnements diversifiés.

Enfin, les contributions de cette thèse marquent une avancée significative vers la création d'un système de dosimétrie entièrement automatisé, intégré et adaptable. Ces approches réduisent l'intervention humaine à son strict minimum, optimisent les flux de travail cliniques, et ouvrent la voie à une radiothérapie plus efficiente. Ces innovations s'inscrivent dans une perspective d'amélioration continue des soins oncologiques, offrant une meilleure accessibilité et standardisation des traitements.

Cette thèse jette les bases d'un écosystème automatisé et intelligent pour la dosimétrie en radiothérapie, au service des patients et des cliniciens.

List of contributions

Publication

Full-length Article

- "Radiotherapy dose optimization via clinical knowledge based reinforcement learning", Paul Dubois, Paul-Henry Cournède, Nikos Paragios, and Pascal Fenoglietto, *Artificial Intelligence in Medicine* (AIME), 2024

Full-length Presentation

- "Dose Volume Histograms Guided Deep Dose Predictions", Paul-Henry Cournède Nikos Paragios Paul Dubois, Carlos Santos Garcia and Pascal Fenoglietto, *Société Française de Physique Médicale* (SFPM), 2024, Dijon, France

- "Radiotherapy dose optimization via clinical knowledge based reinforcement learning", Paul Dubois, Paul-Henry Cournède, Nikos Paragios, and Pascal Fenoglietto, *Artifcial Intelligence in Medicine* (AIME), 2024, Salt Lake City, Utha, USA

Poster Presentation

- "A Novel Framework for Multi-Objective Optimization and Robust Plan Selection Using Graph Theory", Dubois, Paul and Paragios, Nikos and Cournède, Paul-Henry and Temiz, Gizem and Marini-Silva, Rafael and Bus, Norbert and Fenoglietto, Pascal *European Society for Radiotherapy and Oncology* (ESTRO), 2024, Glasgow, UK

- "Clinically Dependent Fully Automatic Treatment Planning System", Paul Dubois, Pascal Fenoglietto, Paul-Henry Cournède, and Nikos Paragyos. *American Society for Radiation Oncology* (ASTRO), 2024, Washington DC, USA

- "Attention mechanism on dose-volume histograms for deep dose predictions", Paul-Henry Cournède Pascal Fenoglietto Paul Dubois, Nikos Paragios, *Société Française de Radio Oncologie* (SFRO), 2024, Paris, France

ArXiv

- "Radiotherapy Dosimetry: A Review on Open-Source Optimizer", Paul Dubois, *arXiv*, 2023

Teaching

Lectures

- Mathematics Refresher, DSBA 2$^{\text{nd}}$ year master students, ESSEC (2021, 2023, 2024)
- Deep Learning and NLP, Engineering 3$^{\text{rd}}$ year master students, CentraleSupélec (2023, 2024)

Teaching Assistant

- High-school students internship Co-supervision (June 2024)
- Reinforcement Learning (Winter 2024)
- Algorithmes et Complexité (Winter 2022-2023, Winter 2023-2024)
- Systèmes d'Information et Programmation (Autumn 2023)
- Natural Language Processing (Winter 2022)
- Reconnaissance Visuelle (Spring 2022)
- Coding Weeks (Autumn 2021, Autumn 2022)
- Optimisation (Autumn 2021)

Others

- SFPM: Participation to the contest "My PhD in 180 seconds" (June 2024)
- Artificial Intelligence and Philosophy "discussion", Association Cinéma et Culture Auterive (May 2024)
- Weekly Seminar, βiomathematics - MICS - CentraleSupélec: "DVH guided deep dose prediction" (May 2024)
- Popular Science Talk, Info@Lèze: "Intelligences Artificielles Génératives" (January 2024)
- Christmas Day Seminar, MICS - CentraleSupélec: "Do you understand where your models live?" (December 2023)
- Weekly Seminar, βiomathematics - MICS - CentraleSupélec: "Introduction to treatment planning in radiotherapy" (December 2023)

- Popular Science Talk, Info@Lèze: "Intelligences Artificielles: Mythes et Réalités" (July 2023)
- ISEP Scientific Day Presentation: "Automatic Dose Optimization for Radiotherapy" (June 2023)
- ISEP Panic Night Tutorial: "Solving Nim's Game: Genetic Algorithm Approach" (January 2023)
- Popular Science Talk, Info@Lèze: "Comment envoyer un secret avec un haut-parleur?" (September 2022)
- Presentation to police scientific research team, Fort de Issy-les-Moulineaux "Intelligences artificielles pour une reconnaissance vocale sécurisée" (June 2022)
- High School Workshop, Info@Lèze: "Genetic Algorithms" (June 2022)
- Pint of Science Talk: "I.A.: Generator vs Discriminator" (May 2022)
- High School Workshop, Info@Lèze: "Math on Mars" (May 2022)
- High School Workshop, Info@Lèze: "Math with Jupyter" (May 2022)

Formations

- BIP – Advanced Processing of Biomedical Signals and Images (October - November 2024)
- SaclAI School - Deep Learning and Signal Processing (February - March 2024)
- Interfaces Doctoral School Day (March 2024)
- Interfaces Back to School Day 2022 (January 2023)
- Climate Workshop and Engineering Sustainability (May 2024)
- Oenology (February - May 2023)
- Ruche user introduction (March 2024)
- Writing skills in Science "ADVANCED" (May - July 2022)
- AI 4 Health (January 2022)
- Theatrical techniques for pedagogy (February - March 2024)

List of acronyms

AAPM **A**merican **A**ssociation of **P**hysicists in **M**edicine

AI **A**rtificial **I**ntelligence

AIME **A**rtificial **I**ntelligence in **Me**decine (formely **A**rtificial **I**ntelligence in **M**edecine **E**urope)

API **A**pplication **P**rogramming **I**nterface

ARIR **A**daptive **R**easoning **i**n **R**adiotherapy

ASTRO **A**merican **S**ocie**t**y for **R**adiation **O**ncology

BER **B**ase **E**xcision **R**epair

BOO **B**eam **O**rientation **O**ptimization

CBCT **C**one **B**eam **C**omputed **T**omography

CDF **C**umulative **D**istribution **F**unction

CNN **C**onvolutional **N**eural **N**etwork

CT **C**omputed **T**omography

CTV **C**linical **T**arget **V**olume

DAFT **D**irect **A**ffine **F**eature **T**ransforms

DAO **D**irect **A**perture **O**ptimization

DKFZ **D**eutsches **K**rebs**f**orschungs**z**entrum (German Cancer Research Center)

DL **D**eep **L**earning

DSB **D**ouble-**S**trand **B**reak

DVH **D**ose-**V**olume **H**istogram

ESTRO **E**uropean **S**ocie**t**y for **R**adiotherapy and **O**ncology

FMO **F**luence **M**ap **O**ptimization

Gy **G**ra**y**

ICRU **I**nternational **C**ommission on **R**adiation **U**nits and Measurements

IMRT **I**ntensity **M**odulated **R**adio**t**herapy

KBP **K**nowledge-**B**ased **P**lanning

KBRP **K**nowledge-**B**ased **R**adiotherapy **P**lanning

LINAC **Lin**ear **Ac**celerator

LS **L**eaf **S**equencing

MAE **M**ean **A**bsolute **E**rror

MCO **M**ulti-**C**riteria **O**ptimization

ML **M**achine **L**earning

MLC **M**ulti-**L**eaf **C**ollimator

MMR **M**is**m**atch **R**epair

MRI **M**agnetic **R**esonance **I**maging

MSE **M**ean **S**quared **E**rror

NER **N**ucleotide **E**xcision **R**epair

NTCP **N**ormal **T**issue **C**omplication **P**robability

OAR **O**rgan **a**t **R**isk

PCA **P**rincipal **C**omponent **A**nalysis

PTV **P**rincipal **T**arget **V**olume

RL **R**einforcement **L**earning

RNN **R**ecurrent **N**eural **N**etwork

RNS **R**eactive **N**itrogen **S**pecies

ROS **R**eactive **O**xygen **S**pecies

RT **R**adio**t**herapy

SFPM **S**ociété **F**rançaise de **P**hysique **M**édicale

SFRO **S**ociété **F**rançaise de **R**adiothérapie **O**ncologique

SSB **S**ingle-**S**trand **B**reak

TCP **T**umor **C**ontrol **P**robability

TLR **T**oll-**L**ike **R**eceptor

TPS **T**reatment **P**lanning **S**ystem

VMAT **V**olumetric **M**odulated **A**rc **T**herapy

WHO **W**orld **H**ealth **O**rganization

List of Figures

List of Tables

Contents

Background

Abstract

The background chapter of this PhD provides a comprehensive overview of key concepts in cancer treatment and radiotherapy. If you already know about radiotherapy and multi-leaf collimator, I strongly advise to skip this chapter.

This chapter begins by outlining the nature of cancer, its phases, stages, risk factors, and common types of treatments (with their advantages and disadvantages). Then, the physics of radiotherapy is explored, with a focus on ionizing radiation, and biological effects of radiation. This chapter also presents the patient journey in radiotherapy, from diagnosis and treatment prescription to planning and follow-up. Key technologies used in radiation therapy, such as multi-leaf collimator (MLC) linear accelerator (LINAC) are introduced. Lastly, this chapter covers the irradiation techniques, and details major steps in the dosimetry process: beam orientation optimization (BOO), fluence map optimization (FMO), leaf sequencing (LS), and direct aperture optimization (DAO).

1.1 Medical context

1.1.1 About cancer

Cancer is a complex disease that can affect many parts of the body. This malady is characterized by the uncontrolled growth of cells that can invade and destroy surrounding tissues. Cancer is a leading cause of death worldwide. In 2022, the World Health Organization (WHO) estimated 20 million new cancer cases and 9.6 million deaths linked to cancer [**?**]. Cancer affects about 20% of the population, and is responsible for 1 in 10 deaths.

Cancer characteristics Cancer is characterized in various manners, starting with an cell proliferation. Cancerous cells reprogram cellular metabolism to support their growth [**?**], they can also stop cell growth arrest mechanisms, and usually manage to evade apoptosis (programmed cell death). Cancer cells can escape the immune system, and change their cellular response phenotypic via plasticity. At some point, cancer cells can get the ability to undergo a sufficient number of successive cell cycles of growth and division to generate macroscopic tumors. To support their growth, they create new blood vessels to get nutrients. Finally, they can escape and form metastasis, and will eventually provoke senescence [1].

Conditions leading to cancer Cancer is a complex disease. First, cancer is caused by mutations in the DNA. These mutations can be inherited or acquired. Second, cancer is embraced by epigenetic reprogramming, i.e., gene expression changes (not caused by changes in the DNA sequence). Third, cancer is often associated with an inflammatory context; inflammation can promote cancer growth and spread. Finally, cancer is often associated with a disruption of the microbiota (the microbial community living in and on the human body). This disruption can promote cancer growth and spread.

Phases of cancer Cancer develops in several phases.

Initiation The first phase is initiation: Mutations in the DNA transform a healthy cell into a cancer cell.

Promotion The second phase is promotion or "tumorigenesis". During this phase, the cancer cell grows and divides uncontrollably to form a tumor cluster of cells. This growth is promoted by changes in gene expression and other factors [**?**]. It may also create new blood vessels to get nutrients and oxygen.

Evolution The final phase is evolution. The tumor will first grow locally, then regionally, invading and damaging surrounding tissues. Finally, the cancer cell will spread to other

[1] deterioration of functional characteristics

body parts, forming metastasis. Metastasis is the leading cause of death in cancer patients [**?**].

Cancer stages Cancer is classified into stages [**?**].

- Stage 0: 'in situ neoplasm'; it means a group of abnormal cells in an area of the body. The cells may develop into cancer in the future.
- Stage 1: the cancer is small and contained within the organ it started in.
- Stage 2: the tumor is larger than in stage 1, but the cancer hasn't started to spread into the surrounding tissues.
- Stage 3: the cancer is larger; it has started to spread into surrounding tissues and cancer cells in the lymph nodes nearby.
- Stage 4: the cancer has spread from where it started to another body organ. This spread is also called secondary or metastatic cancer.

Doctors use the TNM system to describe the cancer stage [**?**].

T stands for the size of the Tumour; it can be 1, 2, 3, or 4, with one being small and four being large.

N stands for the number of lymph Nodes affected; it can be between 0 and 3. 0 means no lymph node contains cancer cells; 3 means many lymph nodes contain cancer cells.

M stands for the existence of Metastasis in another part of the body; it can be 0 (no spread) or 1 (cancer has spread).

Most common cancers According to the WHO, the most common cancers are lung, breast, colorectal, prostate, skin, and stomach cancer. This thesis mainly focuses on prostate cancer, which is among the most common ones.

Risk factors Tobacco use, alcohol consumption, unhealthy diet, physical inactivity, and air pollution are risk factors for other cancer types. However, the leading risk factor for prostate cancer is age. Thus, it touches all social populations evenly and is unavoidable.

1.1.2 Treatment types

There are three main types of cancer treatment: surgery, radiation therapy, and chemotherapy. The choice of treatment depends on the type and stage of cancer, the patient's age and general health, and other factors.

1.1.2.1 Surgery

Surgery is the most effective cancer treatment [**?**]. It involves removing the tumor and surrounding tissue. Surgery is often used to treat early-stage cancer that has not spread to other parts of the body. For surgery to be possible, the tumor must be located in a place the surgeon can easily access. Surgery can be followed by other treatments, such as radiation therapy or chemotherapy, to kill any remaining cancer cells.

Advantages Surgery is considered a curative treatment modality; cancerous tissues are entirely removed, leading to disease eradication. Being a localized intervention, it primarily affects the targeted area with minimal systemic side effects. Additionally, surgical procedures are typically performed in a single session, unlike other treatment modalities (e.g., radiotherapy) that may require multiple cycles.

Disadvantages Surgery is invasive, and it can be painful. The main disadvantage, is that it can only be used for localized cancer (with no metastasis) accessible to the surgeon.

1.1.2.2 Chemotherapy

Chemotherapy is a treatment that uses drugs to kill cancer cells. It is systemic, meaning it can reach cancer cells anywhere in the body. Therefore, it usually has strong side effects. Chemotherapy is often used to treat cancer that has spread to multiple parts of the body (i.e., metastatic cancer).

Depending on how advanced the cancer is, chemotherapy can be used to cure, control, or relieve symptoms (palliation).

Advantages Chemotherapy can be used to treat cancer that has spread to multiple parts of the body. It can also be used to relieve symptoms and improve quality of life.

Disadvantages Chemotherapy is a heavy treatment, with strong side effects. It can also weaken the immune system, making the patient more prone to infections. Finally, newer drugs tend to be very expensive.

1.1.2.3 Radiation therapy

Radiation therapy is a treatment that uses high-energy radiation to kill cancer cells. It is semi-local, meaning that it only affects the tumor, and the tissues traversed by the radiation beams [**?**]. Radiation therapy is curative most of the time. It can be used alone or in combination with other treatments.

Radiation therapy can be delivered in two ways: external radiation therapy and internal radiation therapy. External radiation therapy uses a machine to deliver radiation to the tumor from outside the body. Internal radiation therapy uses radioactive materials placed directly into or near the tumor. This thesis focuses on external radiation therapy.

Advantages Radiation therapy is a non-invasive treatment, with limited side effects. It is relatively localized, and can be used to treat cancers that are not accessible via surgery.

Disadvantages Radiation therapy still targets healthy cells. Depending on the patient's response, it may cause side effects.

1.1.2.4 Other treatments

Cancer research is very active, and new treatments are constantly being developed. These treatments are often used in combination with others.

Immunotherapy Immunotherapy is a treatment that uses the body's immune system to fight cancer. It can boost or change how the immune system works to find and attack cancer cells. It is a systemic treatment.

Targeted therapy Targeted therapy is a treatment that uses drugs to target specific molecules that are involved in cancer growth. It is a systemic treatment.

Hormone therapy Hormones are proteins or substances the body makes that help control how specific cell types work. Hormone therapy is a treatment that uses drugs to block or lower the amount of hormones in the body that are involved in cancer growth. It is a systemic treatment.

Stem cell transplant A stem cell transplant is a treatment that uses stem cells to replace cells damaged or destroyed by cancer treatment. It is a systemic treatment.

1.2 Physics of Radiotherapy

Radiation therapy uses high-energy radiation to kill cancer cells.

1.2.1 Ionizing radiation

Ionizing radiation has enough energy to remove tightly bound electrons from atoms, creating ions. X-rays and gamma rays are both electromagnetic radiations that are ionizing and high-energy photons. Some particle radiations, such as particles, beta particles, and neutrons, are also ionizing, but radiotherapy uses photon radiations.

X-rays are produced by accelerating electrons to collide with a target material and are used in medical imaging and (external) radiation therapy. In contrast, gamma rays originate from the radioactive decay of specific atomic nuclei and are used in (internal) radiation therapy.

Because ionizing radiation therapy can damage the DNA in cells and lead to cell death, it is used in radiation therapy for treating cancer.

1.2.2 Photon interactions

Photon-matter interactions within an absorbing medium undergo stochastic (i.e., random) processes. Four types of interactions (figure 1.1) are possible for photons; their occurrence depends on the atomic number, matter, and the energy of the incident photon [**?**]. Three of the four interactions generate secondary ionizing particles that deposit energy in the medium.

Rayleigh scattering The Rayleigh scattering (figure 1.1a) does not change the energy of the incident photons and consequently has no direct consequence on the body. Rayleigh scattering predominantly occurs with low-energy photons (typically < 100 keV).

Photoelectric absorption The photoelectric absorption effect (figure 1.1b) is the process by which an atom absorbs a photon, and an electron is ejected from the atom. The photon ceases to exist, and its energy is transferred to the electron. The ejected electron, called a photoelectron, can ionize other atoms, leading to dose deposition. The photoelectric effect is the dominant interaction for low-energy (< 100 keV) photons.

Compton scattering Compton scattering (figure 1.1c) is the process by which an atom scatters a photon, and ejects an electron from the atom. The photon is scattered at an angle, and part of its energy is transferred to the electron. The emitted electron is called a Compton electron, which can ionize other atoms, leading to dose deposition. Compton scattering is the dominant interaction for medium-energy (≈ 0.1 to ≈ 10 MeV) photons.

Pair production Pair production (figure 1.1d) is when an atomic nucleus absorbs a photon and creates an electron-positron pair. The photon ceases to exist, and its energy is transferred to the electron-positron pair. The positron rapidly interacts with another electron of the matter, producing two photons emitted at 180° from each other. The electron can ionize other atoms, leading to dose deposition. Pair production is the dominant interaction for high-energy (> 10 MeV) photons.

1.2.3 Photon attenuation

The photon beam will be attenuated as it passes through the medium, and its intensity will decrease. The dose deposition in the medium is proportional to the intensity of the photon

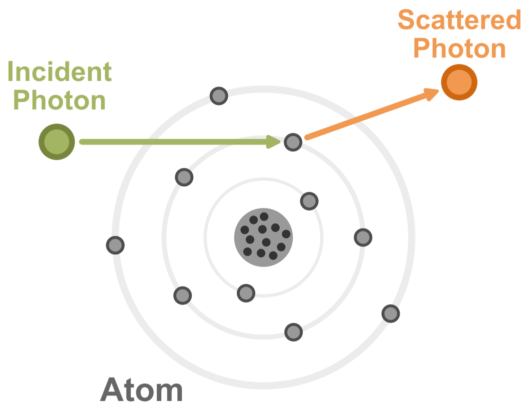

(a) Diagram of Rayleigh Diffusion.

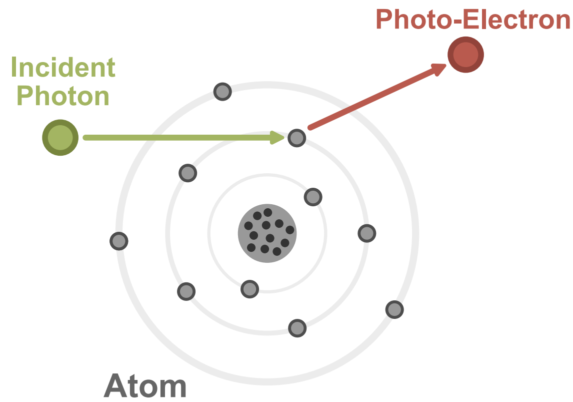

(b) Diagram of Photoelectric Absorption.

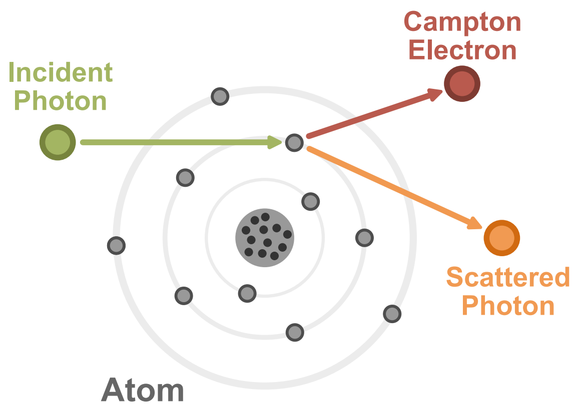

(c) Diagram of Compton Scattering.

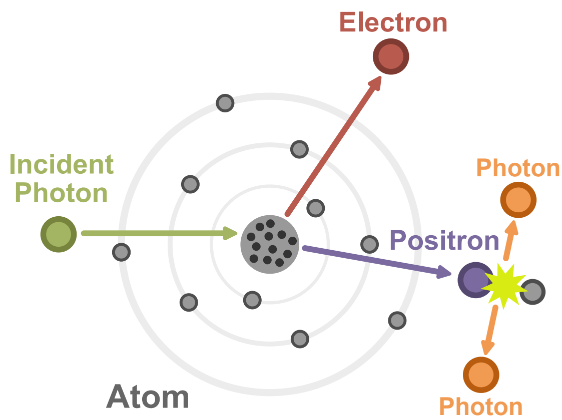

(d) Diagram of Pair Production.

Figure 1.1: Diagrams of photon interactions with matter observed in the kilo and mega-voltage energy range.

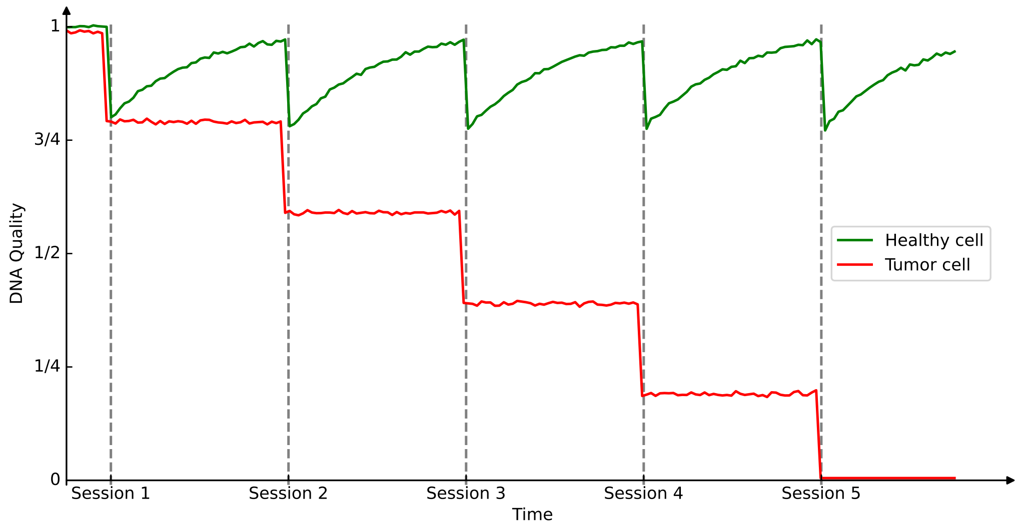

Figure 1.2: Quality of the the DNA in healthy and tumor cell after radiotherapy sessions.

beam. The attenuation of the beam follows an exponential law concerning the depth of the medium traversed (Lambert-Beer law) [**?**]:

$$I(x) = I_0 \exp(-\mu x)$$

where I is the intensity of the photon beam after passing through a thickness x of the medium, I_0 is the initial intensity of the photon beam, and μ is the attenuation coefficient of the medium.

1.3 Biological effect on cells

Ionizing radiation can damage the cells leading to cell death in various ways.

1.3.1 Radiation effects on DNA

Ionizing radiation damages the DNA [**?**] in cells and leads to cell apoptosis[2], necrosis[3], or senescence. Radiation induces DNA damage through both direct and indirect mechanisms: Directly, it causes single-strand breaks (SSBs), double-strand breaks (DSBs) [**?**], DNA crosslinks, and DNA-protein crosslinks [**?**]. Indirectly, radiation generates reactive oxygen species (ROS) and reactive nitrogen species (RNS), further contributing to DNA damage.

[2]process of programmed cell death
[3]death of most or all of the cells in an organ or tissue

DNA repair Cells have mechanisms to repair DNA damage. There are several types of DNA repair mechanisms, including base excision repair (BER), nucleotide excision repair (NER), mismatch repair (MMR), and double-strand break repair (DSBR). Cancer cells often have defects in DNA repair mechanisms, making them more sensitive to radiation therapy [**?**]. This repair mechanism being available only for healthy cells leads to cell death only for cancerous cells when their DNA is too damaged to survive (see figure 1.2).

1.3.2 Radiation affects the plasma membrane

Radiation significantly impacts the biological properties of the plasma membrane by affecting its composition, structural integrity, and functional capabilities. Radiation exposure can alter the fluidity and permeability of the cell membrane, affecting the transport of ions and molecules into and out of the cell. Additionally, radiation causes corrosive damage, and damage to the membrane can initiate signaling events that are important for the apoptotic response [**?**]. These changes can have cascading effects on various cellular processes, highlighting the critical role of the plasma membrane in maintaining cellular homeostasis under stress conditions.

1.3.3 Radiations and cell organelles performances

Radiation exerts significant detrimental effects on various cellular organelles, impacting their functionality and overall cellular health [**?**]. One critical target of radiation damage is the endoplasmic reticulum, where radiation can disrupt protein folding and processing, leading to cellular stress and apoptosis. Additionally, ionizing radiation induces alterations in ribosomal structure and function, impairing protein synthesis and compromising cellular homeostasis. Mitochondria, the cell's powerhouses, also exhibit altered behavior following radiation exposure, including disruptions in energy production and initiating apoptotic pathways. Furthermore, lysosomes, essential for cellular waste processing and recycling, suffer damage upon irradiation, potentially accumulating cellular debris and impairing cell function. These collective effects highlight radiation's broad and profound impact on cellular organelle performance [**?**].

1.3.4 Radiation alters the biological behavior of cells

Radiation profoundly influences the biological behavior of tumor cells and the immune system, impacting critical aspects of cancer progression and immune response. It affects tumor cell proliferation, often reducing the ability of cancer cells to multiply by damaging their DNA and cellular structures. Radiation also influences tumor cells' invasion and metastasis potential either by directly impairing their motility or altering the tumor microenvironment to make it less conducive to cancer spread. Additionally, radiation can modulate cancer-promoting inflammation, either by inducing pro-inflammatory signals that support tumor growth or by disrupting the inflammatory milieu to hinder cancer progression.

1.3.5 Radiation effects when combined with immunotherapy

Radiation can be used alongside immunotherapy. The effect of both treatments is more significant than the sum of their impact if used alone.

Ray-Enhanced Anti-CTLA-4 Immunotherapy Radiation therapy can enhance the efficacy of immune checkpoints [4] based therapy, such as anti-CTLA-4 immunotherapy [5] , a treatment that blocks the CTLA-4 protein in T cells, thus boosting the immune system's response against cancer cells. The combination of radiation and anti-CTLA-4 immunotherapy has shown promising results, as radiation-induced tumor cell death releases antigens that can further stimulate the immune system [**?**]. This synergy can improve tumor control and potentially better clinical outcomes than either treatment alone.

Radiation Combined with Anti–PD-1/PD-L1 Immunotherapy Combining radiation with anti–PD-1/PD-L1 immunotherapy [6] has shown significant success. Anti–PD-1/PD-L1 therapies block the PD-1/PD-L1 pathway, which tumors exploit to evade immune detection. Radiation therapy can augment this effect by increasing the immunogenicity of the tumor, thereby making cancer cells more susceptible to immune attack [**?**].

TLR-Mediated Immunologic Effects of Radiation Therapy Radiation therapy can also exert immunologic effects through Toll-like receptors (TLRs), a class of proteins involved in pathogen recognition and activation of innate immunity. Radiation can activate TLRs on immune cells, producing cytokines and chemokines that enhance the immune response against tumors. This TLR-mediated effect contributes to the synergy between radiation and immunotherapies, leading to more robust anti-tumor responses [**?**].

While this thesis does not focus on biological aspects, one should remember that radiation affects cells in various ways, and cancer therapy is complex.

---

[4] The immune checkpoints are regulators of the immune system; they prevent the immune system from attacking all cells indiscriminately. Tumor cells sometimes exploit this mechanism to evade immune surveillance.

[5] Cytotoxic T-lymphocyte-associated protein 4 (CTLA-4) is a protein receptor that downregulates immune responses (it acts as an "off" switch). Blocking this receptor induces lymphocyte activation and cytokine production and has an in vivo antitumor effect.

[6] Programmed cell Death protein 1 (PD-1) is a protein present on the surface of immune cells, T lymphocytes, and is a component of the immune checkpoint. The T lymphocyte can interact via PD-1 with a tumor cell presenting protein Programmed Death-Ligand 1 (PD-L1) on its surface. This interaction inactivates the T lymphocyte and consequently inactivates one of the immune system's defense mechanisms against tumor cells. Researchers have developed antibodies that bind to PD-1 or PD-L1, called anti-PD-1 or anti-PDL-1 antibodies. Blocking the immune checkpoint by preventing the interaction between PD-1/PD-L1 can lift the inactivation of the immune system, which can then fight the tumor cell again.

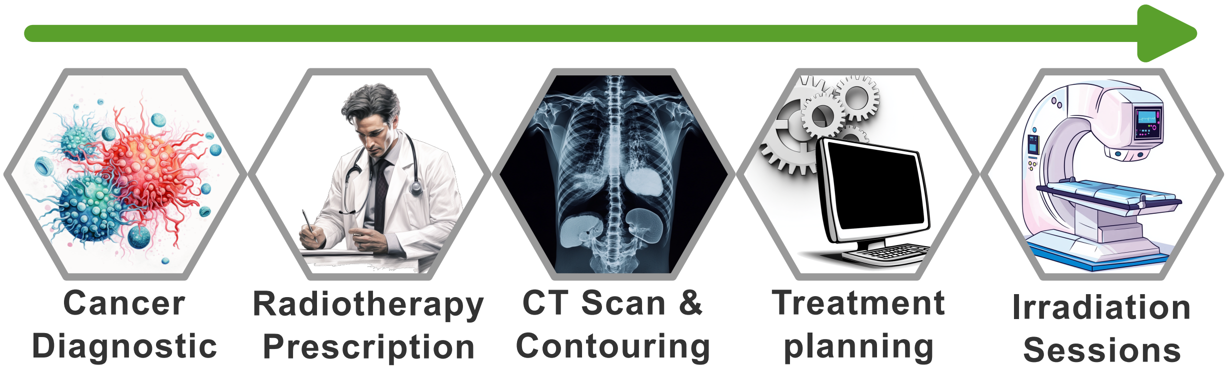

Figure 1.3: Typical radiotherapy patient path.

1.4 Patient Path

The radiotherapy patient path encompasses several critical stages, each essential for the effective treatment of cancer. This section outlines the sequential steps of radiotherapy, from initial detection and diagnosis to follow-up care.

1.4.1 Diagnostic

Patients diagnosed with a tumor can go through several paths: surgery, radiotherapy, immunotherapy, chemotherapy, or any combination. Doctors will choose the most appropriate treatment(s) based on evidence they have (biopsy, radios, et cetera). This manuscript will focus on the radiotherapy path.

1.4.2 Radiotherapy Prescription

Following a confirmed diagnosis and the choice of radiotherapy treatment, the oncologist develops a prescription. This prescription specifies the type, dosage, and frequency of radiation treatment tailored to the patient's specific cancer type, location, and stage. The doctors define minimal tumor irradiation and maximum damage to surrounding healthy tissues. Most of the time, templates are used and fine-tuned to fit specific patients.

1.4.3 CT scan and Contouring

A computed tomography (CT) scan is performed to obtain detailed images of the patient's anatomy. These images are used to delineate the tumor and surrounding organs at risk. Automatic segmentation delineated the contour organs on each slice. Medical doctors previously did this task, and it was heavily time-consuming. Nowadays, artificial intelligence performs with only minor human correction needed [**?**] [**?**]. After the emergence of AI for contouring, this manuscript will tackle the treatment planning problem.

The CT scan also provides the spatial information necessary for precise irradiation simulation.

1.4.4 Treatment Planning

The treatment planning process involves developing a detailed plan specifying the patient's radiation dose distribution. Advanced software calculates the optimal arrangement of radiation beams to achieve the desired dose while minimizing exposure to healthy tissues. This thesis registers new advances in the planning step. Plans must be reviewed and approved by doctors.

1.4.5 Irradiation Sessions

Irradiation sessions, or treatment delivery, is the actual irradiation of the patient. Cone Beam Computed Tomography (CBCT) is usually done to reposition the patient with the scan so that all organs align with the planning CT. Nowadays, the tendency is to reduce the number of irradiation sessions (the old typical five weeks of five sessions is now usually two weeks of five sessions).

1.4.6 Follow-up

After the completion of radiotherapy, patients enter the follow-up phase. Regular follow-up appointments are scheduled to monitor the patient's response to treatment, manage any side effects, and detect any signs of recurrence.

1.5 Machines

The discovery of X-rays by German physicist W. C. Roentgen in 1895 marked a pivotal moment in medical science. Only one year later, in 1896, Despeignes began using radiotherapy in France. Victor Despeignes delivered 15-30 minutes with 80 irradiation sessions (so-called "fractions") to relieve the pain of patients with stomach cancer [**?**].

Since then, machines have become more powerful and more complex. Modern machines can deliver mega-voltage radiation [**?**], which are sufficiently high to destroy tumors in minutes. However, such high-power treatments will irreversibly damage healthy tissues. Hence, as the machines became more powerful, constructors built more complex modulation mechanisms to preserve organs at risk.

1.5.1 Molds

The first kind of modulation used was molds: their purpose was to stop the irradiation before it reached the body. By strategically obscuring the rays, organs can be spared, as they will receive a small amount of irradiation dose, while the tumor will receive a fatal

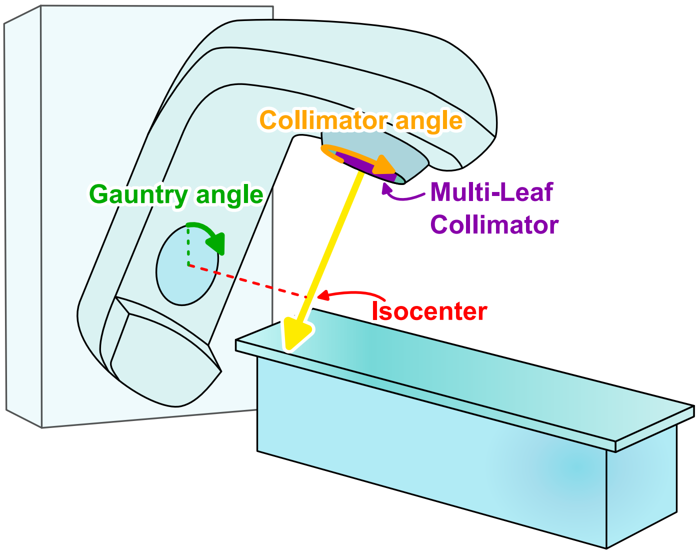

(a) Sketch of a Multi-Leaf Collimator.

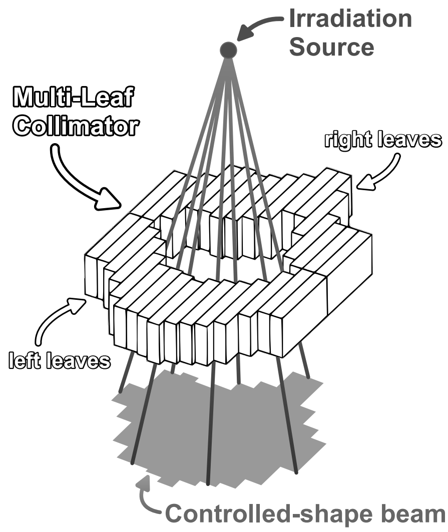

(b) Sketch of a Multi-Leaf Collimator Filtering the Irradiation Source.

Figure 1.4: MLC-LINAC Machines Irradiation Filtering System.

dose. Molds had significant limitations due to their single-use nature. It was necessary to create a custom mold for each patient as their anatomy differs. Typically, three molds were required for the three irradiation angles. Modern technology avoids single-use molds using motorized blockers to stop the rays and dynamically modulate the radiation beam.

1.5.2 Multi-Leaf Collimator - Linear Accelerators

Multi-**l**eaf **c**ollimator (MLC) technology combined with **Lin**ear **Ac**celerators (LINAC) was a revolution in the radiotherapy world [**?**] [**?**]. They are capable of turning around the patient to deliver irradiation from multiple angles (figure 1.4a). Moreover, an array of motorized leaf pairs can shape the radiation beam with high precision (figure 1.4b). Additionally, MLC systems are sometimes equipped with jaws, which help to shape the beams better. The MLC-LINAC is the most common type of radiation therapy machine used today. This manuscript will focus on the MLC-LINAC system due to its widespread use and versatility in clinical settings.

1.5.3 Tomotherapy

Tomotherapy systems have an irradiation head that rapidly rotates around the patient, equipped with a single layer of binary blockers that can be activated and deactivated almost instantaneously [**?**]. The tomotherapy machines follow a helical path [**?**], rotating around the patient while simultaneously moving along their body.

1.5.4 CyberKnife

CyberKnife systems are another non-invasive alternative to conventional MLC-LINAC radiotherapy machines with higher flexibility [?]. These CyberKnife machines have the irradiation head mounted on a robotic arm, which allows a vast array of motions around the patient. This flexibility enables the delivery of even more complex-shaped doses. CyberKnife technology is particularly beneficial for treating unusual tumors in challenging or sensitive body areas.

1.5.5 Brachytherapy

Brachytherapy involves the placement of a radioactive source directly inside the body of the patient [?]. This technique allows for delivering localized high-dose radiation. Although brachytherapy involves an invasive procedure, it significantly minimizes radiation exposure to surrounding healthy tissues. The localized character of brachytherapy makes it a good treatment option for some types of cancer.

1.6 Irradiations techniques

This section describes the main irradiation techniques that can be used with MLC-LINAC machines. The techniques have evolved over the years of MLC usage. Better irradiation techniques improve tumor targeting while keeping exposure of healthy tissues to a minimum.

1.6.1 3-Dimensional Conformal Radiotherapy

Three-Dimensional Conformal Radiotherapy (3D CRT) shapes radiation beams to closely fit the contours of the tumor. The MLC leaves are positioned to match the tumor's contour projection on a plane perpendicular to the radiation rays, typically using three angles. Such shaping of the beams can be done with mold (which is single-use) or with an MLC. Although 3D CRT targets the Principal Target Volume (PTV) more than Organs At Risk (OARs), modern techniques provide superior sparing of healthy tissues. Consequently, advanced and less naive methods have largely supplanted 3D CRT in contemporary clinical practice.

1.6.2 Intensity Modulated RadioTherapy

Intensity Modulated RadioTherapy (IMRT) represents a significant advancement over 3D CRT by taking better advantage of the MLC capabilities. Instead of delivering radiation with uniform intensity from each angle, IMRT dynamically adjusts the beam intensity to improve patient outcomes [?].

Number of Beams The choice of the number of beams in IMRT is a balance between treatment complexity and effectiveness. Using many beams can evenly spread the unwanted dose across all organs, but adds complexity to treatment planning and prolongs the delivery time, which can increase patient movement and reduce dose precision. Conversely, fewer beams simplify planning and shorten treatment time but may result in less optimal dose distribution. Research indicates that 50 beams are needed for "nearly optimal IMRT" [**?**]. Beams at exactly 180 degrees from each other tend to have (very) similar influence on the dose distribution on the patient. Therefore, dosimetrists tend to choose an odd number of equispaced beams. In practice, the number of beams used is below 25.

1.6.3 Volumetric Modulated ArcTherapy

Volumetric Modulated Arc Therapy (VMAT) enhances IMRT by allowing the MLC LINAC head to rotate while delivering radiation. Unlike IMRT, which stops the head at specific positions around the patient, VMAT continuously irradiates while rotating. This technique can better distribute the unwanted dose and reduces the irradiation time [**?**].

However, the mechanical constraints of the machine complicate the optimization problem for VMAT compared to IMRT, making the optimization more computationally intensive. Studies have demonstrated that, IMRT with a Sliding Window and more than 7 angles can achieve equally effective dose distribution [**?**] [**?**]. While demonstrated with IMRT Sliding Window, the techniques developed in this manuscript apply to VMAT, given sufficient computational resources.

1.7 Dosimetry steps

Dosimetry aims to design a treatment plan (i.e., machine instructions) that delivers the best possible dose for the patient. The "best" dose is difficult to define, so doctors formulate high-level clinical dose requirements. These requirements are abstract, so transitioning to machine instructions requires a series of sub-steps. For IMRT, three main steps are typically followed: Beam Orientation Optimization (BOO), Fluence Map Optimization (FMO), and Leaf Sequencing (LS).

1.7.1 Beams Orientation Optimization

Beam orientation optimization (BOO) is the initial dosimetry step. This step determines the optimal number of radiation beams and their respective angles. The beams' orientation significantly impacts the dose distribution within the patient: beams close to each other tend to have similar effects on the body. In contrast, far-apart beams tend to create doses impacting different tissues in the body. There is one exception to this rule of thumbs: Beams exactly 180° from each other can have a similar biological effect because rays will follow the same line, just entering the body from opposite directions. Despite its importance, the practical benefits of BOO are questionable. Research [**?**] suggests that an extensive BOO process offers only slight improvement over more straightforward strategies, like using equispaced beam angles. When using equispaced beams, it's common to use an odd number of beams to avoid beams at exactly 180° having the same effect. Employing an odd number of beams is standard practice when utilizing equispaced beam arrangements. This approach avoids beams positioned at precisely 180° from each other, with similar clinical effects (as mentioned before). Therefore, this manuscript will assume the use of an odd number of equispaced beams and no further BOO.

1.7.2 Fluence Map Optimization

Fluence map optimization (FMO) is the critical step in the IMRT planning process. FMO aims to create fluence maps, i.e., a two-dimensional radiation intensity distribution on each beam's cross-sectional area. The fluence maps should be optimized to shape the dose distribution according to the treatment plan's objectives. At this stage, the physical constraints of the MLC still need to be considered; the primary focus is on achieving the desired dose distribution within the patient. The output of FMO is a set of idealized fluence maps for each beam.

1.7.3 Leaf Sequencing

Leaf Sequencing (LS) determines the specific positions and movements of the MLC leaves. The objective is to ensure that the delivered fluence map closely approximates the ideal fluence map generated during the FMO step. This approximation must be attained while considering the physical limitations of the treatment machine, such as irradiation power, leaf speed, or collimator speed, along with a soft constraint on the total treatment duration.

Step and Shoot The "Step and Shoot" technique in IMRT involves sequentially moving the MLC leaves to different positions to deliver varying radiation intensities. This technique for leaf sequencing is relatively simple computationally.

The fluence maps are divided into discrete levels (figure 1.5). Then, the MLC leaves are positioned so that the open area of the irradiation head matches the level set (figure 1.6). Note that convex level sets can all be matched with the MLC leaves; if the level set is concave, changing the collimator angle may allow the leaves to match the level set shape (figures 1.7a, 1.7b, 1.7c). Each level set is delivered as a static beam in sequence. As the level sets are refined, the irradiation time increases Dosimetrists must set a tradeoff between achieving greater accuracy and maintaining an efficient treatment time.

Sliding Window The "Sliding Window" technique employs a continuous sweep motion of the MLC leaves. This approach enables the delivery of any continuous, positively defined fluence within the irradiation window of the MLC-LINAC. In contrast with step and shoot, a sliding window is more computationally intensive: Finding the appropriate leaf motions

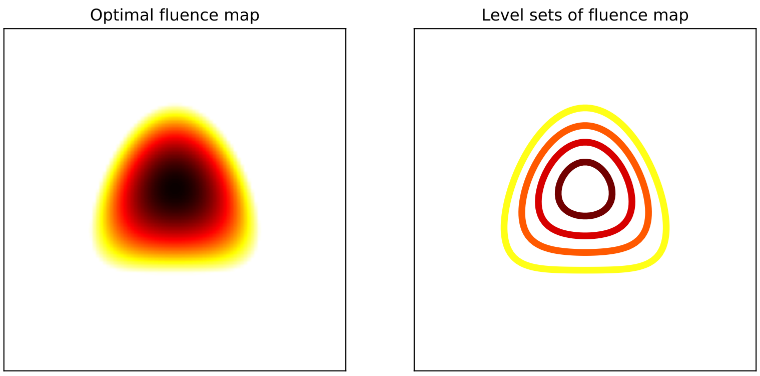

Figure 1.5: Example of a fluence map discretization.

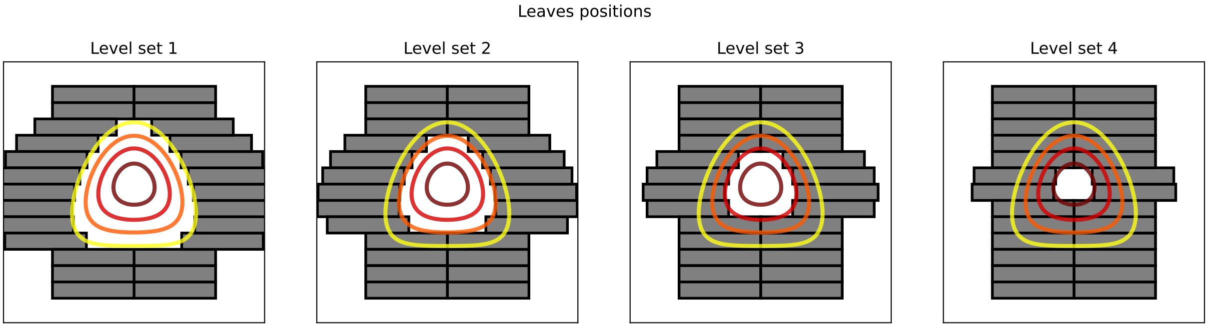

Figure 1.6: Example of level set matching with leaves.

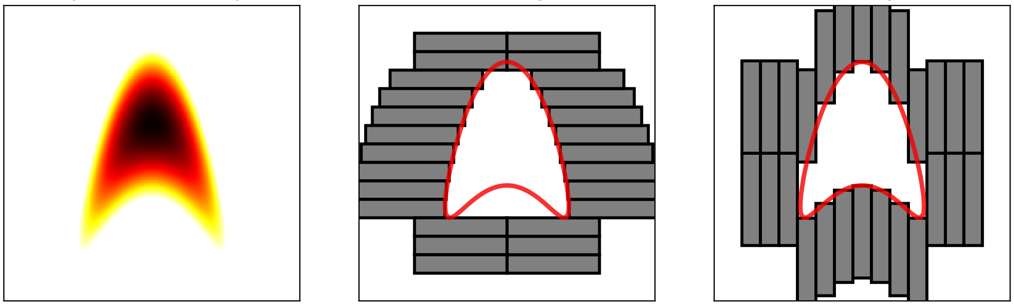

(a) Example of a concave level set matched with leaves.

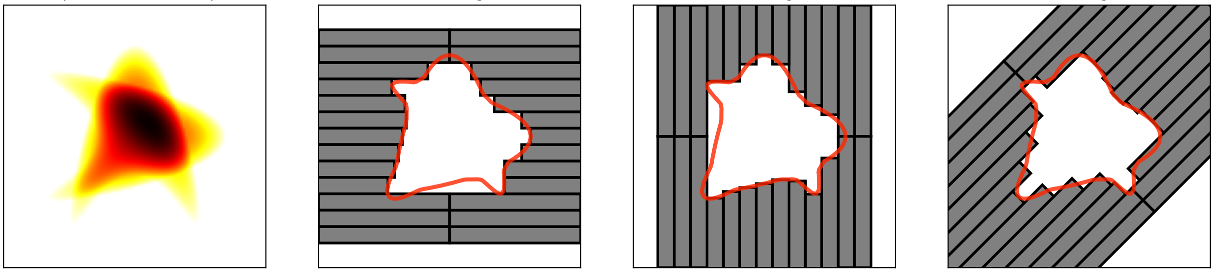

(b) Example of a more complex concave level set matched with leaves.

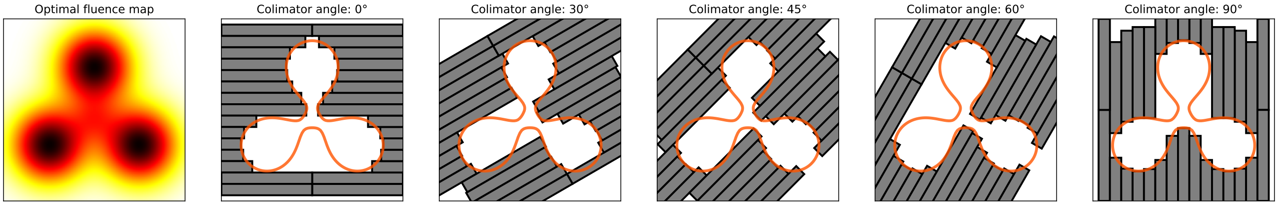

(c) Example of a concave level set impossible to match with leaves.

Figure 1.7: MLC leaves can not always be set to shape level sets of fluence functions.

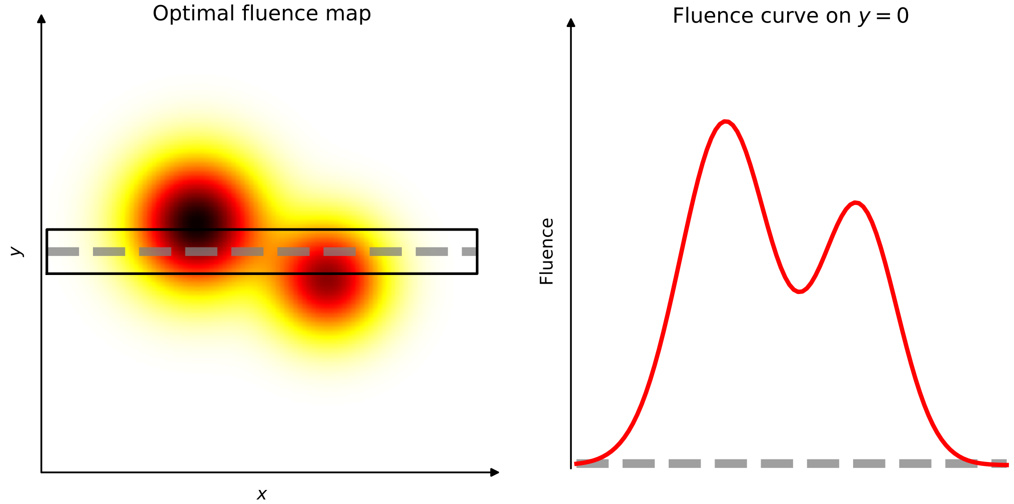

Figure 1.8: Example of a fluence map segmentation along a leaf pair axis.

requires solving a linear programming problem for each pair of leaves (sometimes called "Inverse Sliding Window Algorithm").

The fluence is segmented in a one-dimensional fluence curve along each leaf pair axis (see figure 1.8). Suppose the motion of the leaves is from left to right: The difference between the time the right and left leaves pass by a point determines the amount of irradiation delivered at that point. The greater the time difference, the more rays will be sent from that point (in figure 1.9a and 1.9b, the time laps between left and right leaves passing a point is proportional to the fluence delivered at that point). One needs to carefully move the opening (right) and closing (left) leaves to deliver the correct amount of rays at each point of the fluence map. Solving a linear programming problem allows a leaf pair to deliver any fluence within arbitrary approximation in a reasonable amount of time (figure 1.9). A playground to calculate the leaf's motion for an arbitrary fluence is available here: https://mics-lab.github.io/PresentationJuin2023PRFD/demo.

The sliding window technique is used most of the time, as delivery time is much (about twice) faster [**?**]. This manuscript assumes the use of this technique, focusing on optimizing the fluence distribution.

1.7.4 *(Optional)* Direct Aperture Optimization

Direct Aperture Optimization is mainly used in VMAT and occasionally employed to enhance IMRT plans. Unlike traditional approaches, which separate fluence map optimization from leaf sequencing, DAO directly optimizes the motion of the MLC leaves.

In VMAT, applying conventional leaf sequencing to any arbitrary fluence map is not feasible.

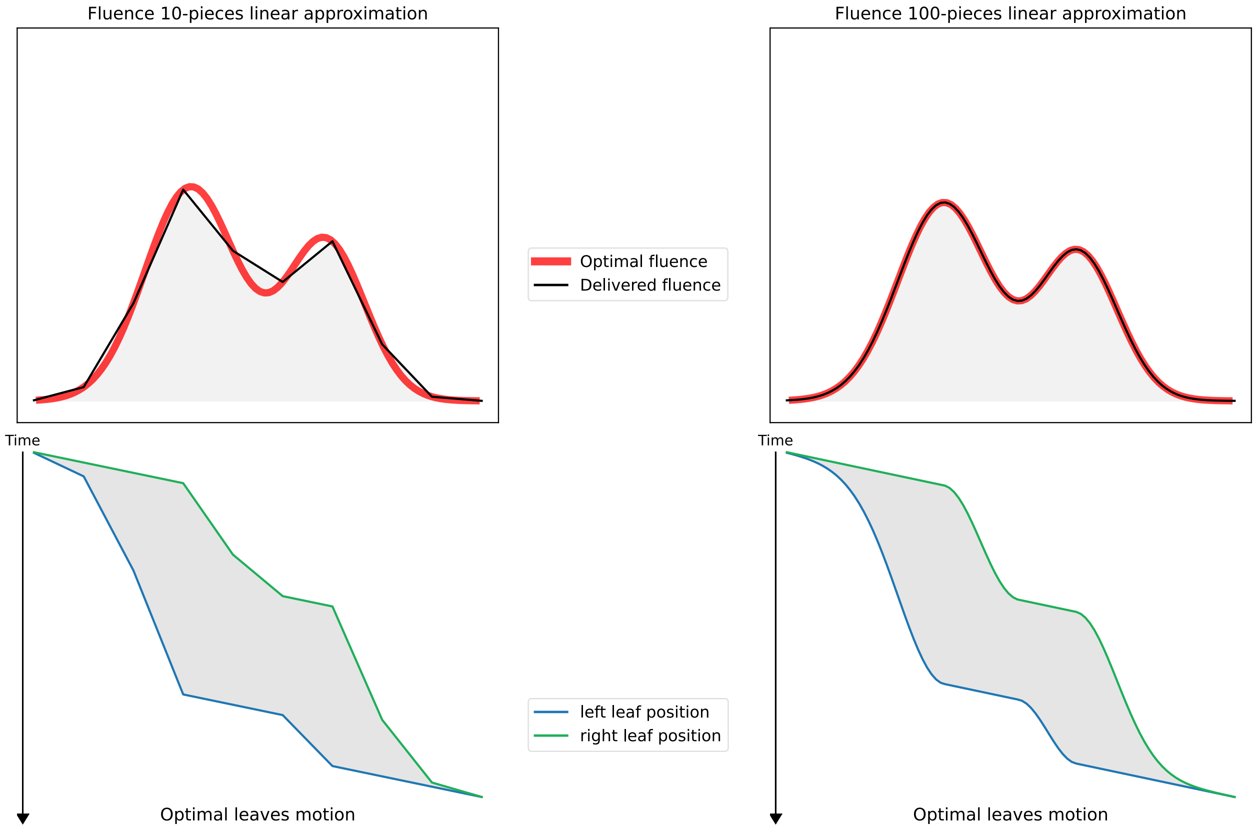

(a) Example of a fluence curve leaf sequencing, with the fluence approximated by a 10-pieces linear function.

(b) Example of a fluence curve leaf sequencing, with the fluence approximated by a 100-pieces linear function.

Figure 1.9: Fluence curve can be approximated with arbitrary error.

Therefore, DAO is essential, as it is the only optimization method capable of generating a VMAT treatment plan.

When applied to IMRT, DAO can refine the treatment plan by directly adjusting the aperture shapes to better align with the desired dose distribution while accounting for the physical constraints of the treatment machine. However, as this manuscript is not focused on leaf sequencing, it assumes that no additional DAO is applied following conventional leaf sequencing.

1.8 Simulation

Throughout the dosimetry process, several approximations are employed. First, the assumption is that each bixel (beam pixel) operates independently. This approximation fails to account for interactions between adjacent bixels. Additionally, during FMO, ideal fluence maps are generated without considering the physical limitations of the treatment machine, such as the width of the multi-leaf collimator leaves (often 5mm). Furthermore, the effects of beam penumbra and the scattering of radiation within the patient's body are often simplified or neglected in the FMO. Given these approximations, re-simulation of the treatment plan is critical to verify that the machine instructions deliver a dose distribution closely aligned with the expected outcomes.

1.9 Treatment Planning Systems

Treatment Planning Systems (TPS) are the crucial tools that calculate the precise machine (MLC) motions according to the dosimetrists priorities and the irradiation technique chosen.

1.9.1 Manufacturer

Eclipse™ (Varian)
Eclipse™ [**?**], developed by Varian, is one of the most widely used TPS globally. It supports VMAT with one or multiple arcs, and IMRT with any number of beams. Eclipse™ integrates with Varian's suite of treatment machines, and integrates an automatic contouring tool [**?**].

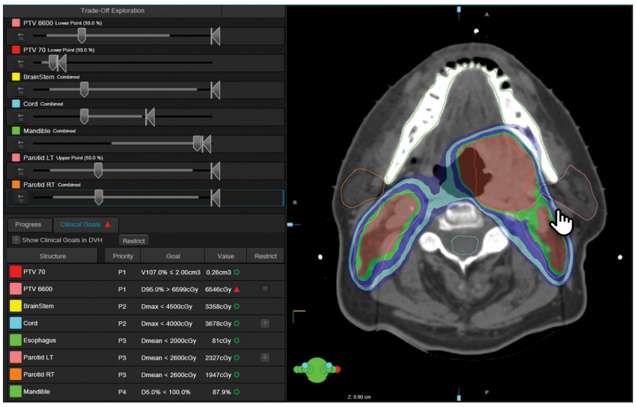

Advertisement screenshot of Eclipse™ (Varian's TPS).

ONE® | Planning (Elekta)
ONE® | Planning [?] is Elekta's TPS, and is also widely used, supporting IMRT and VMAT. It is renowned for its speed with high-precision dose calculation using the Monte Carlo method [7].

Advertisement screenshot of ONE® | Planning (Elekta's TPS).

Precision® (Accuray)
Developed by Accuray, Precision® [?] is the dedicated TPS for CyberKnife and TomoTherapy systems.

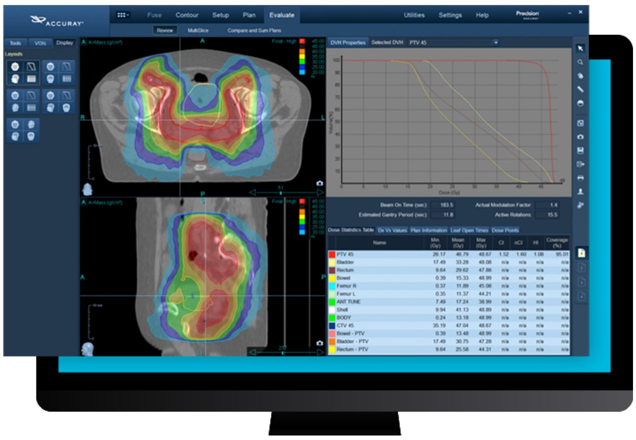

Advertisement screenshot of Precision® (Accuray's TPS).

1.9.2 Non-manufacturer

[7]Monte Carlo methods are a class of computational algorithms that rely on repeated random sampling to obtain numerical results.

RayStation (RaySearch)
RayStation [?], developed by RaySearch Laboratories, is a TPS known for its advanced optimization algorithms. Unlike manufacturer-specific systems, RayStation can output plans for a wide range of linear accelerators and imaging devices. It offers robust support for various treatment techniques, including VMAT, IMRT, 3D-CRT, Cyberknife, and TomoTherapy.

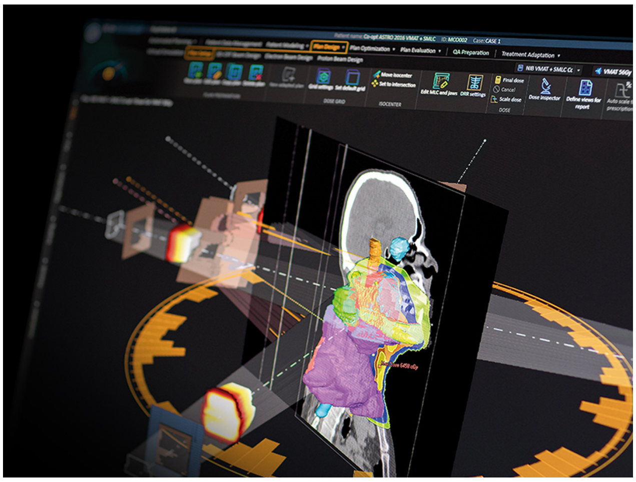

Advertisement screenshot of RayStation (RaySearch's TPS).

matRad (German Cancer Research Center - DKFZ)
matRad [?] is an open-source TPS developed by the German Cancer Research Center (DKFZ) for research and education. While not intended for clinical use, matRad offers a flexible platform for testing and developing new treatment-planning algorithms.

matRad

AutoPlan (TheraPanacea - Unpublished)
AutoPlan is the upcoming TPS from TheraPanacea, designed to incorporate artificial intelligence and machine learning into the treatment planning process.

Introduction

Abstract

This chapter provides a comprehensive overview of the current landscape in radiotherapy planning. We begin by re-contextualizing the field and outlining the critical challenges and limitations traditional methods face. The state of the art is then explored, detailing advancements in automated rule implementation, knowledge-based radiotherapy planning, and Multi-Criteria Optimization (MCO). We address the pivotal role of automated and knowledge-based techniques in improving treatment efficiency. The commercial solutions, such as Pinnacle AutoPlanning, Eclipse RapidPlan, and RayStation are discussed. We identify unresolved problems within the field, setting the stage for the subsequent sections of the thesis.

2.1 Context

Cancer remains one of the leading causes of mortality worldwide, with its incidence projected to rise in the coming decades [**?**, **?**]. As our understanding of cancer biology evolves and diagnostic techniques improve, the demand for effective and personalized treatment strategies continues to grow [**?**]. Radiotherapy has emerged as a cornerstone in cancer management, either as a standalone treatment or in combination with other modalities such as surgery, chemotherapy, and immunotherapy [**?**, **?**]. Radiotherapy leverages ionizing radiation to damage cancer cells' DNA, impeding their ability to proliferate and ultimately leading to cell death [**?**]. The efficacy of radiotherapy lies in its ability to deliver precise doses of radiation to tumor volumes while minimizing exposure to surrounding healthy tissues [**?**]. This delicate balance between tumor control and normal tissue toxicity underscores the importance of treatment planning in radiotherapy [**?**].

The advent of advanced imaging technologies [**?**], coupled with sophisticated delivery systems like Multi-Leaf Collimator Linear Accelerators (MLC-LINACs), Tomotherapy units, and CyberKnife systems, has revolutionized the field of radiation oncology [**?**, **?**]. These technological advancements have paved the way for highly conformal treatment techniques. Intensity-Modulated Radiation Therapy (IMRT) and Volumetric Modulated Arc Therapy (VMAT) techniques offer unprecedented levels of dose sculpting, allowing for escalated doses to tumors while better sparing organs at risk [**?**, **?**, **?**]. However, the increased complexity of modern radiotherapy techniques has led to a corresponding increase in the complexity of treatment planning [**?**, **?**]. The process of creating an optimal treatment plan involves multiple steps, including Beam Orientation Optimization (BOO) [**?**, **?**], Fluence Map Optimization (FMO) [**?**, **?**, **?**], Leaf Sequencing (LS) [**?**, **?**, **?**], and (sometimes) Direct Aperture Optimization (DAO) [**?**, **?**, **?**]. Each step requires careful consideration of numerous variables and constraints, making the planning process time-consuming and labor-intensive [**?**].

In this context, this thesis aims to explore and advance the radiotherapy treatment planning automation field, focusing on developing novel algorithms and methodologies to enhance treatment plans' efficiency, quality, and consistency. By building upon the foundational knowledge of radiotherapy physics, biology, and clinical workflow, we seek to contribute to the ongoing evolution of radiation oncology and, ultimately, to improve outcomes for cancer patients.

2.2 Problematic

Traditional manual radiotherapy planning procedures are inherently subjective and time-consuming. The reliance on individual planner expertise often leads to variability in treatment plan quality[**?**, **?**, **?**, **?**]. This treatment plan diversity can induce inconsistencies in patient care. While efforts have been made to enhance consistency [**?**], significant variability among planners and institutions persists. There is a pressing need for more standardized planning approaches. The automation of treatment planning processes presents a promising solution to these challenges.

Moreover, the time-intensive nature of manual optimization [**?**] and the growing demand for radiotherapy services have created a pressing need to develop automated approaches to streamline the radiotherapy planning process. Automation enables the treatment of more patients and facilitates exploring a broader range of treatment options.

By applying computational algorithms and artificial intelligence, automated planning systems offer the potential to enhance radiotherapy treatment delivery significantly. These systems can improve patient throughput and resource allocation by reducing planning time and increasing the efficiency of radiotherapy departments. Automated planning can improve plan quality and consistency, reducing variability and ensuring optimal treatment outcomes. Furthermore, the ability to enable rapid re-planning facilitates adaptive radiotherapy, allowing for adjustments to treatment plans in response to changes in tumor volume or patient anatomy. Finally, automated systems can explore a more expansive solution space, potentially discovering novel and innovative planning strategies that may improve treatment outcomes.

However, the development and implementation of automated planning systems pose challenges. These challenges include the creation of robust optimization algorithms, integrating with existing Treatment Planning Systems, and validating against current clinical standards.

2.3 State of the Art

2.3.1 Research

Automated rule implementation and reasoning An automated computer program with predefined rules and so called "if-then" [1] structures is a solution for implementing simple clinical guidelines. In this context, the treatment planning system directly interprets patient anatomy and dosimetric requirements, simulating the decision-making process traditionally employed in manual treatment planning [**?**]. By adhering to a structured, logical framework derived from human-defined protocols, automated reasoning in radiotherapy (ARIR) can significantly reduce the need for manual intervention, particularly for repetitive tasks.

Some modern TPS vendors have incorporated ARIR solutions, offering scripting capabilities that enable users to customize the planning process. For instance, the Varian Eclipse [**?**] system includes an application programming interface (API) that facilitates user-defined scripting functions.

[1] Also known as "expert" systems.

Knowledge-based radiotherapy planning Knowledge-based radiotherapy planning (KBRP) represents an objective methodology for incorporating patient-specific data and historical experience into the treatment planning process [**?**]. By automating the optimization of KBRP, it is anticipated that a viable alternative to the current human-centric treatment planning paradigm can be established. A prevalent KBRP approach involves leveraging a database of historical benchmark plans to learn patient-specific dosimetric parameters and generate new treatment plans. Automated KBRP tools effectively set optimization parameters based on the desired dose-volume histogram. Previous studies have reported notable dosimetric improvements in treatment plans generated by KBRP approaches compared to benchmark data, particularly regarding sparing organs at risk [**?**, **?**].

Conventional techniques Memorial Sloan Kettering Cancer Center developed advanced optimization tools, including hierarchical constrained optimization, convex approximations, and Lagrangian methods. These tools addressed the complexity and enhanced the speed, quality, and accessibility of standardized yet personalized care [**?**].

Multi Criteria Optimization In DVH-based inverse optimization used by most commercial TPS, a cost function must be defined to solve the minimization problem. This function combines data from all volumes of interest as a weighted sum of penalties from each DVH constraint. The weighting coefficients reflect tradeoffs between the target(s) and different OARs. However, this approach requires online re-optimization if dosimetric preferences change during plan evaluation, making it time-consuming to find the optimal balance. Multi-criteria optimization (MCO) was introduced to address this, enabling the simultaneous generation of multiple "anchor" plans. Each anchor plan optimizes one OAR's DVH criterion for maximal sparing without compromising tumor target dosimetry [**?**, **?**]. These plans form a hypersurface in the N-dimension space, where N is the number of independent OAR dosimetric constraints. Referred to as the Pareto surface, this hypersurface contains the optimal plans following different dosimetric criteria.

Wish list MCO can also be applied in an a priori approach, where dosimetric preferences are defined before inverse optimization. In this method, a fully automated process generates a single optimal plan without the need for human interaction [**?**]. Breedveld et al. introduced this approach in their work on IMRT Cycle (iCycle) [**?**], where the optimal plan is guided by a predefined "wish list" of dosimetric criteria, each assigned a specific priority.

Pareto surface narrowing In theory, MCO requires generating numerous plans to construct the Pareto surface, which can be time-intensive, even with automation. However, Craft and Bortfeld analyzed head and neck IMRT plans and demonstrated that only a few plans are needed to form a Pareto database [**?**]. Using objective correlation matrices and principal component analysis (PCA) of beamlet solutions, Craft and Bortfeld showed that if N independent dosimetric criteria are defined, $N + 1$ plans are sufficient to construct a feasible Pareto surface. This insight facilitated the practical clinical use of MCO, first implemented in the RayStation TPS [**?**].

Pareto surface exploration Previous research has explored Pareto optimal tradeoffs in various domains. Gebru et al., for instance, investigated methods for evaluating Pareto optimality [**?**]. Similarly, Cilla et al. conducted a comprehensive analysis of Pareto fronts [**?**]. These studies provide valuable insights into the principles and techniques associated with Pareto optimization. Craft et al. proposed a method for generating multiple Pareto optimal dose distributions, allowing clinicians to make informed decisions based on their specific preferences and clinical contexts [**?**]

2.3.2 Commercial

Pinnacle AutoPlanning AutoPlanning in the Pinnacle TPS is an automated radiotherapy planning tool that optimizes treatment plans based on user-defined prescriptions and organ-at-risk constraints. AutoPlanning was initially used for prostate cancer and expanded to more complex treatments. Determining best practices for the optimal use of AP remains a challenge [**?**]. Most patients are treated using VMAT techniques, with most treatment plans being generated solely by AP without requiring additional manual adjustments [**?**]. However, the dose calculation engine is recognized as an area with potential for improvement.

Eclipse Rapidplan RapidPlan (Varian) is a knowledge-based planning (KBP) tool that predicts dose-volume histograms (DVHs) based on patient anatomy and treatment parameters, using principal component analysis to model correlations between dosimetric and geometric features. RapidPlan has been used at Institut du Cancer Avignon-Provence, with 83% of plans meeting clinical criteria in a single optimization [**?**]. However, fine-tuning objectives for optimal trade-offs can be time-consuming, and the model's performance is limited by the variability of the training database.

RayStation auto-planning RayStation TPS Auto-Panning demonstrated similar or better target coverage, conformity, and organ-at-risk sparing than manual planning, with a significant reduction in manual operation time but increased computer processing time [**?**]. The planning process depends on the use of IronPython-based automated scripts. However, the qualifications required to develop and manage these scripts and the responsibility in case of failure still need to be clarified.

mCycle The autoplanning solution mCycle, developed by Elekta, utilizes an a priori multi-criteria optimization algorithm. Leon Berard Cancer Center (Lyon, France) tested the solution and found all plans were considered clinically acceptable, with an optimization time between 30 and 60 minutes [**?**]. However, obtaining a robust wish list is complex and center-dependent. There needs to be an extensive discussion with the clinical team to assign the plan constraints and priority for each OAR objective.

2.4 Unsolved problems

Numerous approaches have been investigated to automate the radiotherapy treatment planning process. Despite these efforts, a consensus on the optimal method has yet to be established, and few automated solutions have been adopted in clinics. The challenges associated with automating radiotherapy treatment planning remain a significant area of inquiry within the field. This thesis addresses this critical issue by proposing advancements in key areas that may contribute to developing a fully automated treatment planning system.

2.5 Thesis overview

This section provides a comprehensive summary of the forthcoming chapters of this thesis.

2.5.1 Fluence Map Optimization

Chapter 3 is dedicated to developing computational methods for FMO. The chapter begins by assessing the discretization strategies. Naive approaches for optimization are explored, stepping up to a formalization of the classical FMO problem. A significant focus is placed on incorporating medical constraints and the corresponding importance factors associated with each constraint, which are critical in ensuring clinically viable treatment plans. The performance of various optimization algorithms is evaluated and compared, providing insights into their relative efficiencies in solving the FMO problem. This primary work was published in the form of an ArXiV article.

2.5.2 Semi-automation

Using graph-based analysis

Chapter 4 explores the interrelationships between radiotherapy treatment plans by defining a distance metric. This distance is then used to cluster plans into meaningful groups. The clustering forms a basis for developing a semi-automated framework for treatment plan optimization. Leveraging graph-based methodologies, this approach reduces the need for manual intervention in the planning process while ensuring the generation of high-quality plans. The potential of this semi-automated framework to streamline clinical workflows was presented at the 2024 European Society for Radiotherapy and Oncology (ESTRO) conference.

2.5.3 Full-automation

With reinforcement learning and conventional treatment optimization techniques

Chapter 5 addresses the limitations of classical optimization techniques in fully automating the treatment planning process. This chapter introduces a framework that integrates reinforcement learning with conventional optimization. The reinforcement learning agent is driven by clinical expertise and can be specialized to center-specific guidelines. The techniques found have been published through a peer-reviewed journal article, a presentation at the Artificial Intelligence in Medicine (AIME) 2024 conference, and a poster presentation at the American Society for Radiation Oncology (ASTRO) 2024 meeting.

2.5.4 Hybrid-automation

Via target DVHs deep dose and dose mimicking technique

The final research chapter, Chapter 6, presents a hybrid approach to automating treatment planning. This approach combines deep learning for dose prediction with target DVHs and plan-mimicking strategies. This methodology bridges the gap between fully automated AI-driven techniques and traditional planning methods, offering a more adaptable and clinically feasible solution. The hybrid model provides a mechanism for mimicking high-quality plans from experienced planners. This research has been presented at the French Society of Medical Physics (SFPM) and the French Society for Radiation Oncology (SFRO) 2024 meetings.

Dosimetry Optimization

Abstract

Biological tissues are sensible to radiations in a non-linear manner [**?**], and slight variations in dose can have significant biological effects. Organs have differing sensibilities to radiation, which increases further the difficulty in formulating the goals to achieve when designing a radiation dose. Some organs can tolerate high cumulative doses if the radiation is well distributed. In contrast, others may withstand high doses at localized points ("hot spots") but cannot handle large doses overall. To address these differences, clinicians impose dose-volume histogram constraints in addition to the prescribed dose. Although the ideal objective is to minimize or eliminate radiation exposure to organs, achieving $0\,\mathrm{Gy}$ is impossible. The necessity of finding compromises drives the need for advanced optimization techniques to generate fluence maps that best satisfy the medical constraints. Therefore, various techniques can be used to calculate fluence maps (i.e., performing the critical fluence map optimization step). In this chapter, we explore some fluence map optimization techniques.

3.1 Discretization

The optimization process starts with transforming the continuous nature of both the radiation field and the human body into discrete elements. This transformation enables calculations with modern computers.

3.1.1 Fluence Map Discretization: Bixels

Fluence maps are broken down into discrete elements called "bixels" (**be**am **el**ements). Bixels represent small and independent beams of radiation (see a visualization figure 3.1).

The width of each bixel is constrained by the width of the multi-leaf collimator leaves. Modern multi-leaf collimator systems typically have a leaf width of 0.5 cm.

The height of a bixel can be selected arbitrarily, as the leaf can move continuously. Nevertheless, square bixels (akin to image pixels) are commonly used and will be employed throughout this manuscript.

It is essential to know that since negative energy rays are physically infeasible, we need to ensure that each bixel value is non-negative[1]. Bixels whose beams do not affect the planning target volume are typically excluded from calculations to improve computational efficiency. Activating these bixels could only degrade dose quality by increasing the dose to organs at risk without benefiting the dose distribution within the planning target volume.

3.1.2 Human Body Discretization: Voxels

The human body of the patient is also divided into discrete elements, as it is a three-dimensional object; the elements are "voxels" (**vo**lume **el**ements). Each voxel represents a small portion of tissue within the patient's body, and will determine the granularity of the dose computed.

The maximum resolution of the voxel grid is defined by the planning image, which is typically a CT scan. It is common practice to resample the planning image to reduce computational demands. In this manuscript, where new techniques are explored, we have opted to resample the voxel grid to a resolution of 5 mm, ensuring a balance between computational efficiency and accuracy.

Additionally, to further optimize the computational process, only voxels corresponding to the planning target volume (PTV) and organs at risk (OARs) are retained for calculations. This selective approach reduces unnecessary computation.

[1] In practice, to ensure positive bixel values, we use the absolute value element-wise.

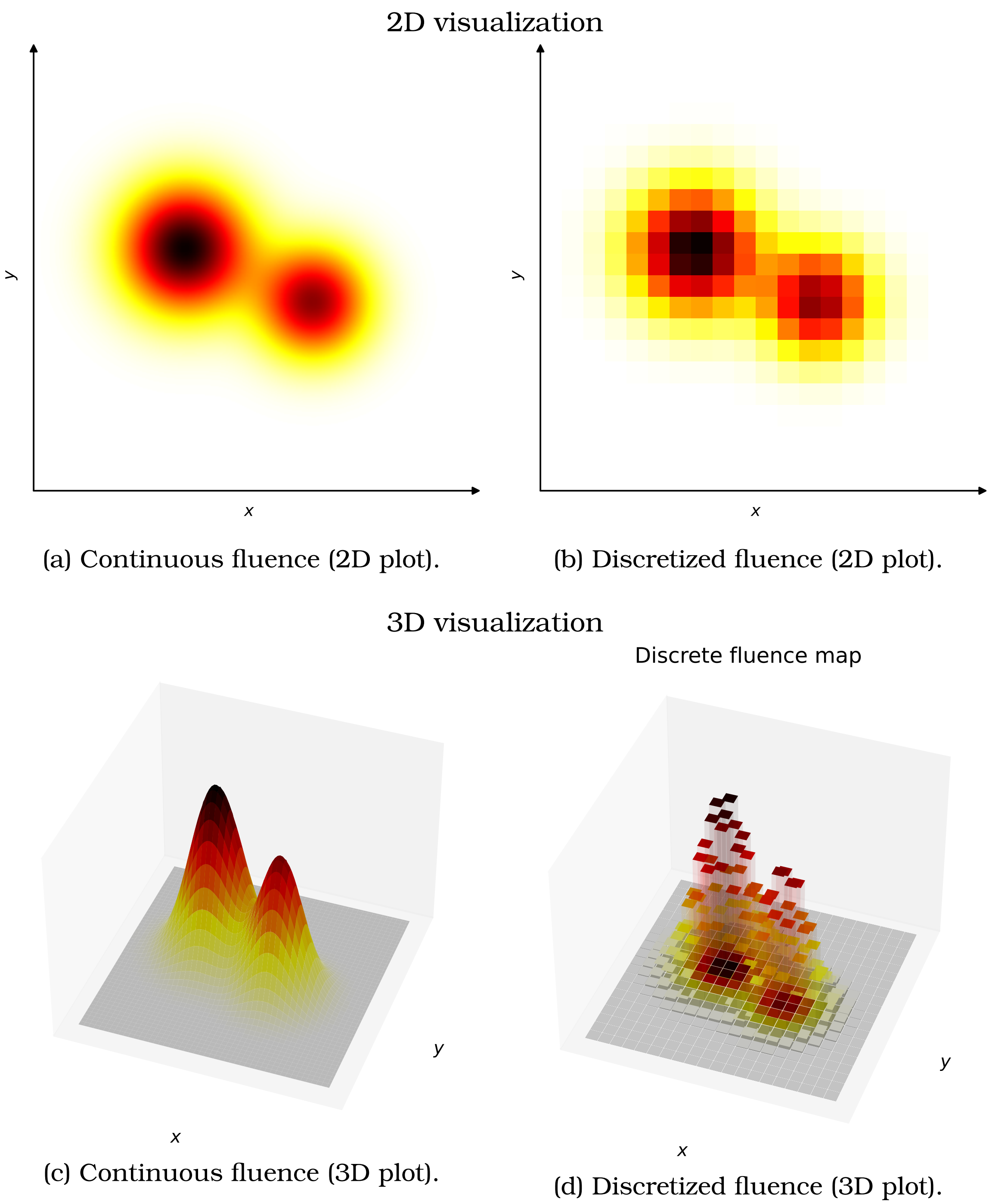

(a) Continuous fluence (2D plot).

(b) Discretized fluence (2D plot).

(c) Continuous fluence (3D plot).

(d) Discretized fluence (3D plot).

Figure 3.1: Example of a fluence discretized to 20×20 bixels.

3.1.3 Dose-Influence Matrix

The Dose-Influence Matrix (or DI-Matrix) links the discretized fluence map (the bixels values) and the discretized dose distribution within the patient (the dose on each voxel). This matrix defines how the radiation from each individual bixel influences the dose delivered to every voxel in the patient's body.

We start by converting the 2D fluence map, composed of individual bixel values, into a column vector $\mathbf{b}$. Similarly, we represent dose distribution in the patient's 3D space as a vector d, where each entry corresponds to the dose in a specific voxel. The DI-Matrix $\mathbf{L}$ governs the relationship between these vectors b and d via the matrix-vector multiplication $\mathrm{d} = \mathbf{L}\mathrm{b}$ [2]. This mathematical operation computes the total dose at each voxel by summing the contributions from all active bixels (here, we assume that the effect of bixels is linear).

The DI-Matrix is constructed by simulating the radiation delivered by each individual bixel. For each bixel, the jaws of the multi-leaf collimator are virtually opened to allow only that specific beamlet to go through. A radiation transport model calculates the dose deposited in each voxel, considering the beam's spread and attenuation as it travels through the body. The resulting 3D dose deposition fills one column of the matrix $\mathbf{L}$, corresponding to that bixel's influence on all voxels. Repeating this process for each bixel generates the entire DI-Matrix.

The accuracy of the dose calculation depends on the precision of the DI-Matrix. Simple models like pencil beam approximations, which assume a linear trajectory with minimal scattering, are considered too coarse. In contrast, more advanced simulations, such as Monte Carlo methods, provide a detailed and accurate dose calculation, although at a higher computational cost. In this manuscript, we employ collapsed cone convolution techniques (via TheraPanacea dose engine), which balance efficiency and accuracy.

3.2 Naive Optimization Method

A natural starting point in dose optimization is to attempt to directly achieve the delivery of a uniform dose, equal to the prescription, on all voxels within the PTV, and no dose elsewhere. We can attempt to find the bixels values delivering this dose by solving a least squares problem. We attempt to find the fluence map b that minimizes the difference between the actual dose d and the target dose $\mathrm{d}_{\text{target}}$, which is set to the prescribed dose within the PTV.

Formally, the optimization problem can be stated as:

$$\min_{\mathbf{b}} \ \|\mathbf{d}_{\text{target}} - \mathbf{L}\mathbf{b}\|^2, \quad \mathbf{b} \geq 0$$

[2]In practice, we compute $\mathbf{d} = \mathbf{L}|\mathbf{b}|$, where $|\mathbf{b}|$ is absolute value of $\mathbf{b}$ element-wise to ensure positive bixel values.

where $\mathbf{d}_{\text{target}}$ is the target dose vector, defined as follows for a prescription of pGy:

$$\mathbf{d}_{\text{target}} = p \cdot \mathbb{1}_{\text{PTV}}$$

Here, $\mathbb{1}_{\text{PTV}}$ is the indicator vector for PTV that is equal to 1 for voxels within the PTV and 0 elsewhere.

To solve this problem, we perform a least squares minimization to find the optimal fluence map $\mathbf{b}$, where the matrix-vector multiplication $\mathbf{Lb}$ yields the dose distribution $\mathbf{d}$ across the entire patient volume.

However, this method is often inadequate in practice, as it attempts to solve the system based solely on the prescribed dose within the PTV, while neglecting any constraints on doses to the organs at risk. Since no constraints are imposed on the OAR doses, this naive optimization can result in high doses to critical structures, leading to unacceptable treatment plans. As a result, more sophisticated optimization methods that incorporate dose constraints on OARs and account for dose-volume constraints are necessary to achieve clinically viable treatment plans.

3.3 Constraints and Importance Factors

In order to obtain clinically acceptable doses, we need to incorporate the clinical aims in the optimization.

3.3.1 Constraints Formulation

Different organs exhibit varying sensitivities to radiation, which influence their dose tolerance limits [**?**] [**?**]. Normal tissues are categorized as serial, parallel, or mixed, based on the functional organization of their sub-units. This classification determines the appropriate absorbed dose limits for normal tissues.

Serial organs (figure 3.2a), such as the spinal cord or esophagus, are characterized by a functional dependence on the integrity of every sub-unit. Damage to even a tiny region in these tissues can result in the loss of the organ's overall function. In contrast, parallel organs (figure 3.2b), such as the lung or liver, possess a reserve capacity where damage to a portion of the tissue does not necessarily impair overall function, as long as a critical volume remains intact.

We define two DVH value measures, $V_{X\,\text{Gy}}$ and $D_{X\%}$, for a structure S. For a given dose $d : \mathbb{R}^3 \to \mathbb{R}^+$, $V_{X\,\text{Gy}}$ is defined as the volume of the three dimensional structure $S \subseteq \mathbb{R}^3$ that receives a dose equal to or higher than X Gy, that is:

$$V_{X\,\text{Gy}} = \frac{\text{Vol}\left(\left\{p \in S \subset \mathbb{R}^3 \mid d(p) \geq X\right\}\right)}{\text{Vol}\,(S)}.$$

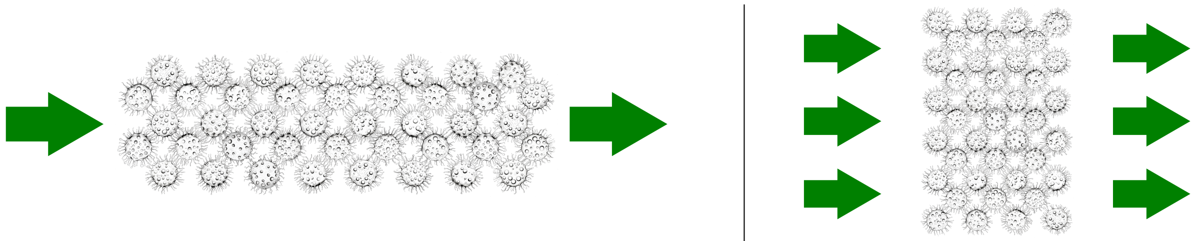

(a) Organ functioning in a serial-like way.

(b) Organ functioning in a parallel-like way.

Figure 3.2: Organs functioning types.

This formula can be approximated using the discretized dose on voxels $\mathbf{d}$:

$$V_{X\,\text{Gy}} \approx \frac{\#\{v \in S \mid \mathbf{d}_v \geq X\}}{\#\,\{v \in S\}}$$

with $v \in S$ voxels of the structure S, $\mathbf{d}_v$ the dose of $\mathbf{d}$ associated with voxel v, and $\#$ refers to voxel count.

Similarly, we define $D_{X\,\%}$ as the minimal dose (in Gy) delivered to the $X\,\%$ most irradiated region of the structure, that is:

$$D_{X\,\%} = \min\,\{d(p) \mid p \in S_{X\,\%}\}$$

where $S_{X\,\%} \subseteq S$ is the $X\,\%$ most irradiated region of S. Again, it can be approximated using the discretized dose on voxels $\mathbf{d}$:

$$D_{X\,\%} \approx \min\,\{\mathbf{d}_v \mid v \in S_{X\,\%}\}$$

where $v \in S_{X\,\%}$ are the $X\,\%$ most irradiated voxels of S.

For parallel-like structures, dose–volume reporting specifying $V_{D\,\text{Gy}}$ is commonly used, with $D\,$Gy adapted to the specific organ. For instance, **[?]** demonstrated a correlation between the incidence and severity of lung pneumonitis and $V_{20\,\text{Gy}}$, the volume of the lung receiving more than $20\,$Gy. In parallel-like structures, the median absorbed dose ($D_{50\,\%}$) provides a valuable measure of the total dose delivered to the organ at risk.

For serial-like organs, it is recommended to report $D_{2\,\%}$ as the maximum absorbed dose, as $D_{0\,\%}$ is subject to noise.

Finally, for organs with a mixed parallel-serial structure, it is advised to report $D_{50\,\%}$, $D_{2\,\%}$, and $V_{D\,\text{Gy}}$, with $D\,$Gy selected based on the threshold beyond which there is a significant risk of serious complications.

3.3.2 Optimization Problem

After the doctors have formulated maximal dose constraints for each OARs, and PTV coverage constraints $\mathcal{C}$, we can formulate the mathematical optimization problem.

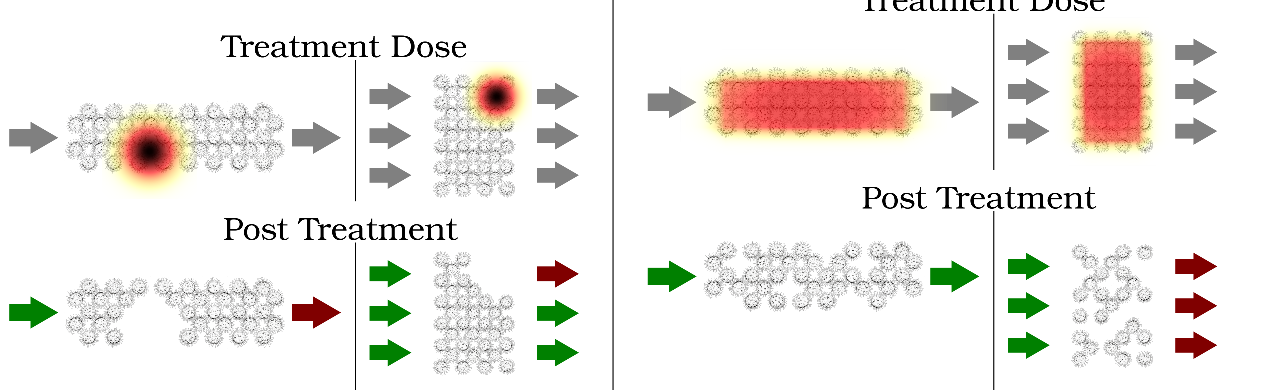

(a) Irradiation of organs at risk with one heat point.

(a1) Serial organ dies.

(a2) Parallel organ survives.

(b) Irradiation of organs at risk with spread heat dose.

(b1) Serial organ survives.

(b2) Parallel organ dies.

Figure 3.3: Irradiation type survival of organs serial-like and parallel-like.

Constraints $c \in \mathcal{C}$ are formulated as $c = (S, D, V, \pm)$ where D is in Grey, V is a %, and $\pm$ means the constraint is maximal/minimal.
E.g.: $c_{PTV+} = (\text{PTV},\ 76\,Gy,\ 95\,\%,\ +)$ means that for the PTV structure, we need $D_{95\%} \geq 76\,\text{Gy}$ (or, equivalently, $V_{76\text{Gy}} \geq 95\%$); this is a very typical constraint [**?**]. This constraint example is illustrated in figure 3.4c and 3.4d.
E.g. (bis): $c_{\text{organ}} = (\text{organ},\ 25\,Gy,\ 20\,\%,\ -)$ means that for the 'organ' structure, we need $D_{20\%} \leq 25\,\text{Gy}$ (or, equivalently, $V_{25\text{Gy}} \leq 25\%$). This constraint example is illustrated in figure 3.4a and 3.4b.

We only calculate a voxel-discretized version $\mathbf{d}$ of the dose $d : \mathbb{R}^3 \to \mathbb{R}^+$, using a bixel-discretized version $\mathbf{b}$ of the fluence maps $f^\theta : \mathbb{R}^2 \to \mathbb{R}^+$ for each selected angle θ. Hence, we formulate the optimization problem on the discretized information.

Ideal Case In the ideal case, it is possible to meet all constraints, and we try to minimize further the dose $\mathbf{d}$ on the OARs. Mathematically, we find the values for $\mathbf{b}$ giving dose $\mathbf{d} = \mathbf{L}\mathbf{d}$ such that all DVH constraints $\mathcal{C}$ are satisfied, and $\sum_{v \in \text{OARs}} \mathbf{d}_v^2$ is minimum (where $\mathbf{d}_v$ is the dose on voxel v, and $v \in$ OARs are the voxels v belonging to an OAR):

$$\min_{\mathbf{b}} \sum_{v \in \text{OARs}} \mathbf{d}_v^2 \quad \text{with } \mathbf{d} = \mathbf{L}\mathbf{b},\ \mathbf{b} \geq 0 \text{ and such that } \forall c \in \mathcal{C}, c \text{ is satisfied.}$$

Practical Case In practice, constraints formulated by the doctors are too hard to satisfy. Hence, we create one objective function f_c for each constraint $c \in \mathcal{C}$, which decrease as we

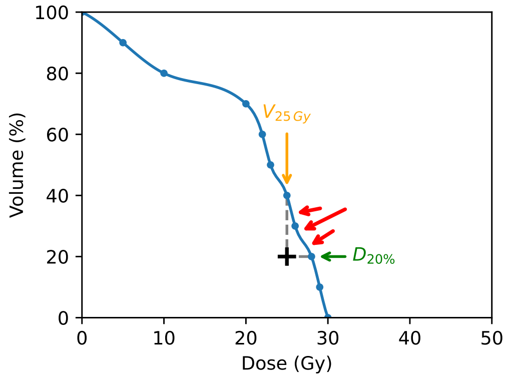

(a) Maximal dose constraint not met.

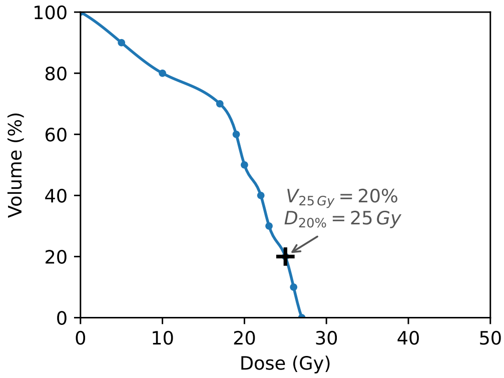

(b) Maximal dose constraint met.

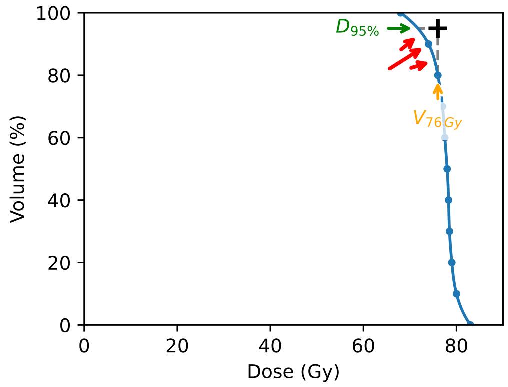

(c) Minimal dose constraint unmet.

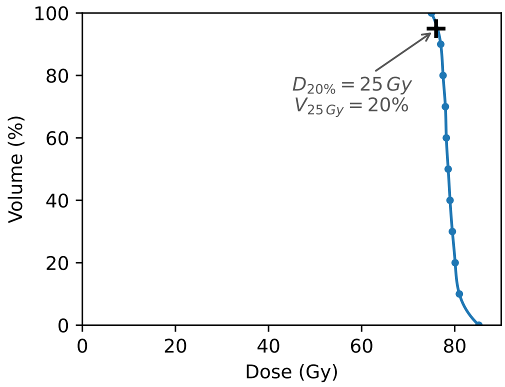

(d) Minimal dose constraint met.

Figures 3.4a, 3.4b: Typical DVH of an OAR, with visualization of the maximal dose constraint $D_{20\%} \leq 25\,\mathrm{Gy}$ (or $V_{25\mathrm{Gy}} \leq 20\,\%$). Figure 3.4c, 3.4d: Typical DVH of a PTV, with visualization of the minimal dose constraint $D_{95\%} \geq 76\,\mathrm{Gy}$ (or $V_{76\mathrm{Gy}} \geq 95\,\%$). Note that dose-volume objectives then turn to points on dose-volume histograms. The relevant DVH curve must stay above (in the case of a minimal dose constraint), or under (in the case of a maximal dose constraint) this point to pass the constraint.

get closer to satisfying the constraint. The optimization problem becomes:

$$\min_{\mathbf{b}} \sum_{c\in\mathcal{C}} w_c f_c(\mathbf{d}) \quad \text{with } \mathbf{d} = \mathbf{L}\mathbf{b},\ \mathbf{b} \geq 0$$

with w_c importance factor of constraint c.

Penalization functions Given a constraint $c = (S, D\,\text{Gy}, V\,\%, \pm)$, multiple approaches can be considered for defining an objective function f_c. Here, we explore three commonly used methods (also visually explained in figure 3.5):

1. **Penalizing the lower** $100 - V\,\%$ **dose voxels**: This method penalizes a fixed number of voxels but tends to be noisy since the lower $V\%$ voxels can fluctuate with each optimization iteration.
2. **Penalizing voxels with dose** $> D\,Gy$: This approach yields a convex objective function.
3. **Penalizing the lower** $100 - V\,\%$ **dose voxels with dose** $> D\,Gy$: This method is the most advanced method; Note that once the constraint is satisfied, no voxel is penalized. However, for the same reason as the first approach, this penalization remains prone to noise.

Turning off penalization is possible once a constraint is met (this is useful for the first two methods presented above). In our implementation, we chose not to do so, so when a constraint is on the edge of being met, the penalization does not turn on and off every other optimization iteration.

Once the set of penalized voxels is selected, the penalization power p must be determined, with typical choices being $p = 1$ or $p = 2$. We opt for penalizing voxels with a dose greater than D Gy and set $p = 2$. This choice makes the objective function convex a weighted sum of convex functions. Desirable properties, such as the existence of a unique global minimum once the values of w_c are fixed, follow from the convexity of the objective function.

Finally, the mathematical formulation of the objective function associated with the constraint $c = (S, D, V, \pm)$ is:

$$f_c(\mathbf{d}) = \sum_{v\in S} (\mathbf{d}_v - D)_+^2 \,.$$

The global minimization problem becomes

$$C(w, \mathbf{d}) \quad \text{with } \mathbf{d} = \mathbf{L}\mathbf{b},\ \mathbf{b} \geq 0$$

where $w = \{w_c \mid c \in \mathcal{C}\}$, the set weights or importance factors of each constraint, are to be determined, and

$$C(w, \mathbf{d}) = \min_{\mathbf{b}} \sum_{c\in\mathcal{C}} w_c \sum_{v\in S} (\mathbf{d}_v - D)_+^2$$

is the total cost function. Note that the problem changes as w evolves. It is by adjusting w that dosimetrists may guide the optimizer towards a clinically acceptable plan.

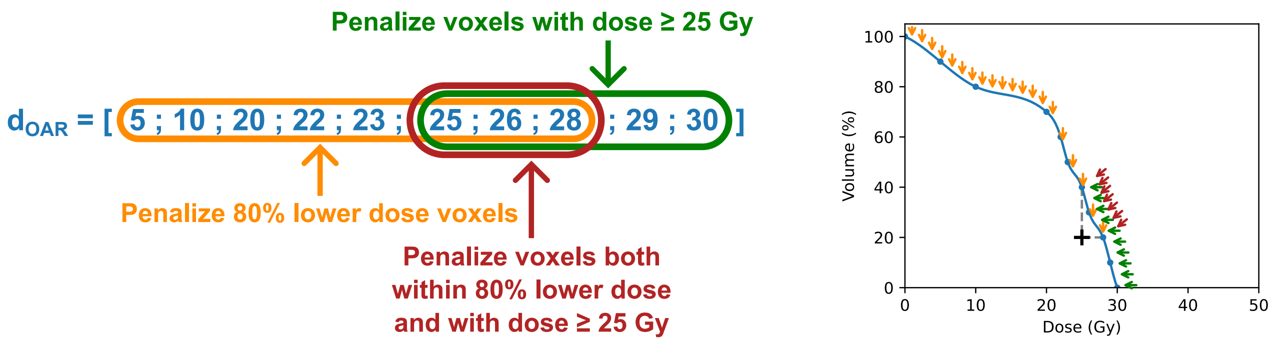

(a) Penalizations of constraint $D_{20\%} < 25\,\text{Gy}$ on a structure of 10 voxels.

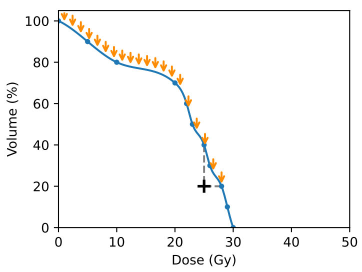

(b) Penalizing the lower $20\,\%$ dose voxels.

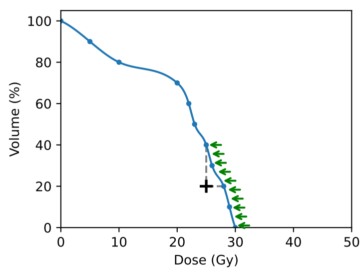

(c) Penalizing voxels with dose greater than $25\,\text{Gy}$.

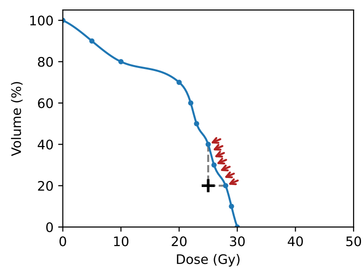

(d) Penalizing the lower $20\,\%$ dose voxels with dose greater than $25\,\text{Gy}$.

Figure 3.5: Typical penalization of a dose on an OAR according to the maximal dose constraint $D_{20\,\%} \leq 25\,\text{Gy}$.

Bixel regularization For optimal leaf sequencing, it is preferable to have smooth bixel values, meaning that adjacent bixels should have minimal variation in their values. A regularization term was incorporated to achieve this, penalizing discrepancies in bixel values relative to their neighboring bixels using a squared penalty function.

3.3.3 Balancing the Importance Factors

The importance factors w_c play a crucial role in the optimization process. These weights allow dosimetrists to prioritize certain clinical constraints over others. Properly balancing these factors ensures that the most critical aspects of the treatment plan are emphasized while still striving to meet all constraints.

The constraints associated with the PTV, ensuring the destruction of the tumor, conflict with the protection of the OARs. Hence, the optimization process becomes a trade-off between satisfying different constraints. For example, increasing the dose of the PTV will inadvertently increase the dose of nearby OARs. Carefully tuning of the importance factors ensures that the optimization algorithm directs the fluence maps towards a solution that balances the therapeutic benefits with the risk of complications.

Due to the unique geometry of each patient, an optimal dose plan cannot be applied universally. The optimization must be recalculated for every patient. Dosimetrists customize the dose to meet the specific needs of each individual patient by taking into account clinical priorities, spatial relationships, and physician expertise. This process is time consuming, and remains manual; this manuscript tackles the problem of treatment planning.

The contouring task used to be a manual operation but is now done automatically, thanks to the progress of artificial intelligence on segmentation tasks [**?**] [**?**]. After the emergence of AI for contouring, this manuscript tackles the problem of automatic treatment planning.

3.4 Dose Mimicking

Dose mimicking is a technique used to reproduce a dose distribution as closely as possible. This task is typically needed when a patient changes machine: the leaves might not have the exact same shape, and their movements (the treatment plan) must be recalculated. However, the optimal 3D dose spread remains the same, and one only needs to replicate it (or mimic it) with another machine.

Hence, dose mimicking involves the optimization of a new treatment plan to match the dose profile of an existing plan, which is typically derived from either a prior treatment or a reference plan considered clinically acceptable. This differ from the naive approach in section 3.2: the dose distribution that we try to replicate is not manually set. The target dose was achieved before either on the same machine, or on a similar MLC. Hence, the task of mimicking it should be "easier".

Formally, the optimization problem can be stated the same way as in section 3.2:

$$\min_{\mathbf{b}} \ \|\mathbf{d}_{\text{target}} - \mathbf{L}\mathbf{b}\|^2$$

with $\mathbf{d}_{\text{target}}$ the previously target dose, instead of the manually defined one.

3.5 Optimization Algorithm Review for Dosimetry

The selection of an optimization algorithm is critical. Different algorithms may converge to various local minima when dealing with non-convex objective functions, potentially leading to significant outcome variations. To mitigate this issue, we have designed the objective function to be convex, ensuring all optimization methods converge to the same global minimum. In this study, we benchmark the computational complexity and convergence rates of various algorithms. These findings are intended to provide valuable insights for the development of TPS.

3.5.1 Data

We focused on evaluating the various open-source optimizers. We used the widely recognized TG-119 [**?**] cases as a benchmark for evaluating radiation therapy plan optimization. The TG-119 dataset provides specific dose goals, which we incorporated into our proposed cost function. The TG-119 multiple PTVs is a theoretical case unlikely to happen in real life. However, the other cases represent a comprehensive set of what dosimetrists could encounter daily.

We also used one typical case of prostate cancer from ICM. For this case, doctors had provided specific dose goals that we again incorporated into our proposed cost function.

3.5.2 Open-source Optimizers

We tried to have a comprehensive set of available open-source optimizers.

(Stochastic) Gradient Descent Is an optimization algorithm that iteratively updates the model parameters in the direction of the negative gradient of the objective function. In our case, it is not stochastic since it calculates the gradient using the current solution[3] [**?**].

Conjugate Gradient Is an iterative optimization algorithm commonly used to solve systems of linear equations or quadratic optimization problems. It iteratively computes conjugate directions and updates the solution along them, aiming to minimize the objective function [**?**]. Conjugate Gradient is often applied in scenarios where the Hessian matrix is unavailable or computationally expensive.

[3] Our objective function has all its inputs as parameters, so there is no notion of stochasticity.

Newton Newton's method is an iterative optimization algorithm that uses the second-order derivative (Hessian matrix) to find the minimum of a function. It updates the current estimate by considering both the first-order derivative (gradient) and the second-order derivative [**?**].

SLSQP (Sequential Least Squares Programming) is a sequential quadratic programming algorithm for constrained optimization. It iteratively solves a sequence of quadratic programming subproblems to find the optimal solution subject to constraints [**?**].

RMSprop (Root Mean Square Propagation) is an optimization algorithm that addresses the problem of diminishing learning rates in traditional gradient descent methods. It divides the learning rate by the root mean square of the past gradients, which helps to stabilize and speed up convergence [**?**].

BFGS-based

Pure BFGS (Broyden-Fletcher-Goldfarb-Shanno) is a quasi-Newton method that approximates the Hessian matrix using updates based on gradient information. It performs a line search to determine the step size that minimizes the objective function along the search direction [**?**].

L-BFGS (Limited-memory BFGS) is a variation of BFGS that uses a limited-memory approach to approximate the Hessian matrix. It stores a limited number of past gradient and parameter values to compute an approximate inverse Hessian matrix efficiently [**?**].

Adam-based

Pure Adam (Adaptive Moment Estimation) is an optimization algorithm combining ideas from adaptive learning rates and momentum methods. It computes adaptive learning rates for each parameter based on estimates of the first and second moments of the gradients [**?**].

RAdam (Rectified Adam) is a variant of the Adam optimizer that introduces a rectification term to stabilize the adaptive learning rate. It aims to address some convergence issues that may occur in Adam by dynamically adjusting the variance of the adaptive learning rate [**?**].

NAdam (Nesterov Adam) combines the Nesterov accelerated gradient method with the Adam optimizer. It incorporates Nesterov momentum into the Adam update rule to improve convergence and provide better generalization [**?**].

AdamDelta Is another variant of the Adam optimizer that replaces the second moment estimates (variance) with a delta parameter. It eliminates the need for storing and updating the moving average of the squared gradients, which can be beneficial in memory-constrained settings [**?**].

Adamax Is an extension of the Adam optimizer that uses the gradients' infinity norm (max norm) instead of the L2 norm. It is designed to handle sparse gradients more effectively and can be particularly useful in deep learning models [**?**].

Rprop (Resilient Backpropagation) is an optimization algorithm specifically designed for neural networks. It adaptively updates the weights based on the gradient sign, adjusting the step size. Rprop performs weight updates independently for each weight parameter [**?**].

Other optimizers variations In addition, we tested AdamW, Adagrad, and ASGD. However, AdamW and Adagrad behaved similarly to Adam, and ASGD behaved similarly to SGD. For readability purposes, we did not include them in the results plots.

3.5.3 Results

Newton's method Based on the iterations-wise graph analysis, Newton's method performs best, consistently achieving a stable converged state within ten steps across all four examined cases. However, Newton's method steps are computationally expensive since it uses a second-order derivative (the Hessian) that is difficult to compute.

It is widely recognized that Newton's method excels in optimizing convex functions [**?**]. Our objective function is convex by construction; hence, this optimization algorithm is particularly effective.

LBFGS vs BFGS It would be expected that BFGS performs better than LBFGS in terms of iterations but not in terms of time (since LBFGS is a fast approximation of the BFGS technique). However, we observe that LBFGS outperforms BFGS even on the iterations-wise graph. This performance suggests that the limited memory approximation is biased towards suitable directions in these problems.

Best Algorithms Besides Newton's method, three algorithms have similar performances: Adam, Adamax, and LBFGS. Adam and Adamax appear to have more "wavy" cost curves, while LBFGS cost decreases more stably. These observations are valid both in terms of iteration and time.

TGG 119 Multiple PTVs (figure 3.6a) is the smallest problem, and the real ICM prostate case (figure 3.6d) is the largest problem (in terms of patient/organs/structure volume size); TGG 119 fake head and neck (figure 3.6b) and TGG 119 fake prostate (figure 3.6c) have similar

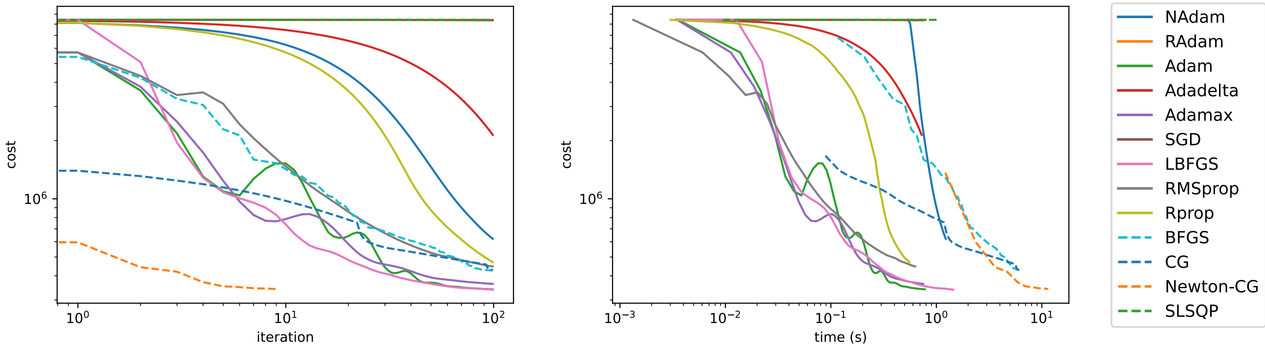

(a) TGG 119: Multiple PTVs.

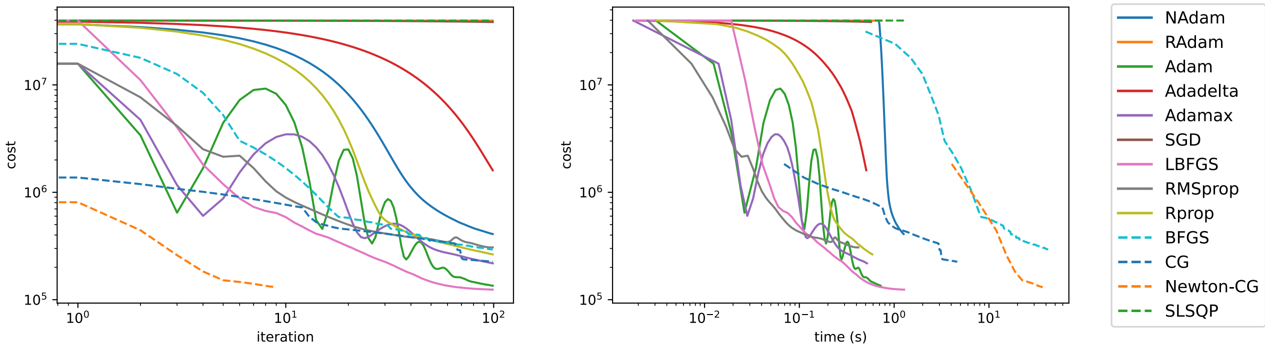

(b) TGG 119: Head and Neck.

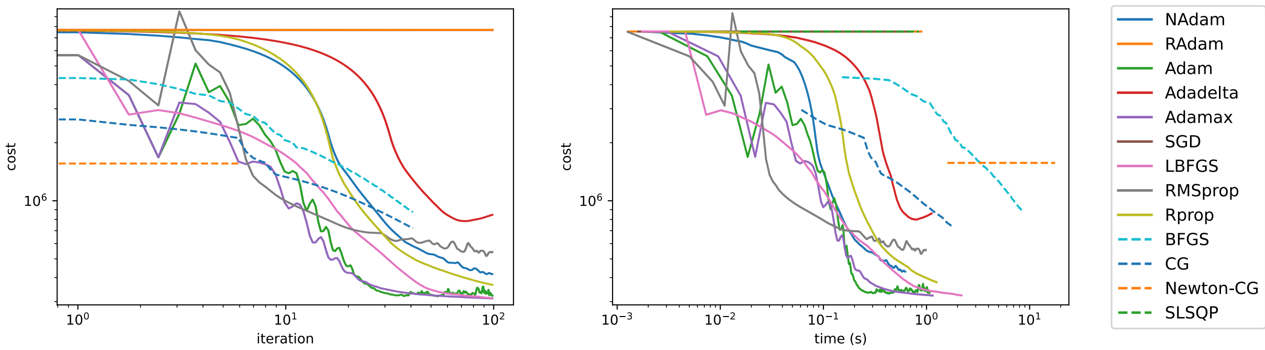

(c) TGG 119: Prostate.

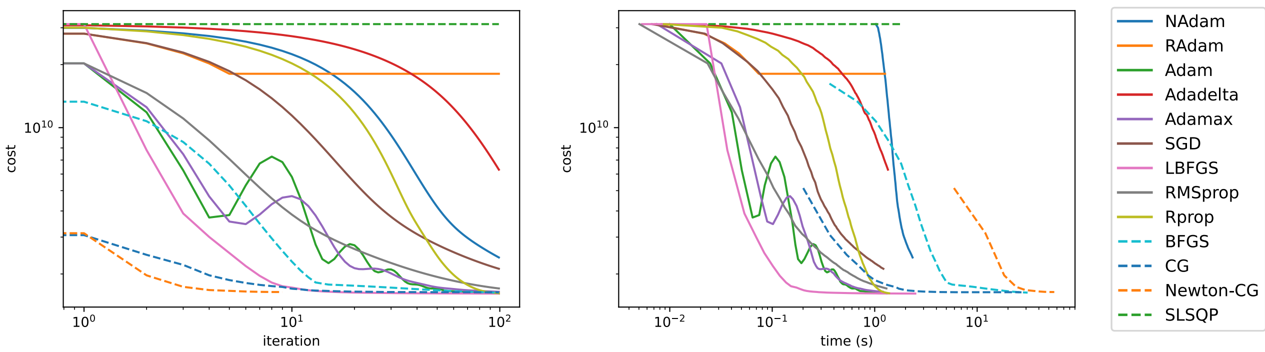

(d) Prostate from ICM (Institut régonal du Cancer de Montpellier).

Figure 3.6: Evolution of the objective function value ('cost') through optimization iterations and computation time for four typical dosimetry cases.

sizes. Notably, an observable trend indicates that as the problem size increases, LBFGS outperforms both Adamax and Adam optimization algorithms.

Therefore, we will use the LBFGS algorithm in the rest of this manuscript.

3.5.4 Discussion

In the future, if new techniques are developed making computing the Hessian much faster, we recommend using Newton's optimization algorithm. However, to our knowledge, computing the Hessian remains intrinsically long, not only in our implementation.

Hence, we recommend using the LBFGS algorithm for the problem of dose optimization in radiotherapy; it is the fastest to converge and converges steadily on the tested cases.

Doses Relationship

Abstract

Fluence Map Optimization (FMO) requires selecting importance factors for each clinical constraint, which reflect the relative priority of achieving specific dose goals. These importance factors significantly influence the resulting dose distribution, as varying their values can lead to diverse treatment outcomes. This chapter investigates the relationship between the chosen importance factors and the resulting dose distributions. We aim to understand how different configurations affect the trade-offs between conflicting clinical objectives. This analysis provides insight into optimizing importance factors to achieve the most clinically effective treatment plans.

4.1 Distance Between Doses

In this section, we aim to establish a robust metric for quantifying the distance between different dose distributions. Such a distance should provide a numerical comparison that reflects the clinical discrepancies between two dose distributions. By developing a distance measure that captures these nuances, we can better evaluate and compare treatment plans.

A non-trivial task Quantifying the difference between two dose distributions, particularly regarding clinical impact, is inherently challenging. This complexity arises because not all patient anatomy regions contribute equally to treatment outcomes. Dose variations in critical structures may significantly influence clinical effects, while similar variations in less critical areas may have negligible impact. Moreover, the potential for dose compensation (underdosing in one region counterbalancing overdosing in another) further complicates the development of a reliable metric for comparing dose distributions. This compensatory effect is only sometimes applicable, making establishing a standardized method for assessing dose distribution clinical differences challenging.

Dose Evaluation To assess the quality of a dose distribution, dosimetrists primarily focus on DVHs as the key information. While they also consider aspects of the three-dimensional (3D) dose distribution, such as inter-structure dose gradients and the presence, number, and location of hot spots, their primary attention is directed towards the analysis of DVHs, which provide a comprehensive overview of dose coverage and sparing of organs at risk.

4.1.1 Method

Naive Doses Comparison The most straightforward method for comparing two dose distributions, thus defining a distance metric, is to perform a voxel-by-voxel comparison of the dose values. However, this approach overlooks the inherent anatomical structure of the human body and the fact that not all voxels have the same clinical significance. Consequently, even if the voxel-wise distance between two dose distributions is considerable, their overall clinical effects may still be similar.

Pathological example We constructed a simplified example, as illustrated in Figure 4.1. This hypothetical scenario involves a phantom model consisting of a homogeneous water-equivalent material containing a cubic planning target volume (PTV) and a cubic organ-at-risk (OAR). Although this model lacks anatomical realism, it effectively highlights the limitations of using basic voxel-wise comparisons for dose evaluation. It emphasizes the need for more sophisticated techniques to capture clinically relevant differences in dose distributions accurately.

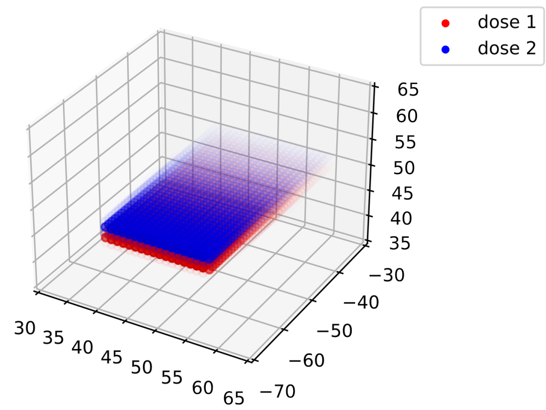

(a) 3D visualization of the two doses on the phantom body.

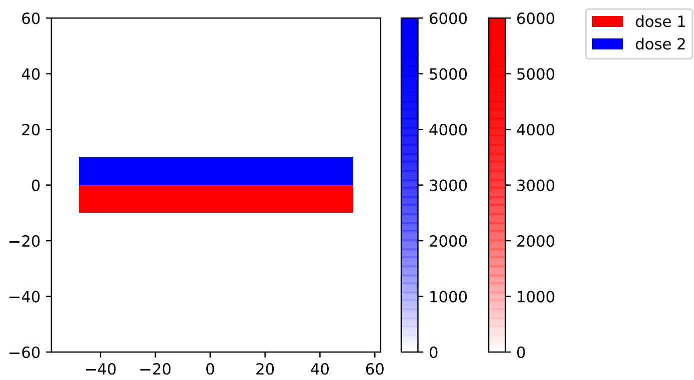

(b) 2D view of the bixels activation of the two doses.

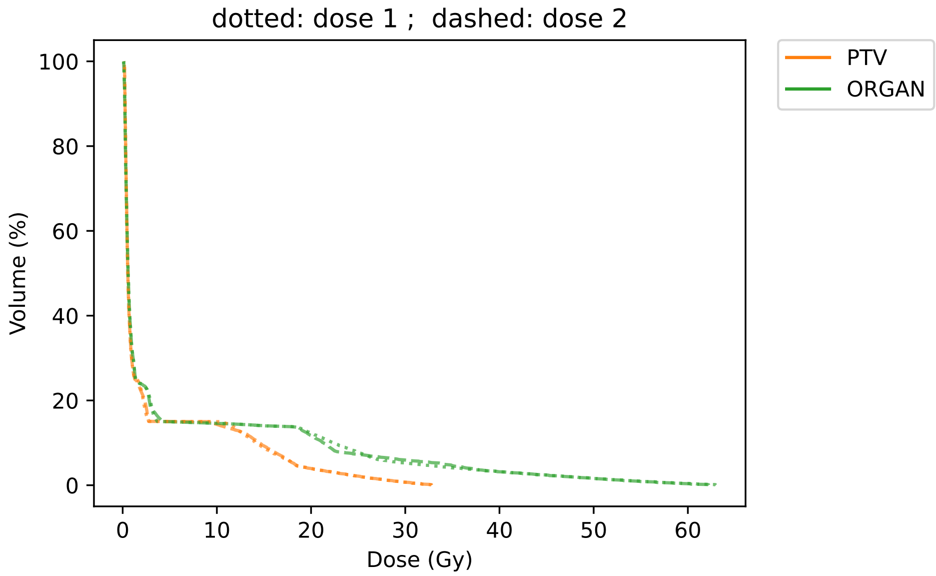

(c) Dose-Volume Histograms of the two doses on the phantom body.

Figure 4.1: Example of two doses that have the same clinical effect (measured from the DVHs), but very different voxel-wise dose values.

4.1.1.1 Doses Samples

We assessed the efficacy of our proposed method for comparing radiation doses using the TG-119 Prostate case, a well-established benchmark for evaluating radiation therapy plans [?]. The TG-119 dataset includes predefined dose objectives, which we utilized to formulate our cost function. We performed optimizations with different weight assignments applied to each constraint to generate varying treatment dose distributions for the same patient case under identical constraints.

4.1.1.2 Distances Between Doses

Comparing Doses Voxel-wise When two radiation dose distributions are closely aligned, the voxel-wise comparison is an effective measure, as it can be assumed that the global distribution is similar. This approach allows for a detailed comparison of local dose variations. Mathematically, given the voxel-wise dose $\mathbf{d}$, the distance between two dose distributions, $\mathbf{d}^1$ and $\mathbf{d}^2$, is defined as the norm of their difference: $\sum_{v\in\mathcal{V}}|\mathbf{d}_v^1 - \mathbf{d}_v^2|$, where v represents the voxels in the set of interest $\mathcal{V}$, and $\mathbf{d}_v^i$ is the dose value at voxel v for dose distribution $\mathbf{d}^i$ [1]. However, voxel-wise distance can become misleading if two regions of equal volume within the same anatomical structure have their dose values swapped. In such cases, the voxel-wise difference would appear large despite the clinical equivalence of the two doses. Furthermore, this method is limited to comparing doses within the same patient, as it requires a direct correspondence between the dose voxels in both distributions.

Comparing Dose Volume Histogram Curves We propose comparing the Dose Volume Histogram (DVH) curves. We have one curve for each structure; we define the distances between doses for each structure, and in the end, we sum up all structures to end up with a single scalar distance between two doses. We can quantify the variation between the two dose distributions in aggregated forms, using the structures.

Discrete DVH Approximation The DVH is obtained after sorting the voxel-wise dose of the structure: Let $\mathbf{d}[s]$ bet the voxel-wise dose of the structure s (therefore, a list, of length $n[s]$, the number of voxels that belong to the structure). Let $\dot{\mathbf{d}}[s]$ be the list above in descending order (i.e. $\dot{\mathbf{d}}[s]_i > \dot{\mathbf{d}}[s]_j$ if $0 < i < j \leq n[s]$). Then, the DVH of s can be approximated by the continuous line composed of the segments linking the following points: $\left(\dot{\mathbf{d}}[s]_i, i/n[s]\right) \quad 0 < i \leq n[s]$. Since we compute the dose voxel-wise, we may only have an approximation of the DVH. However, in practice, most structures of interest have more than a hundred voxels, which makes the DVH approximation very precise.

Since we draw one curve per structure of interest, this capture some of the importance of voxel over others. In fact, when analyzing a dose, doctors look at the dose volume (voxel-wise), but they also take a close look at the DVHs; this is an incentive that DVHs should contain meaningful information.

[1]This is often written as $|\mathbf{d}_1 - \mathbf{d}_2|$, with the summation over voxels implied.

Distance Measure To measure how different two DVH curves, we can imagine several techniques:

- Fréchet distance (treating DVHs as curves in a 2D space)
- Hausdorff distance (treating DVHs as 1D manifolds in a 2D space)
- Wasserstein distance (treating DVHs as probability distributions)
- Kolmogorov-Smirnov test (treating DVHs as probability distributions)
- Total variation between curves (treating DVHs as functions)

We evaluated all the aforementioned distance metrics and propose to retain only the one that yields the most clinically meaningful results.

Fréchet Distance DVH (Dose-Volume Histogram) curves can be interpreted as lines in $\mathbb{R}^2$ [2]. In this context, the Fréchet distance is a well-known metric for assessing the similarity between two curves, particularly useful for comparing poly-lines [**?**]. It measures the minimum distance a particle would travel when simultaneously traversing both curves. In this study, we apply the Fréchet distance to compare the DVH curves of two radiation dose distributions.

Formally, let P and Q represent the curves being compared, with γ denoting a parametrization defined on the interval $[0, 1]$. The positions of a particle moving along curves P and Q at time t are given by $P(\gamma(t))$ and $Q(\gamma(t))$, respectively. The Fréchet distance is defined as:

$$d_{\text{Fréchet}}(P, Q) = \inf_{\gamma} \max_{t \in [0,1]} d(P(\gamma(t)), Q(\gamma(t)))$$

When applied to DVH curves, let $\mathcal{C}_A$ and $\mathcal{C}_B$ denote the discrete DVH curves of two dose distributions. These curves consist of line segments connecting a series of points $\{\mathcal{C}_A(i) = (d_i, v_i),\ 1 \leq i \leq n_A\}$ and $\left\{\mathcal{C}_B(j) = (\tilde{d}_j, \tilde{v}_j),\ 1 \leq j \leq n_B\right\}$; where d_i and $\tilde{d}_j$ denote the dose levels[3], v_i and $\tilde{v}_j$ represent the corresponding volumes, and n_A and n_B are the number of points forming $\mathcal{C}_A$ and $\mathcal{C}_B$[4].

The Fréchet distance, in this case, is defined as the infimum over all possible traversal times. Given that the curves are discrete line segments, the Fréchet distance can be expressed as:

$$d_{\text{Fréchet}}(\mathcal{C}_A, \mathcal{C}_B) = \min_{\substack{j : [\![1, n_A]\!] \to [\![1, n_B]\!] \\ j \nearrow \ (j \text{ increasing})}} \sum_{i=1}^{n_A} dist\left(\mathcal{C}_A(i), \mathcal{C}_B(j(i))\right)$$

[2] In the case of voxel-wise dose approximations, they are represented as poly-lines in $\mathbb{R}^2$.
[3] Derived from **d** after selecting voxels of the structure of interest, and sorting voxels.
[4] Here we are constantly comparing two DVH curves of the same structure on the same patient, so we always have $n_A = n_B$.

$$\text{where } dist\left(\mathcal{C}_A(i), \mathcal{C}_B(j(i))\right) = \sqrt{(d_i - \tilde{d}_{j(i)})^2 + (v_i - \tilde{v}_{j(i)})^2}$$

Here, j represents a (discrete) a parametrization, and $dist\left(\mathcal{C}_A(i), \mathcal{C}_B(j(i))\right)$ is the distance between points $\mathcal{C}_A(i)$ and $\mathcal{C}_B(j(i))$.

One drawback of the Fréchet distance is its computational expense, particularly for structures with a large number of voxels. To mitigate this, we applied the Ramer–Douglas–Peucker algorithm for curve simplification [**?**]. We employed this algorithm with $\epsilon = 0.05$, and after testing on a subset of DVH curves, it was found to accelerate computations by a factor of 3-5, while the calculated Fréchet distance deviated by less than $0.5\,\%$. This method was therefore used in the results presented below.

Hausdorff Distance The Hausdorff distance is another commonly used metric for measuring the similarity between two curves [**?**]. It is defined as the greatest of the shortest distances between any point on one curve and the closest point on the other. Formally, let X and Y be two non-empty sets; the Hausdorff distance between X and Y, denoted $d_{\text{Hausdorff}}(X, Y)$, is given by:

$$d_{\text{Hausdorff}}(X, Y) = \sup_{x \in X} \inf_{y \in Y} dist(x, y)$$

where $dist(x, y)$ represents the distance between points x and y (typically, the Euclidean distance).

In this study, we treat DVH (Dose-Volume Histogram) curves as sets of points in a two-dimensional space $\mathbb{R}^2$, using the Hausdorff distance to quantify their difference. Using the same notation for the DVH curves $\mathcal{C}_A$ and $\mathcal{C}_B$ as previously defined, the discrete Hausdorff distance is computed as:

$$d_{\text{Hausdorff}}(\mathcal{C}_A, \mathcal{C}_B) = \max_{i \in [\![1, n_A]\!]} \min_{y \in \mathcal{C}_B} dist(\mathcal{C}_A(i), y)$$

where $\mathcal{C}_B$ is represented by the set of points

$$\left\{ \left((1-\lambda)\tilde{d}_j + \lambda \tilde{d}_{j+1}, (1-\lambda)\tilde{v}_j + \lambda \tilde{v}_{j+1} \right) \mid \lambda \in [0,1]\,, j \in [\![1, n_B - 1]\!] \right\}.$$

Wasserstein Distance The Wasserstein distance, also known as the Earth Mover's Distance, is a metric used to quantify the difference between two probability distributions [**?**]. Formally, given two probability distributions μ and ν defined on a metric space X, the Wasserstein distance, denoted $d_{\text{Wasserstein}}(\mu, \nu)$, represents the infimum cost of transporting the mass of distribution μ to match distribution ν, where the transportation cost is determined by the distance metric $dist$ on X. It is defined as:

$$d_{\text{Wasserstein}}(P, Q) = \inf_{\gamma \in \Gamma(\mu, \nu)} E_{(x,y)\sim\gamma}\left[dist(x, y)\right]$$

where $\Gamma(\mu, \nu)$ represents the set of all possible joint distributions $\gamma(x, y)$ with marginals μ and ν.

In our analysis, we treat DVH (Dose-Volume Histogram) curves as probability distributions and employ the Wasserstein distance to assess their differences. This metric has the distinct advantage of capturing both local and global variations between the curves, offering a more comprehensive comparison. However, it can be computationally demanding, particularly when dealing with DVHs of large anatomical structures.

Kolmogorov-Smirnov Distance Another distance metric commonly used to compare DVH curves is the Kolmogorov-Smirnov (KS) distance [**?**]. The KS distance measures the maximum vertical separation between two curves and is particularly well-suited for comparing non-parametric distributions, such as DVH curves.

Mathematically, let the two DVH curves be represented by functions f and g, mapping dose levels to volume ratios. The KS distance, d_{KS}, is then defined as:

$$d_{KS} = \sup_{x \in \mathbb{R}^+} |f(x) - g(x)|.$$

In the case of discrete DVH data, f and g are piecewise linear, continuous functions from $\mathbb{R}^+$ to $[0, 1]$, with their values set to zero beyond the maximum dose level.

Total Variation Distance We propose a distance metric that computes the integral of the absolute difference between two DVH (dose-volume histogram) curves. This metric is straightforward to compute and provides a balanced measure of local and global differences between the curves [**?**]. Additionally, it is computationally efficient and well-suited for analyzing large structures with many voxels. This approach yielded the most consistent and clinically relevant results among the metrics tested. As such, we selected this distance measure for our analysis.

Traditionally, the total variation distance is defined as the integral of the absolute difference between two DVH curves. While the dose domain is theoretically unbounded, the volume domain is bounded between $0\,\%$ and $100\,\%$. To avoid integrating over an unbounded dose domain, we opted to reverse the axes, placing dose on the y-axis and volume on the x-axis and subsequently integrating the absolute difference in dose over the volume range $[0, 1]$.

Mathematically, standard DVHs are described by $V : \mathbb{R}^+ \to [0, 1]$. For two DVHs $V(d)$ and $\tilde{V}(d)$, the total variation distance is given by:

$$d_{\text{TotalVariation}} = \int_0^{+\infty} |V(d) - \tilde{V}(d)|\, dd$$

However, in our approach, we express DVHs with dose as a volume function, denoted $D : [0, 1] \to \mathbb{R}^+$. Thus, for two DVHs $D(v)$ and $\tilde{D}(v)$, the total variation distance becomes:

$$d_{\text{TotalVariation}} = \int_0^1 |D(v) - \tilde{D}(v)|\, dv$$

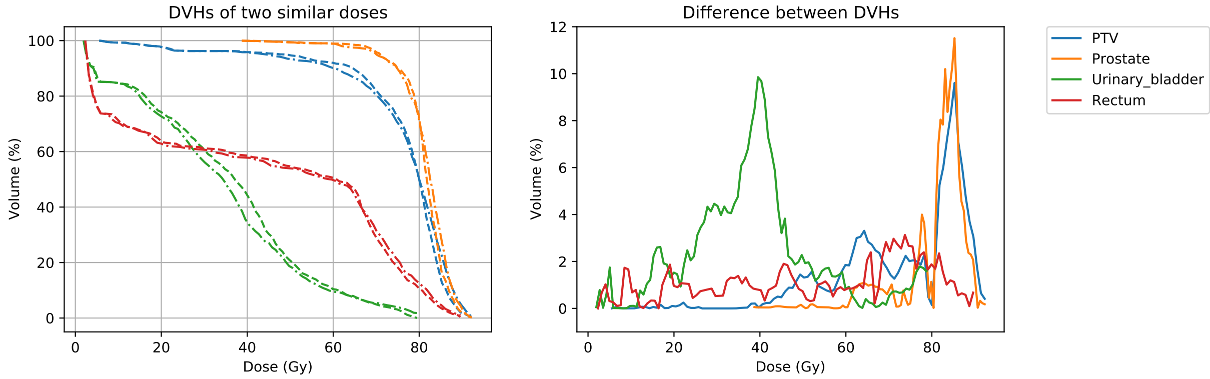

(a) Classical DVH (dose on the x-axis).

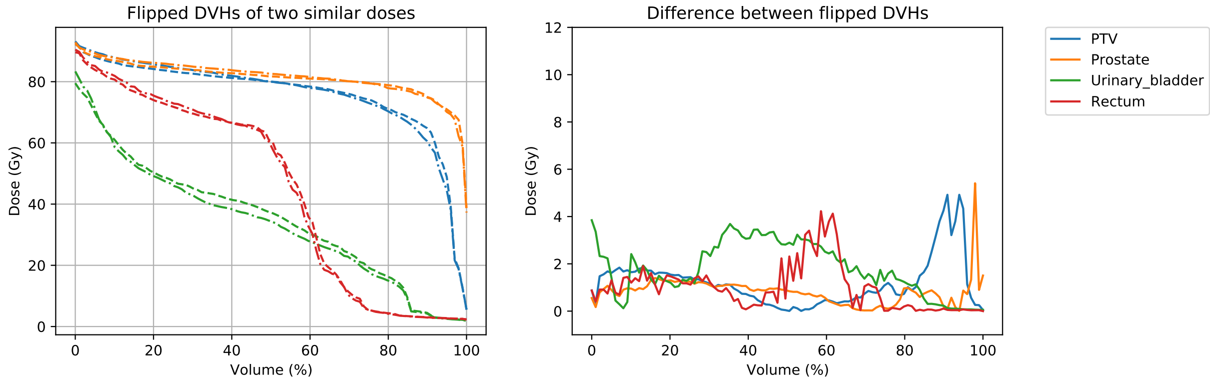

(b) Flipped axes DVH (volume on the x-axis).

Figure 4.2: DVHs: Comparison of classical and flipped axes styles.

While the theoretical value of the integral remains unchanged, we prefer integrating over the finite volume domain $0, 1]$ instead of the unbounded dose domain $\mathbb{R}^+ = [0, +\infty[$. An illustration highlighting the differences between the classical DVH and the version with swapped x- and y-axes is presented in Figure 4.2. The two compared doses were optimized on the TG-119 phantom prostate case, using different weights (1 and 3) for the PTV objective.

As Figure 4.2 shows, the difference between DVHs exhibits less noise (fewer fluctuations) when the dose is on the x-axis. This observation suggests a reduction in numerical error, providing additional motivation to place the volume on the x-axis.

Computing the total variation distance is computationally efficient, requiring only $\mathcal{O}(n_s)$ operations per structure, where n_s represents the number of voxels in the structure of interest, s. Overall, this method achieves a good balance between capturing local and global differences in DVH curves.

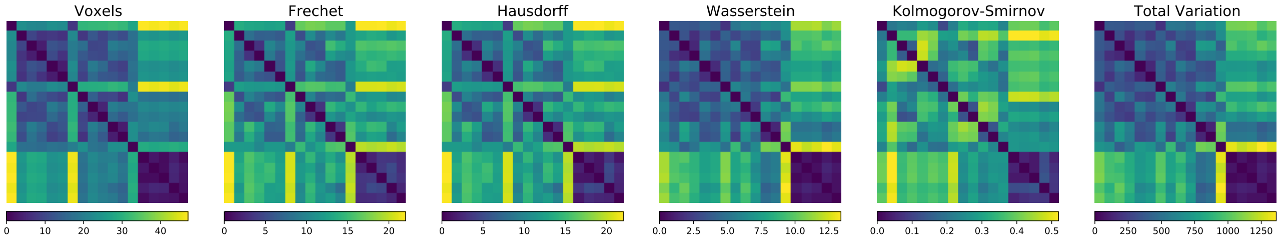

Figure 4.3: Pairwise distances between doses
(with different distances calculation method)

4.1.2 Results

4.1.2.1 Dose Distances Comparison

We optimized each constraint with all weights initially set to 1 but sequentially increased one to 3, 10, and 100. This process resulted in 18 distinct dose distributions, which were compared using the distance metrics described earlier. We calculated the pairwise distances for each pair of doses, effectively constructing the adjacency matrix of a fully connected graph, where each optimized dose corresponds to a node. See Figure 4.3 for comparing the adjacency matrices.

Ideally, the distance metric should satisfy the following criteria:

- It should match the voxel-wise distance when the voxel-wise difference is small.
- It should remain small in cases where the voxel-wise distance is significant. However, the clinical significance of the two doses is similar, even if the doses are voxel-wise different.

From the pairwise distances shown in Figure 4.3, we make the following observations:

- The Fréchet and Hausdorff distances behave similarly to the voxel-wise distance, indicating that they are too sensitive. Thus, they are not suitable for our purpose.
- The Kolmogorov-Smirnov distance appears to degenerate, likely capturing noise due to numerical approximations in the DVH calculations. Therefore, it is also not suitable for our purpose.
- The Wasserstein and Total Variation distances produce more clinically relevant results. As a result, we chose to focus further analysis on these two metrics.

4.1.2.2 Link between Total Variation and Wasserstein

The adjacency matrices for the Wasserstein and Total Variation distances exhibit substantial similarity. This similarity is expected, as the two metrics are equivalent in this context, given that we employed the Earth Mover's Distance (Wasserstein distance with $p = 1$). The Total Variation distance can be regarded as a particular case of the Wasserstein distance.

The Wasserstein distance, also known as the Earth Mover's Distance, provides a metric for quantifying the distance between two probability distributions. Let X and Y be two distributions with cumulative distribution functions (CDFs) F and G, respectively. The Wasserstein distance between them is formally defined as:

$$W_p(F, G) = \inf_{\pi \in \Pi(F,G)} \left(\iint_{x,y \in \mathbb{R}^2} |x - y|^p d\pi(x, y) \right)^{1/p}$$

where $\Pi(F, G)$ represents the set of all possible joint distributions with F and G as marginals.

In contrast, the Total Variation distance between the two curves F and G is defined as:

$$\text{TotalVariation}(F, G) = \int_{x \in \mathbb{R}} |F(x) - G(x)| dx$$

When the Wasserstein distance is computed with $p = 1$, it becomes equivalent to the Total Variation distance:

$$W_1(F, G) \equiv \text{TotalVariation}(F, G).$$

Thus, the only expected differences between these two distance metrics in our analysis should arise from numerical errors.

4.1.2.3 Bounding of Total Variation and Voxel Distance

The Voxel Distance can bound the Total Variation distance. However, the reverse is impossible, as illustrated by the example in the introduction, where two doses exhibit nearly identical dose-volume histograms but significantly different voxel-wise distances.

In the following, we provide a bound for the Total Variation distance of a single DVH, which can be generalized to the sum of the Total Variation distances across all DVHs.

This proof demonstrates that while the Voxel Distance constrains the Total Variation distance, the converse does not hold, especially when voxel-wise variations do not translate to clinically meaningful differences in the global dose distribution.

We aim to compare two dose distributions on a structure, d and $\tilde{d}$ (we suppose that d and $\tilde{d}$ are lists containing only the values on the voxels of the structure).

Sorting lists

Lemma 1. *Let $\dot{l}, l^* \in \mathbb{R}^n$. Let $\dot{l}$ be sorted and $\dot{l^*} \in \mathbb{R}^n$ be sorted version of l^*. Then, we have:*

$$|\dot{l} - l^*| \geq |\dot{l} - \dot{l^*}|$$

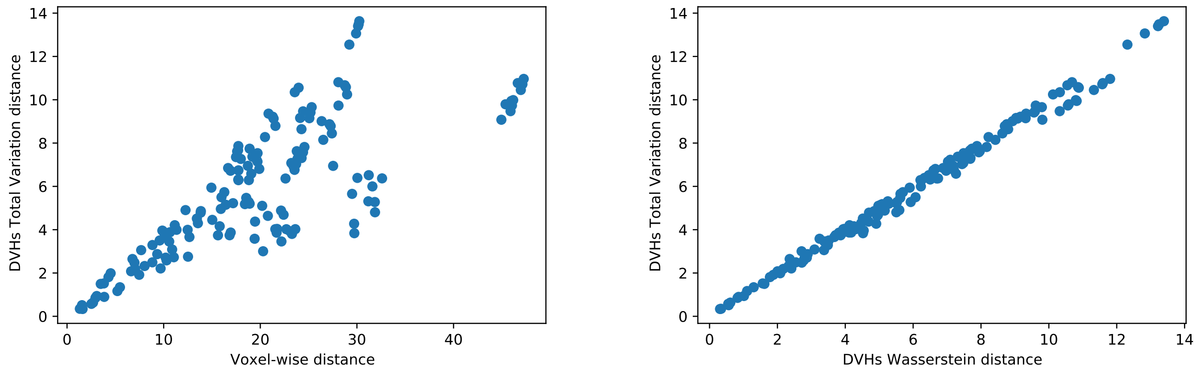

(a) DVHs Total Variation vs Voxel-wise. (b) Total Variation vs Wasserstein.

Figure 4.4: Comparing Distances

Proof. Suppose $a < b$ and $c < d$, and WLOG, $a \leq c$.
We have $|a-d| = |a-c| + |c-d|$ so $|a-d| + |b-c| = |a-c| + |c-d| + |b-c|$ using triangle inequality ($|c-d| + |b-c| \geq |b-c|$): $|a-d| + |b-c| \leq |a-c| + |b-d|$.
Thus, with $\dot{l}$ sorted, swapping elements l_i and l_j ($i < j$) of l^* decreases $|\dot{l} - l^*|$ if $l_i \geq l_j$. Applying, bubble sort on l^*, we obtain $\dot{l^*}$ doing only permutations satisfying the condition just stated.

Hence, we obtain $|\dot{l} - l^*| \geq |\dot{l} - \dot{l^*}|$ at the end of the bubble sort. □

Corollary 1. *Let $l, l^* \in \mathbb{R}^n$. Let $\dot{l}, \dot{l^*} \in \mathbb{R}^n$ be sorted version of l, l^*. Then:*

$$|l - l^*| \geq |\dot{l} - \dot{l^*}|$$

Proof. The order in which we perform $|l - l^*| = \sum_{k=1}^{n} |l_k - l_k^*|$ can be chosen, so $|l - l^*| = \sum_{k=1}^{n} |l_{\sigma(k)} - l_{\sigma(k)}^*|$ (with σ a permutation of $[\![1, n]\!]$). Taking σ such that $l_{\sigma(i)} \leq l_{\sigma(j)}$ for $i < j$ and using lemma finishes the proof. □

Proof Outline Suppose the voxel-wise difference is ε-small (i.e. $|d_i - \tilde{d}_i| < \varepsilon$). Then, the total variation of the unsorted vector doses is $|d - \tilde{d}| < n_{\mathcal{S}}\varepsilon$. Let $\dot{d}$ be sorted d and $\dot{\tilde{d}}$ be sorted $\tilde{d}$. Then, by Corollary 1, we have: $|\dot{d} - \dot{\tilde{d}}| \leq |d - \tilde{d}| < n_{\mathcal{S}}\varepsilon$.

Therefore, if d and $\tilde{d}$ are sufficiently close, $\varepsilon \to 0$ and $|\dot{d} - \dot{\tilde{d}}| \to 0$.

Conclusion Thus, voxel-wise very close doses distributions will also have close DVHs distances, which ensure DVHs distances are non-degenerative.

4.1.2.4 Distances Distribution Comparison

Comparing Total Variation and Voxel-wise The bounding of the total variation DVH distance in terms of voxel-wise distance is clearly illustrated in Figure 4.4a, where a linear upper bound can be observed in the scatter plot. However, specific pairs of doses are closer regarding DVH distance than initially anticipated based solely on voxel-wise comparisons. This observation underscores the need for a more nuanced analysis beyond voxel-wise comparison, as it may overlook clinically relevant similarities between dose distributions.

Comparing Total Variation and Wasserstein Figure 4.4b shows that the two DVH distances are nearly perfectly proportional. This result aligns with expectations, given that they are mathematically equivalent. The only difference lies in the integration axis in the total variation distance, which accounts for the small fluctuations observed, likely due to accumulated numerical error.

4.1.3 Discussion

In this section, we introduce a novel metric for comparing radiation doses. This metric offers the advantage of being insensitive to dose changes in certain regions, provided they are compensated in other regions, thus achieving the intended objective. This property makes the metric particularly useful in various applications, including dose mimicking and determining early stopping criteria for fluence map optimization.

Despite the advantages, this distance metric has certain limitations. A notable drawback is its inability to capture spatial dose distribution, which may pose challenges in specific cases. Pathological examples exist where two DVHs appear similar, but the clinical interpretation differs significantly. Other factors, such as the spatial distribution of the dose within the target volume or surrounding tissues, can play a pivotal role in the treatment's effectiveness. To cover this, incorporating hot points in the metric could help. However, it remains to be seen how to do it in a clinically meaningful way.

For instance, two dose distributions might deliver the same high dose, with one distributed across several small regions and the other concentrated in a single large region. While the DVHs may appear identical, clinicians would interpret these two dose distributions differently. Such edge cases, however, are sporadic in clinical practice. Nonetheless, for critical cases, we recommend complementing this metric with voxel-invariant approaches and other techniques to evaluate the radiation doses comprehensively.

When comparing two distinct doses, a considerable distance between them may indicate a significant difference in the intensity or frequency of the treatment. However, this does not necessarily imply that one dose is superior. The effectiveness of a dose depends on several other factors, such as the individual patient's characteristics, medical history, and treatment response.

The distance between two doses does not assess which is more effective or clinically appropriate in a specific case. It only acknowledges that they are clinically equivalent or not, and in the latter case, a dosimetrist needs to make a choice. It is essential to account for all relevant factors when evaluating the efficacy of a treatment dose to ensure a comprehensive understanding.

Overall, the proposed dose comparison technique presents a promising tool for radiation dose evaluation. While it has certain limitations, it can serve as a valuable addition to the repertoire of methods employed by radiation oncologists and medical physicists for optimizing treatment plans and improving patient outcomes. Complementing existing techniques offers an additional layer of analysis, contributing to more informed decision-making in clinical practice.

Stop Criterion Defining an adequate stopping criterion for the fluence map optimization process is a critical challenge in radiotherapy dose optimization. In clinical practice, dosimetrists often guide optimization, who may terminate the process when they are satisfied with the outcome. However, the need for fully automated optimization processes requires the establishment of systematic and objective stopping criteria. One potential approach is to compare the clinical effects of two dose distributions and stop when one optimization step does not change the clinical effect. This method can helps evaluate different solutions and determine the optimal point to terminate the optimization process.

4.2 Network of Doses

In this section, we aim to construct a clinically meaningful network of dose distributions, where each node represents a distinct dose distribution, and the edges quantify the relationships between them. By creating such a network, we can identify clusters of similar dose distributions and uncover patterns that reflect clinical relevance. This network-based approach will enable us to visualize better, analyze, and interpret the relationships between various treatment plans, ultimately improving the comparison and optimization of radiotherapy strategies.

Numerous efforts have been made to automate the treatment optimization process in radiation therapy. One promising avenue is the exploration of the Pareto frontier, as discussed in [**?**] and [**?**], which seeks to identify a set of treatment plans that balance conflicting objectives, such as maximizing tumor control while minimizing damage to surrounding healthy tissue. Another approach proposed [**?**] consists of directly extracting leaf movements from patient data to enhance the automation of dose delivery.

Despite these advancements, fully automated approaches have yet to be widely adopted in clinical practice, primarily due to practical limitations and the complexity of translating these methods into routine use. Using doses network analysis, we will propose a hybrid approach that integrates both manual and automated treatment optimization. This method will combine the computational efficiency of automation with the expert judgment of clinicians, ensuring that the final treatment plans are both optimal and clinically relevant.

4.2.1 Methods

Multiple Plans Generation We employed the same dose optimization process as previously described. The cost function utilized in this study is designed to be convex, ensuring that, irrespective of the specific weight assignments given to the objectives, minimizing this cost function will consistently converge to an optimal radiotherapy plan. To generate a diverse set of treatment doses for a given patient case and set of constraints, we optimized the cost function with varying weight assignments for each constraint.

This approach mirrors the current practice in which dosimetrists adjust the weights associated with different dose objectives to guide the optimization engine toward a clinically acceptable solution. By altering these weights, it becomes possible to explore different trade-offs and prioritize certain aspects of the treatment plan, such as sparing healthy tissue or enhancing tumor coverage, according to the patient's specific clinical needs.

Objectives' Weights Generation The weights assigned to each optimization objective dictate the relative importance of each objective in the trade-offs made by the optimization engine. Initially, we begin with a typical weight assignment used in clinical practice. To generate a diverse set of weights, we perturb these initial values by adding random normal noise, resulting in a unique new set of weights.

By repeating this process, we can explore a wide range of potential treatment plans. This thorough exploration provides a nuanced understanding of the trade-offs between competing clinical objectives. The random computational exploration of irradiation strategies extends beyond the capabilities of manual exploration, enabling clinicians to make more informed and tailored decisions based on a broader array of treatment possibilities.

Dose Normalization For consistency across cases, we normalized the doses using the "$D_{50\,\%}$" normalization method, a common practice in radiation therapy. This method normalizes the dose such that the median dose delivered to the PTV equals the prescribed dose, ensuring comparability across treatment plans.

Phantom Patient Our proposed method for clustering radiation doses was evaluated using the TG-119 Prostate case [**?**], a well-established benchmark dataset commonly employed to assess the quality of radiation therapy plans. The TG-119 dataset provides predefined dose objectives, which were incorporated into the formulation of our cost function. This benchmark allows for a robust evaluation of our clustering approach in the context of clinically relevant treatment goals, ensuring that the method aligns with widely accepted standards in radiation therapy planning.

Dose Clustering Techniques

Dose Distance We first needed to establish a method for defining the distance between individual doses to perform the dose clustering. We employed the Euclidean distance between voxel-wise dose distributions as our distance metric. The weight of each edge between two doses was then defined as the inverse of this distance as we sought to maximize the edge weights between similar doses. Defining edge weights as the inverse of the distance between nodes is a common practice in graph theory, as noted in previous works [**?**] [**?**].

Community Detection We employed Louvain's method for community detection to cluster the radiation doses. Louvain's method is a greedy optimization algorithm that aims to maximize the modularity of the graph. Modularity is a metric used to assess the quality of a graph partition by quantifying how well the graph is divided into distinct communities. For our analysis, we utilized the implementation of Louvain's method available in the Python library NetworkX [**?**], which facilitated partitioning the dose similarity graph into meaningful clusters.

Evaluating Communities Split The clustering quality was evaluated using DVHs derived from the different doses. We computed the mean and standard deviation of the DVHs curves for each cluster and the entire dataset.

We analyzed the relative volume doses across four distinct anatomical structures. One hundred one dose values were sampled for each structure, corresponding to volume percentages ranging from $0\,\%$ to $100\,\%$ in equal $1\,\%$ intervals. These values were aggregated into a single vector, resulting in a vector of length 404 for each dose.

To assess the variability within these dose vectors, we calculated the standard deviation for each of the 404 elements in the vector. This measure provides insight into the dispersion of dose values within the structures. By averaging the calculated standard deviations, we derived a scalar metric that quantifies the degree of separation among the clustered doses, reflecting the consistency or variability of the doses within each group.

4.2.2 Results

Visual Clustering Evaluation

Graph Plots In figure 4.5, each node represents a dose. The communities are attributed using Louvain method and are identified by colors. Since the graph is clearly not planar, we choose to plot it in a circular layout (fig. 4.5a) and in a spring layout (fig. 4.5b).

In order to obtain a more precise understanding of the edge weights in the network, one can refer to the adjacency matrix of the edge weights, as depicted in Figure 4.6.

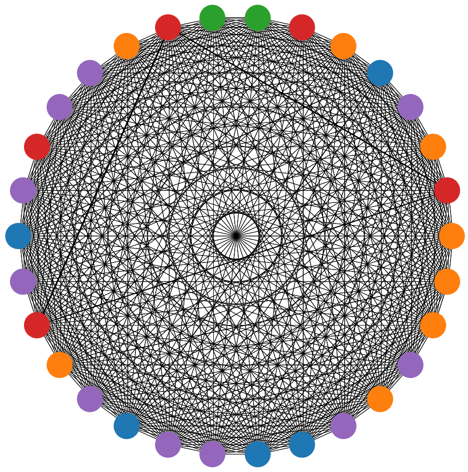

(a) Circular Layout.

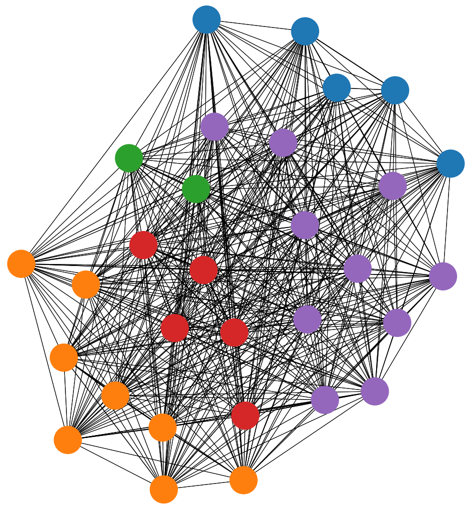

(b) Spring Layout.

Figure 4.5: Plot of the Network
Edges width $\propto$ edge weight $\propto$ $^1/_{\text{distance}}$
Node's color reflects community attribution

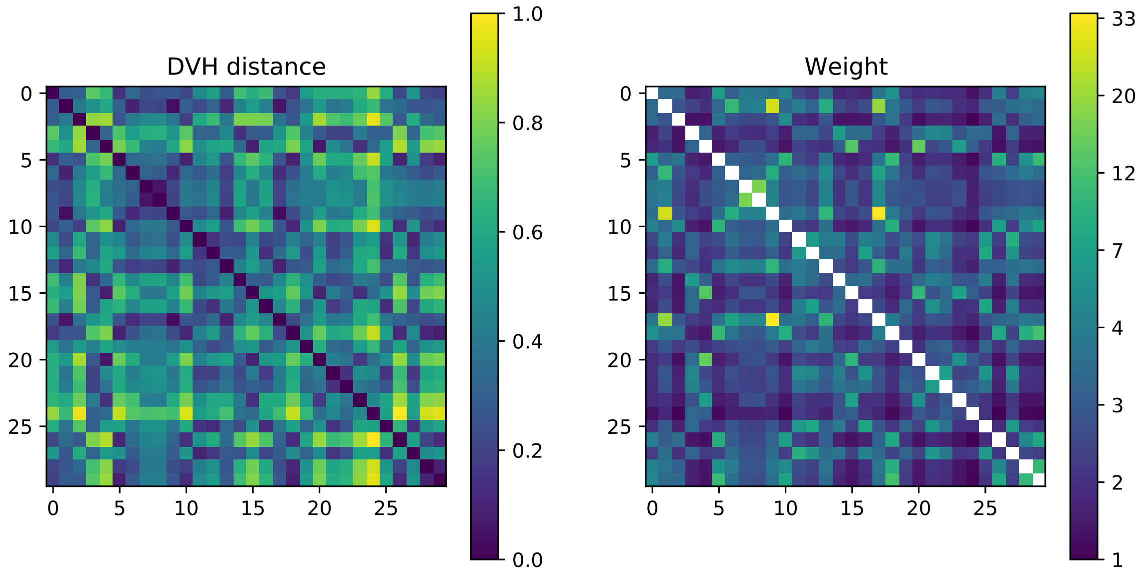

Figure 4.6: Weight Adjacency Matrix of the Network

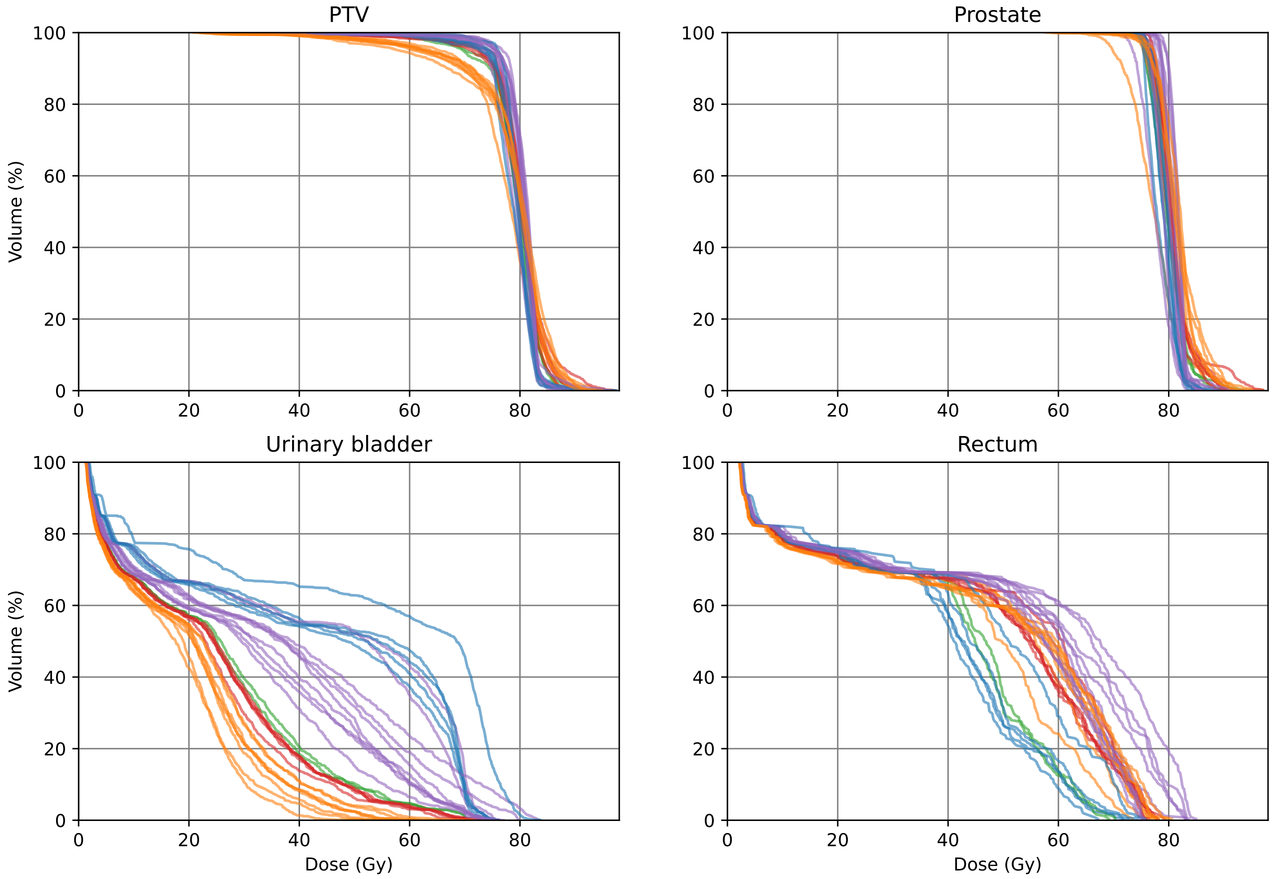

Figure 4.7: Dose-Volume Histogram

DVH Plot Figure 4.7 illustrates the DVHs, with the colors of the plots corresponding to the communities identified in the network analysis. To ensure clarity and prevent confusion, each structure is presented on a separate plot. Notably, our observations align with expectations, as doses assigned to nodes within the same community (indicated by the same color) exhibit nearly overlapping DVHs.

The visualization of DVHs offers critical insights into the distribution of radiation doses across different anatomical structures. The strong alignment between observed dose patterns and community assignments highlights the potential of network analysis to reveal significant patterns within radiation therapy data. By mapping the colors of the DVH plots to the communities identified in the network, we gain a deeper understanding of the relationship between dose assignments and structural characteristics.

This analysis supports the hypothesis that nodes (representing doses) within the same community exhibit similar dose profiles. As a result, these doses could be consolidated, given that they are likely to have comparable clinical outcomes. This method provides an efficient approach to identifying groups of treatment plans that share equivalent therapeutic effects, enabling a more streamlined decision-making process.

Set	Set Size	Mean Standard Deviation
Cluster 1 **(blue)**	5	7.30
Cluster 2 **(orange)**	8	4.51
Cluster 3 **(green)**	2	0.95
Cluster 4 **(red)**	5	2.17
Cluster 5 **(purple)**	10	7.92
All	*19*	*15.54*

Table 4.1: Clustering Quality

Numerical Clustering Evaluation As explained in subsection 4.2.1, we use the mean standard deviation of doses at 101 equispaced values of volume to obtain a scalar value of how far apart are a set of doses; see table 4.1 for results.

The mean standard deviation values for the clusters — 7.30, 4.51, 0.95, 2.17, and 7.92, with an average of 4.57 — are significantly lower (nearly four times) than the mean, standard deviation of the entire network, which is 15.54 (see Table 4.1). This substantial reduction in standard deviation provides clear quantitative evidence that our clustering method yields favorable results.

This quantitative improvement is further corroborated by qualitative insights, as shown in Figure 4.7, where the dose clusters effectively characterize the distribution of radiation doses. The strong alignment between the dose clusters and the DVH patterns reinforces the validity and relevance of our clustering strategy. Our proposed clustering approach performs well in qualitative and quantitative evaluations, underscoring its potential utility in optimizing radiation therapy plans.

4.2.3 Discussion

This study presents a novel approach to clustering doses based on their distributions, providing both quantitative and qualitative evidence of the significance of such clustering. However, clustering doses remains a complex task due to the high dimensionality of dose space and the irregularities in dose distributions. While the results presented in this study are promising, they are not yet ready for clinical implementation. The results suggest that doses within the same cluster likely have indistinguishable clinical effects, which opens up several practical applications.

Regrouping doses into clusters offers valuable insights into clinical practices and introduces new possibilities for optimizing radiotherapy treatment plans. One potential application of dose clustering is to use the identified clusters as a similarity measure for early stopping in optimization processes, leading to potential time savings and computational efficiency. Specifically, if the dose distribution shows convergence with the previous n dose distributions, this could serve as an indication to halt further optimization, thereby improving efficiency.

Moreover, expanding this clustering approach to include doses from multiple patients could provide insight into the treatment practices of different clinical centers, facilitating comparisons of outcomes for similar anatomies.

In the following section, we propose a clinical application of the dose clustering technique that can potentially streamline the optimization process for dosimetrists. This approach could significantly reduce the number of manual interactions, or "clicks," required within the Treatment Planning System, thereby enabling faster and more efficient dose optimization.

4.3 A Novel Framework for Multi-Objective Optimization and Robust Plan Selection Using Graph Theory[5]

4.3.1 Challenges in Current Practices

In recent years, the complexity of treatment planning in radiotherapy has increased substantially, with planners having to balance multiple objectives, such as maximizing tumor control while minimizing damage to surrounding healthy tissue. Despite advances in radiotherapy planning, current practices still face limitations. Traditional approaches often rely on manual fine-tuning of parameters, making it difficult to achieve a globally optimal solution. Multi-objective optimization balances competing goals and is a manual, time-consuming process. Planners must evaluate and adjust multiple treatment plans to account for uncertainties and variations in patient anatomy. This approach is labor-intensive and prone to inconsistencies due to human factors, which can lead to suboptimal patient outcomes. We present a novel framework for multi-objective optimization and robust treatment plan selection based on graph theory to address these challenges. This framework introduces significant automation into the planning process, allowing for more efficient and reliable plan generation.

4.3.2 Proposed Framework

The first step in the framework is the construction of the graph, which is based on the systematic random perturbation of importance factors assigned to clinical constraints. By treating this set of plans as a graph, we can explore the landscape of possible solutions more systematically. It would not be practical to ask doctors and dosimetrists to evaluate dozens of treatment plans.

We use clustering algorithm described in the previous section to regroup doses with similar effects. Clusters of plans, or "communities," emerge based on their proximity in the graph,

[5] Presented at ESTRO 2024.

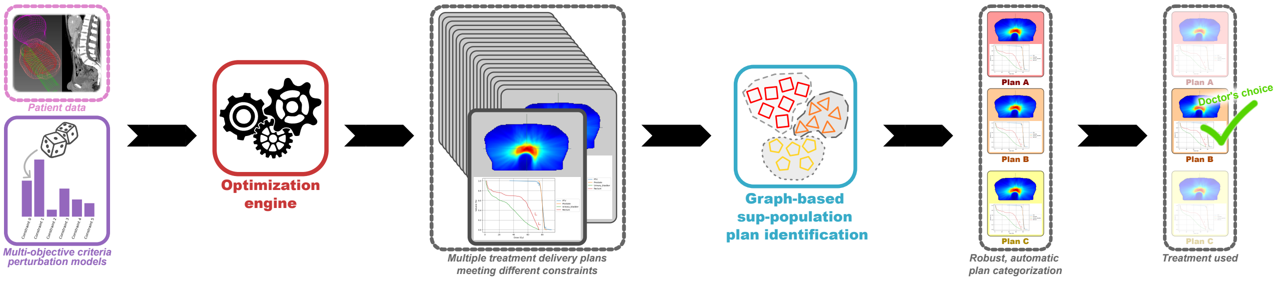

Figure 4.8: Graphical Abstract of the Proposed Process.

allowing us to narrow down the set of candidates for more detailed evaluation. By focusing on these robust communities, we reduce the need for manual intervention in plan selection. Instead of planners having to sift through dozens of plans, the framework automatically highlights the most promising options, significantly reducing both time and effort (see figure 4.8).

This framework represents a shift from the traditional "many-clicks" approach—where planners must manually adjust and evaluate numerous treatment plans—to a "few-clicks" workflow, where the system presents only the most relevant, robust plans for final review. This automation not only saves time but also reduces the risk of human error, leading to more consistent, higher-quality outcomes for patients.

4.3.3 Discussion

The proposed framework transitions from a traditional N-click approach[6] to a more efficient n-click solution[7]. While this shift significantly reduces the time required for plan selection, it still requires dosimetrists and doctors to adapt to a new workflow. This change in habit—moving from manually reviewing and adjusting plans to relying on semi-automated plan suggestions—may pose a barrier to clinical implementation.

For a solution to be adopted in everyday practice, it must minimize the disruption to current workflows. Ideally, this means evolving the framework into a proper 1-click solution, where the system autonomously generates and selects the optimal, robust treatment plan without requiring manual intervention. Such a system would eliminate the need for dosimetrists and doctors to alter their habits and ensure consistent, high-quality outcomes with minimal effort. Achieving this level of automation is essential for widespread clinical adoption. Therefore, future work in this manuscript will focus on refining the framework to meet these demands, bringing it closer to a fully automated, practical tool for radiotherapy planning.

[6]with $N >> 10$
[7]with $10 > n > 1$

Classical Dosimetry Automation

Abstract

In radiation therapy, treatment planning involves balancing competing objectives. The contradictory goals often lack universal prioritization. Expert bias introduces variability in clinical practice, as the preferences of radiation oncologists and medical physicists shape treatment planning. Traditionally, this balance is achieved through manual or semi-manual processes guided by the expertise of clinicians and planners. This chapter explores approaches for fully automating the treatment planning process, focusing on classical optimization techniques constrained by dosimetric objectives.

We will review established methods and propose new agents capable of optimizing dose without human interaction. This innovative approach leverages previously defined dose distance metrics. We aim to streamline and standardize the treatment planning workflow by fully automating the optimization process.

5.1 Meta Optimization Approach

After the FMO step is developed and encapsulated, one may modify the weights used for the FMO iteratively until a condition is met or for a given number of steps. We will, therefore, have one inner optimization (the FMO) and one outer optimization.

Algorithm 1 Meta Optimization Algorithm Outline

```
initialize w
repeat
    initialize b                      ▷ FMO starts
    repeat
        d = Lb                        ▷ differentiable
        c = C(w, d)                   ▷ differentiable
        back-propagate c
        update b
    until FMO stop condition          ▷ FMO ends
    update w
until Meta-optimization stop condition
```

The outer optimization step is not differentiable (or at least not in a reasonable computation time). Hence, we will be looking at gradient-free optimization methods.

5.1.1 Expert Weight Adjustment

Expert systems are computer systems emulating the decision-making of a human expert.

Simple Weight Increase One approach involves increasing the weight of all unsatisfied constraints after each FMO optimization step. This method is advantageous due to its simplicity in terms of implementation and understanding. However, a significant limitation arises when none of the constraints are met, causing the outer optimization loop to stagnate. In such cases, the optimization process remains stationary, usually when too many constraints are enforced. This stationary state arises particularly in complex scenarios with multiple competing constraints and can result in a situation where progress is hindered, preventing the solution from improving over iterations.

Inverse Proportional Weight Increase Another approach involves increasing the weight of each constraint inversely proportional to how close it is to being met, thereby quantifying the degree of constraint satisfaction. For instance, the degree of satisfaction can be quantified by calculating the area between the dose-volume histogram (DVH) constraint and the actual DVH curve; when this area is zero, the constraint is considered fully satisfied.

While this method remains relatively straightforward to implement and provides a more refined adjustment of weights based on how close each constraint is to being met, it can lead to oscillation issues. Constraints may fluctuate between being satisfied and violated across iterations, hindering stable convergence. Although adding momentum to the optimization process could mitigate these oscillations, expert systems of this nature typically require continuous tuning and refinement. As a result, this approach may not be viable for reliable clinical applications where consistent performance is essential.

5.1.2 Metric-Based

Here, we suppose that one can construct a measure of the quality of a plan.

Hill Climbing Hill climbing [**?**] is a simple optimization technique in which the solution iteratively moves toward an improved solution based on a defined metric. In the context of radiotherapy treatment planning, several metrics have been proposed to quantify the quality of a plan, including Normal Tissue Complication Probabilities (NTCP), target coverage, conformity index, and heterogeneity index, among others [**?**, **?**] . This approach offers a systematic way to improve treatment plans by optimizing the chosen metric.

However, defining the correct metric of interest is challenging, as no single metric, nor a combination of metrics, has consistently proven to satisfy radio-oncologists' requirements. In practice, the most reliable method for assessing the quality of a treatment plan remains the manual evaluation of DVHs, which provide a detailed representation of the dose distribution across both the target and the surrounding organs at risk.

Pareto Exploration Researchers have developed algorithms to explore the Pareto surface of dose distributions, yet no consensus has been reached on selecting an optimal dose from this surface. Consequently, Pareto surface exploration is unsuitable due to the absence of an objective quantitative measure for evaluating the quality of a specific plan [**?**]. This limitation similarly constrains other meta-optimization techniques, as they also rely on the availability of a clear, impartial criterion for plan evaluation [**?**, **?**].

Contextual Knowledge Another challenge is the varying difficulty across patients due to their different organ geometry. In "easy" cases, clinicians may require a highly optimized dose distribution regarding the previously mentioned metrics. On the other hand, for "harder" cases, they can afford to be more lenient regarding constraint satisfaction.

This context-aware acceptability criterion adds complexity to the optimization process. It becomes challenging to define general rules not only for ranking treatment plans but also for deciding a plan's acceptability.

5.2 Radiotherapy Dose Optimization via Clinical Knowledge Based Reinforcement Learning[1]

5.2.1 Introduction

Reinforcement learning (RL) is a machine learning paradigm that trains agents to make sequential decisions in dynamic environments [**?**]. Agents learn to optimize their actions to achieve long-term objectives through trial and error guided by rewards or penalties. The decisions taken by dosimetrists when optimizing treatment can be formalized as an RL problem. Moreover, dosimetrists can guide the TPS towards an acceptable plan but usually can not explain their decision while interacting with the TPS. The difficulty in explaining why certain decisions are taken suggests using deep RL over expert-based methods. This setup is similar to image recognition, where one can say a picture represents a car or a boat but struggles to explain why.

The study's primary hypothesis is that all the information needed to decide how to change the weights in the objective function relies on the DVHs. The fact that dosimetrists almost solely use DVH plots supports our hypothesis. In order to learn the actions of dosimetrists who use a TPS to optimize doses, we leverage deep learning. We train an agent that takes the DVHs as the input of the current optimized dose and predicts the evaluation of possible weight changes.

Access to the exact actions taken by human dosimetrists on the TPS is typically unavailable (as clinics do not usually store this data; only the final plan is held). Therefore, we only use the dose distributions of previously treated patients to train our model. This partial availability of data suggests the use of RL.

Reinforcement Learning Paradigm RL agents adapt actions to situations where there are interactions with an environment [**?**]. In order to learn, RL agents only need a reward (scalar value) after performing an action.

In classical RL, we want $V(S_t) = R_t + \gamma V(S_{t+1})$. (so the update is $V(S_t) \leftarrow (1-\alpha)V(S_t) + \alpha\left[R_{t+1} + \gamma V(S_{t+1})\right]$). In the context of dose optimization, the reward R_t is defined as $R_t = \mathcal{E}(S_{t+1}) - \mathcal{E}(S_t)$, where $\mathcal{E}$ is a function that evaluates the quality of a state (such that higher is better; if lower is better, then swap s_t and S_{t+1}).

The evaluation $\mathcal{E}$ can be one or a mixture of the metrics mentioned in the introduction (Section 5.1.2) [**?**] [**?**] [**?**]. This setup may leverage knowledge about which actions to perform instead of guessing randomly, as a meta-optimizer would do. Hence, the RL could gain some computation time compared to a meta-optimization.

However, this technique does not use past plans; it only needs the optimizer inputs (CT, structures contours). We propose using the availability of past treatment plans to more

[1]Presented at AIME 2024.

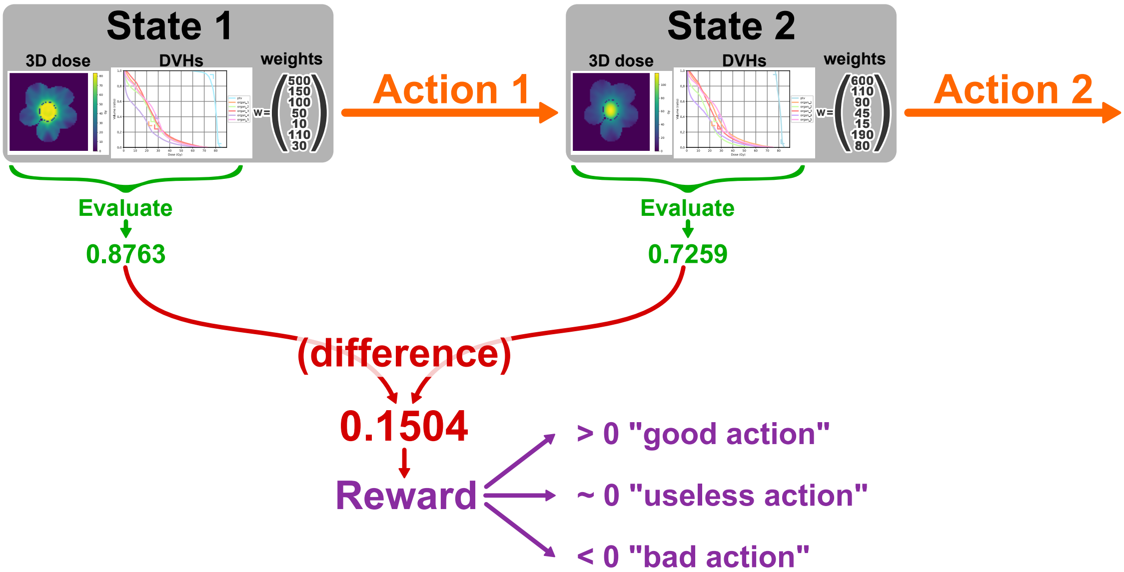

Figure 5.1: Classical reinforcement learning reward for automatic dosimetry.

accurately reflect the complexity of decisions made by dosimetrists and better match their expectations of a fully automatic treatment planning system.

5.2.2 Methods

We present a novel paradigm for reward-based RL agents in dosimetry. This revised reward framework better reproduces human-optimized dose distributions.

Reinforcement Learning Reward As developed in previous work, we can derive a distance between dose plans [**?**]. If we consider the clinical dose of past cases (used for training) as the best achievable one, we can evaluate a dose plan by computing its distance from the clinical dose plan.

Let D_t be the dose associated with S_t, and D_C the clinical dose. We then define $\mathcal{E}(S_t) = \mathcal{D}(D_t, D_C)$. Since, in that case, $\mathcal{E}(S_t)$ should be minimized, we will define the reward as

$$R_t = \mathcal{E}(S_t) - \mathcal{E}(S_{t+1}) = \mathcal{D}(D_t, D_C) - \mathcal{D}(D_{t+1}, D_C).$$

This reward can be interpreted as the "distance gained to the clinical dose".

Architecture We use a dense neural network, which inputs the DVHs and current normalized weight values. It outputs the $Q(s,a)$ value for each possible action a. Dense layers are very prone to overfitting. In order to force the network to actually predict the following evaluation for each possible action, without overfitting, we incorporated a bottleneck in

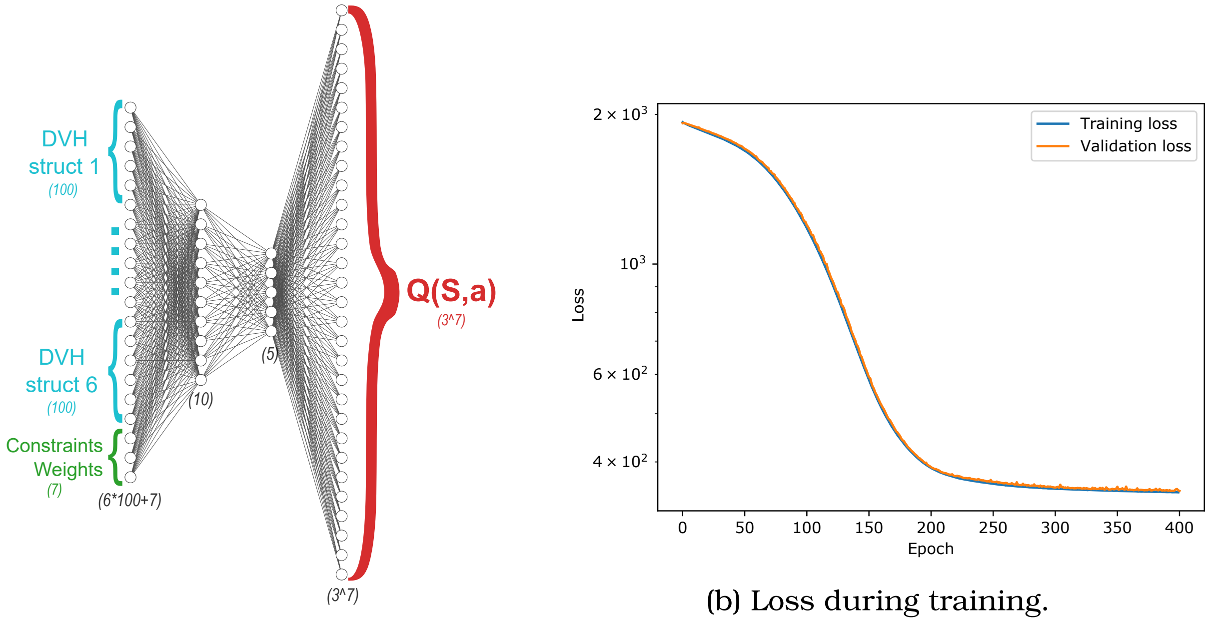

(a) Architecture.

(b) Loss during training.

Figure 5.2: Deep neural network used for the RL agent.

the network (Figure 5.2a). Compressing the information stops the network from overfitting. Networks with such architecture show very little difference between training and validation sets (see Figure 5.2b).

Avoiding Off-Distribution We generated a training set of over 125k actions (this took five days on an NVIDIA GeForce GTX 1080). Despite this relatively large dataset, we have not explored exhaustively the state-actions space, and the network still lands off-distribution. This can easily be spotted when the predicted Q value is greater than the current distance to the clinical dose; we choose to ignore those predictions, and in fact all outlier predictions. The justification is that our set of actions is limited, no action will suddenly drastically improve the plan. It is the combination of several sequential actions that allows good plan optimization. Therefore, while testing, we choose the action with the best prediction, while passing the outlier test just mentioned.

Data We generated synthetic phantom patients and corresponding clinically relevant dose distributions. Variability can arise in clinical practice due to differences in organ contouring methods (manual or automated) and the potential for clinics to delineate different organs. To mitigate this variability in our ongoing research, we employed synthetic patients, ensuring a standardized approach where all patients possess the same number of organs with similar shapes and identical prescription parameters. Future studies will explore the application of this methodology to actual clinical cases.

Constraint type	Structure	Volume	Dose
Minimum	PTV	$95\,\%$	$78.0\,Gy$
Maximum	PTV	$5\,\%$	$82.0\,Gy$
Maximum	Organ 1	$28.4\,\%$	$21.8\,Gy$
Maximum	Organ 2	$33.7\,\%$	$23.7\,Gy$
Maximum	Organ 3	$24.1\,\%$	$26.9\,Gy$
Maximum	Organ 4	$37.6\,\%$	$27.9\,Gy$
Maximum	Organ 5	$20.5\,\%$	$30.8\,Gy$

Table 5.1: DVH constraints used to create the cost function used in the FMO.

Synthetic patients We generated a cohort of 130 patients with bodies modeled as oval axial cross-sections, assigning a uniform density equivalent to water. Within each body, we placed an ellipsoidal planning target volume (PTV) with a slightly different density, sampled from $\mathcal{N}(1, 0.05)$. Five organs at risk (OARs) were also positioned around the PTV, aligned along the axial plane. The exact position and size of organs and PTV were randomized to consider the geometric variability across individuals. This setup was designed to simulate cases analogous to typical prostate cancer scenarios.

Synthetic clinical dose After generating the patient's CT and structures, we needed to create a reference dose that our agent should mimic. We manually set weights and performed a standard optimization. The dose prescription is a standard $80\,Gy$ on PTV, the same across all patients. The table of the clinical DVH constraints used for optimization are detailed in table 5.1 We used a seven-beam IMRT irradiation technique on all the cohorts.

5.2.3 Results

Figure 5.4 shows how the distance between our RL agents performs over five steps on 30 test patients (unseen during the training). A lower distance is interpreted as an improved dose, since it is closer to the best dose, which is the clinical one.

Quantitative Results The network converged on the training data, and validation showed minor overfitting. For testing, we generated 30 brand new cases that we again manually optimized. We then used the RL model to perform the optimization of these 30 unseen cases. On average, our model was able to reduce the dose distance with manually optimized dose by a factor of 3 (from 1.8 at iteration 0 to 0.6 at iteration 4), as shown in Table 5.2.

We remark from the Table 5.2 that the homogeneity score and conformity score give similar results. Classical meta-optimization performs well, but needs a metric to elect the best dose (during the test, the clinical dose is unknown, so the DVHs distance metric is not available). We also observe that clinical doses are not always scoring high (in this test set,

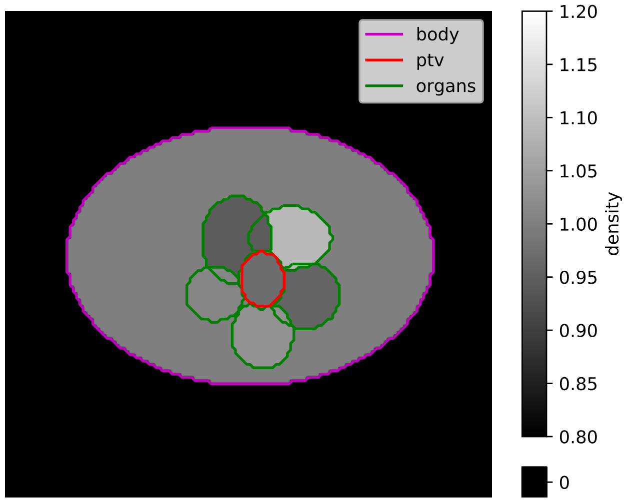

(a) CT

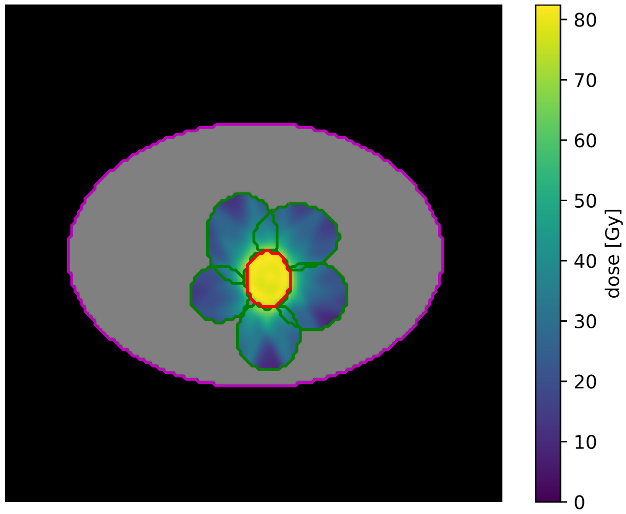

(b) Clinical dose

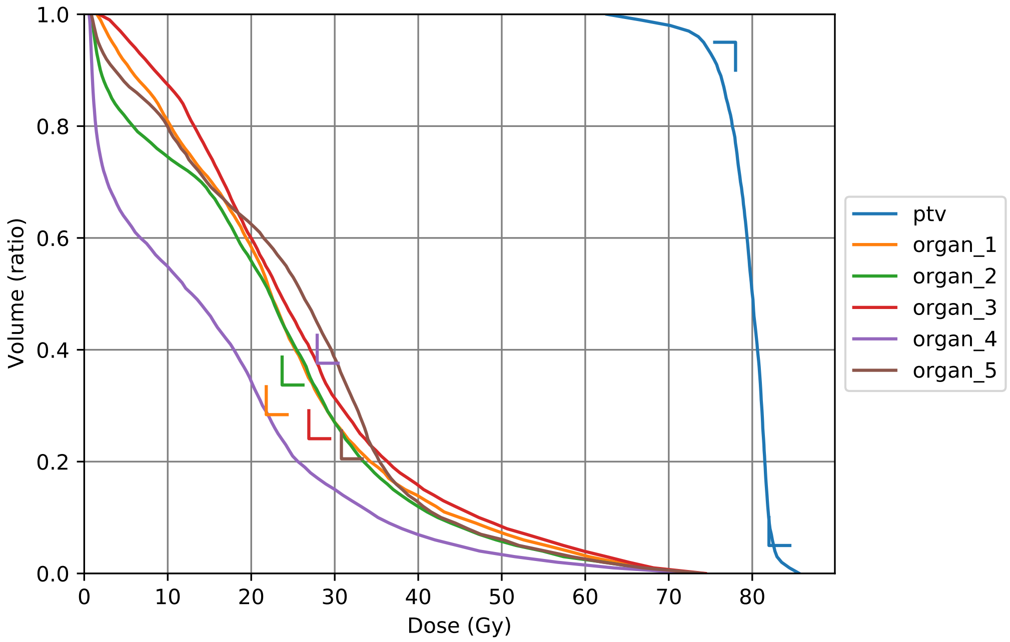

(c) Associated clinical dose **DVH**

Figure 5.3: Example of a (generated) patient's main axial slice (center of the PTV) and DVHs.

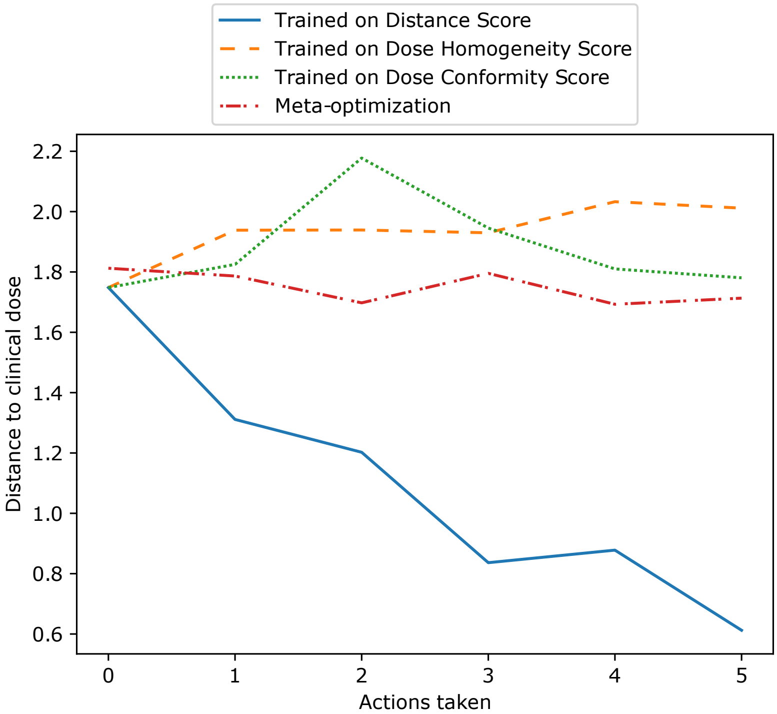

Figure 5.4: Average distance between RL agent's dose and clinical dose.

Agent \ Metric	Mean Final Distance*	Homogeneity Score†	Conformity Score†
RL Distance Score	**0.612**	1.871	0.406
RL Homogeneity Score	2.012	**4.387**	0.567
RL Conformity Score	1.770	4.017	0.507
Meta-optimization	N/A	4.117	**0.610**
Clinical doses	*0*	*1.541*	*0.580*

* distance is imporved performance through a lower score.
† score is imporved performance through a higher score.

Table 5.2: Average performances of four algorithms tested on DVHs distance to clinical dose, dose homogeneity-based score, and conformity-based score.

a high conformity, but low homogeneity compared to automatic techniques). This show the difficulty to create a metric that capture all the complexity of a clinically acceptable dose.

Qualitative Results Figure 5.5 shows the DVHs at each of the first four optimization steps on one of the test patients, unseen by the agent during the training. Our model drastically reduced the dose distance with manually optimized doses. Visual inspection of the DVHs plot shows that the dose optimized by the RL agent is very close to the clinical (manually fine-tuned) one.

5.2.4 Discussion and Conclusion

Our study demonstrates the potential of deep RL for automating radiotherapy treatment plan optimization. A key strength of our approach is its ability to learn from past treatment plans, capturing the complex decision-making processes of human dosimetrists. This data-driven approach avoids the limitations of pre-defined metrics, which may not fully capture the nuances of optimal treatment planning.

However, our study also has limitations. The agent's performance relies on the quality and quantity of available training data. Cases with limited historical data or complex anatomical features may require additional strategies. Moreover, while the agent achieves promising results regarding dose distance reduction, the dose is not guaranteed to be clinically acceptable. Although this study demonstrates the promise of our RL approach in a controlled setting, one final limitation to mention is that extending it to real-world radiotherapy planning would necessitates addressing additional complexities and constraints.

Several avenues exist for further research. Firstly, we plan to investigate strategies for incorporating additional information, such as patient characteristics and anatomical complexities, into the training process. For example, a potential improvement to the current model involves the integration of 3D dose distributions as input. This additional information would

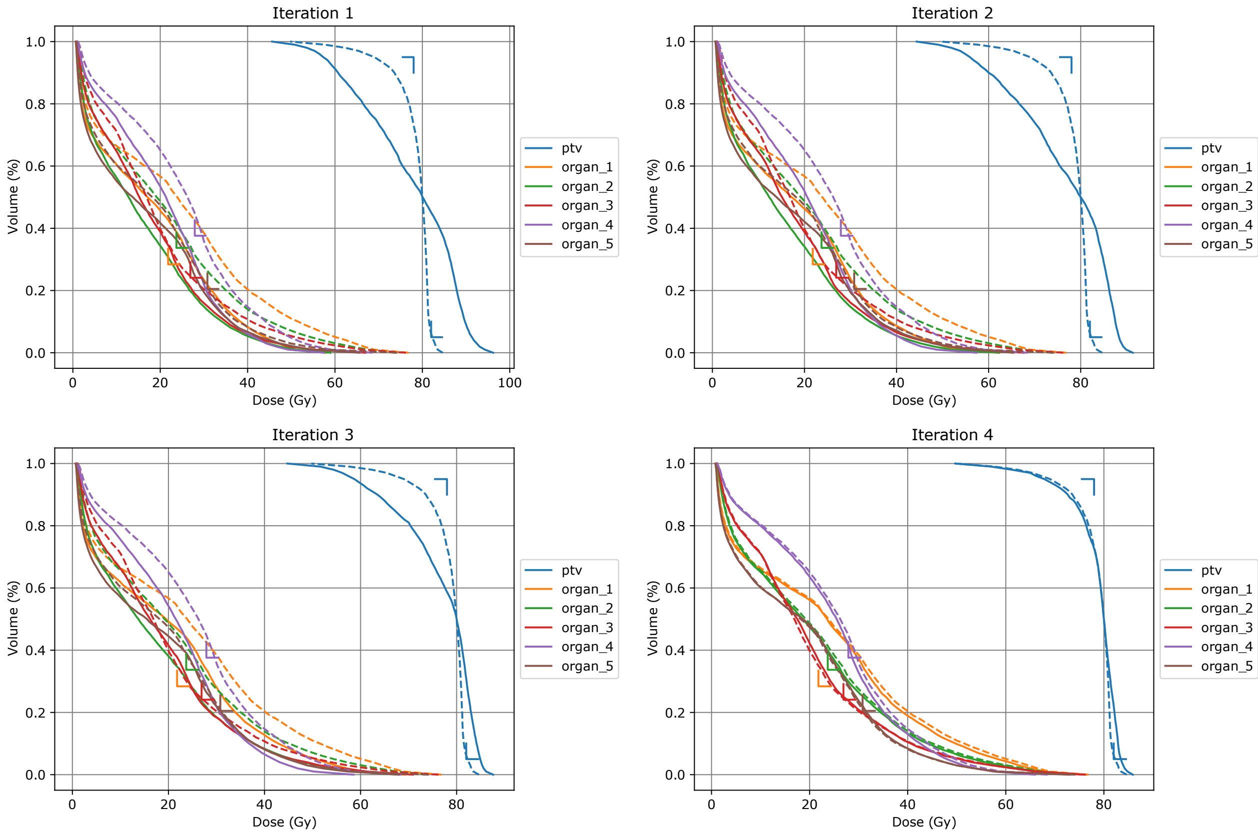

Figure 5.5: RL Agent DVHs after each action taken on a test (unseen) patient. Solid lines are the agent's dose DVHs; dotted ones are the reference dose DVHs (manually fine-tuned).

allow the RL agent to identify dose hotspots within the treatment volume better. This spatial representation of dose delivery would enable the agent to more accurately assess areas of over- or under-dosage, leading to more informed decision-making during plan optimization. Ultimately, the agent is expected to improve the clinical acceptability of the generated treatment plans by using a more comprehensive understanding of the dose landscape and its implications for treatment outcomes.

Secondly, we aim to explore techniques for improving the interpretability of the RL agent's decision-making process. Interpretability is essential for building trust in the system and facilitating its clinical adoption. By developing techniques that allow dosimetrists and clinicians to understand the rationale behind the agent's actions, we can ensure that its decisions align with clinical expertise and best practices. This transparency will support the validation of the agent's performance and provide insights into potential areas for refinement and further optimization.

Our approach differs from previous RL-based methods for radiotherapy planning in two key aspects. First, we avoid relying on pre-defined metrics for evaluation, which can be subjective, and limit the agent's ability to learn complex optimization strategies. Second, compared to traditional meta-optimization approaches, our method leverages past treatment data, potentially leading to more informed decision-making during the optimization process.

This study demonstrates deep RL's feasibility and potential benefits for automating radiotherapy treatment plan optimization. Our approach is capable of directly predicts state evaluations, and shows promise in achieving significant improvements in efficiency and, potentially, treatment outcomes. Further research is needed to address limitations, improve interpretability, and ensure safe clinical integration. This approach could revolutionize radiotherapy planning, leading to more standardized, efficient, and improved patient care.

5.3 Clinically Dependent Fully Automatic Treatment Planning System[2]

In the previous section, we propose a novel approach using RL agents trained to mimic human optimization based on historical dose distributions from past treatments. This section will show that the RL agent developed above method allows for clinic-specific optimization. The RL agent adapts to various clinical practices without requiring additional information beyond the clinic's historical dose data. By tailoring the RL agent's training to the specific dose patterns previously delivered by a clinic, the agent can learn to replicate the clinic's internal standards and guidelines. This approach enables the deployment of a standardized training algorithm across multiple institutions while providing each institution with a personalized model. This system could pave the way for broader adoption of fully automatic TPS in routine clinical settings.

[2]Presented at ASTRO 2024.

5.3.1 Introduction

One area that remains challenging is the complete automation of treatment planning. Current TPS technologies offer either manual treatment planning or a single automatic planning. They fail to consider the wide variation in practices across clinics [**?**], which often leads to sub-optimal treatment plans according to one clinic-specific guideline. Manual planning by dosimetrists remains how most treatment plans are calculated.

There is significant interest in developing a fully automatic TPS that can mimic human decision-making processes while remaining adaptable to different clinics' specific practices. Reinforcement learning has emerged as a promising approach in automated planning because of its ability to adapt to complex environments and learn from interactions with them. In radiotherapy, RL can theoretically adjust the weight of constraints in optimization to achieve clinically acceptable plans. However, current RL systems have struggled to replicate the clinical guideline adaptability of human dosimetrists.

In this section, we propose a solution that leverages the clinic's past treatment data to train RL agents that can optimize treatment plans according to local clinical guidelines. By training one agent per clinic, the system ensures that the RL agents adhere to each clinic's specific standards, potentially making automated TPS more clinically viable. We hypothesize that our clinic-specific RL agents can optimize radiotherapy plans while adhering to the respective institutional standards.

5.3.2 Methods

Training Data We created three clinical doses for each patient, each following a specific guideline. In order to reduce computation time (as this time, we had three different clinics for each patient), we generated a cohort of 50 virtual patients for training and another 20 for testing. Each case was manually optimized to serve as a reference for the RL agent.

Reinforcement Learning Framework We use the same RL framework described in section 5.2.2, where the reward function was designed to penalize deviations from the reference dose distribution by comparing the RL-generated DVHs with those of the training cases. The closer the agent's plan was to the reference, the higher the reward received. This approach differs from traditional RL reward systems that often struggle to provide meaningful feedback in complex medical scenarios like dosimetry, where the "goodness" of a plan is difficult to quantify with a single metric. Most importantly, this approach allows the optimization to fit each center's internal standard practices and guidelines. We created three RL agents, each mimicking the treatment plans of a specific clinic.

5.3.3 Results

Qualitative Evaluation Figure 5.6 summarizes the evolution of the average distance between the reinforcement learning agent's dose and the dose from clinics A, B, and C

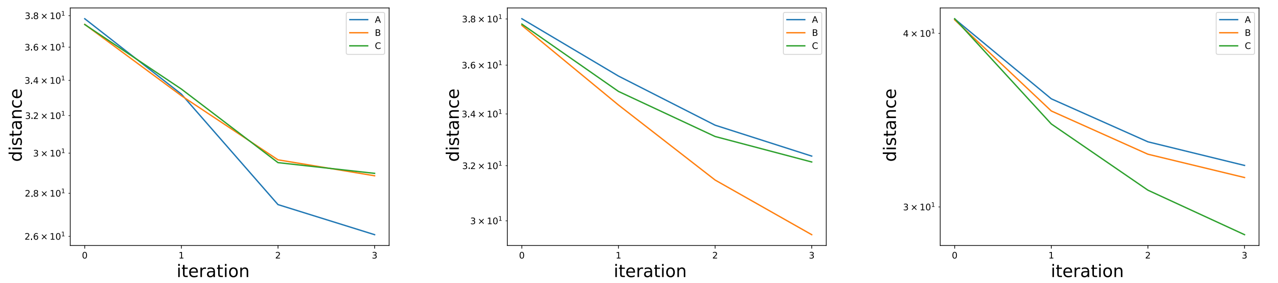

(a) RL agent trained to replicate doses from clinic A.

(b) RL agent trained to replicate doses from clinic B.

(c) RL agent trained to replicate doses from clinic C.

Figure 5.6: Distance between the reinforcement learning agent's dose and the dose from clinics A, B, and C throughout iterations.

RL Agent trained on	Distance to clinic A	Distance to clinic B	Distance to clinic C
Doses from clinic A	**1.6**	2.2	5.1
Doses from clinic B	2.3	**1.3**	2.3
Doses from clinic C	2.7	2.5	**1.6**

Table 5.3: Average distance of each RL agent on each clinical dose on the test set.

throughout iterations of importance wights changes. Each one of the three agents was trained on the dose data of one specific clinic. Throughout iterations, RL agent were able to gradually reduce the distance with the dose they were trained to replicate.

Quantitative Evaluation The table 5.3 summarizes the average DVH differences between the RL-generated plans and the reference clinical plans across the test set. We observe a lower average distance on the diagonal, showing that RL agents trained on specific clinical guidelines successfully mimic the dose type of specific clinics. However, RL agents performed poorly according to other clinics' guidelines.

Mimicking Clinical Guidelines Our results demonstrate that RL agents trained on clinic-specific data can successfully mimic the dose distributions generated by human dosimetrists. Agents trained to optimize according to one clinic's guidelines produced plans that closely matched the previous plans from that clinic. However, agents trained under a specific set of guidelines did not perform well when tested on patients from different clinical guidelines. This finding highlights the importance of tailoring RL agents to individual clinic practices. A general-purpose RL agent trained on mixed clinical data would struggle to produce acceptable plans for any clinic, confirming our hypothesis that RL agents must be clinic-specific to achieve clinically useful results.

5.3.4 Conclusion

The findings of this study suggest that fully automated TPS systems tailored to individual clinics are feasible. We could replicate the human dosimetrists' decision-making process by training RL agents on a cohort of patients treated under a specific set of guidelines. The main advantage of this approach is that it allows each clinic to maintain its internal standards and practices rather than adopting a generic automated planning system that may not suit its unique requirements.

However, there are still limitations to the approach. One fundamental limitation is that RL agents trained on one clinical guideline cannot generalize across different practices. This limitation suggests that each clinic must invest resources into training its own RL models. Additionally, our work so far has focused on phantom cases, and future research is needed to assess the applicability of this method to non-phantom patients.

This study and the one in the previous section have demonstrated the potential for a clinically dependent, fully automatic TPS using RL. We trained RL agents to mimic human optimization by leveraging historical clinical data. This system can adhere to clinic-specific guidelines without requiring physicians to explicitly define them, a task that is often challenging and imprecise. Instead, the system leverages historical treatment data to learn and implicitly replicate the clinical preferences and decision-making processes. This implicit learning reduces the burden on clinicians to formalize their optimization strategies. This idea makes automated treatment planning more likely to be adopted. Future work will involve expanding the cohort to non-phantom patients and conducting testing with human oversight to ensure the safety and efficacy of the system.

Dosimetry Automation via Dose Mimicking

Abstract

The previous chapter discussed automation techniques that enhance classical treatment plan optimization methods. This chapter focuses on novel automation techniques for radiotherapy treatment planning that bypass traditional optimization frameworks. With the advent of deep learning, dose prediction models have emerged, offering an alternative approach to generating treatment plans. These models predict synthetic 3D dose distributions, which can be used in dose mimicking to create clinically deliverable treatment plans. In this chapter, we explore advancements in dose prediction techniques, explicitly focusing on methods that improve the accuracy and adaptability of these predictions. By incorporating additional information, such as Dose-Volume Histograms, we propose methods to make dose prediction models more clinically relevant and capable of generating treatment plans that align with varying prescription protocols and dosimetrist preferences.

6.1 Dose-Volume Histograms Guided Deep Dose Prediction for Radiotherapy Treatment Planning[1]

6.1.1 Introduction

Traditionally, the creation of radiotherapy treatment plans has been a semi-manual process, where dosimetrists finetune importance factors assigned to structures and constraints. A cost function is then used through a classical optimization algorithm to calculate the optimal plan.

In recent years, deep learning in treatment planning has gained attention. Deep learning models can predict the three-dimensional dose distribution based on patient-specific anatomical data derived from medical imaging (CT scans). While the predicted dose distribution may not directly be used as a deliverable treatment plan, it serves as the basis for determining a clinically viable plan through dose mimicking. Dose mimicking is an optimization technique that eliminates the need for manual adjustment of importance factors by dosimetrists. Therefore, the ability to predict a clinically acceptable and near-deliverable 3D dose distribution for any patient presents significant potential for fully automating the radiotherapy planning process. It is important to note that the successful application of dose mimicking [**?**, **?**] requires a target dose distribution that is nearly deliverable; thus, arbitrarily setting the target dose to zero for OARs is not feasible.

However, this approach requires further adaptation to accommodate specific clinical guidelines. A potential solution involves training individualized models for each treatment center, allowing institution-specific practices and guidelines to be incorporated. However, deep learning dose prediction models are computationally large, and implementing separate models for each center is resource-intensive. Furthermore, such models require substantial datasets for effective training. Consequently, smaller treatment centers may lack the necessary data volume to train a comprehensive model adequately. Additionally, a separate model may be required for each prescription type due to the variability in prescription doses, making manual treatment planning necessary for non-standard cases. Finally, clinicians and dosimetrists may prefer manually adjusting treatment plans in some cases. Such adjustments are not feasible within the current model framework.

We propose a novel approach that incorporates target DVHs directly into the input of the deep learning-based dose prediction model. Incorporating DVHs introduces interactivity into the model, allowing adjustments to the target DVH to yield corresponding changes in dose predictions. This methodology enables a workflow where dosimetrists can refine the predicted dose distribution according to specific clinical objectives. Furthermore, by establishing a template target DVH tailored to each clinic, the same model can be deployed across multiple centers while generating 3D dose predictions that align with the specific practices of each institution.

[1] Presented at SFPM 2024.

Related work Previous studies have explored the application of deep learning to DVH prediction in radiotherapy planning. Chung et al., for example, developed a method to predict patient-specific dose-volume histograms (DVHs) [**?**]. Ahmed et al. similarly investigated the estimation of the best feasible DVHs for organs at risk [**?**]. In contrast, our research adopts a reverse approach, utilizing target DVHs to predict clinically acceptable dose distributions. To our knowledge, this innovative paradigm has not been previously explored in the literature.

6.1.2 Material and Methods

Data size We defined a bounding box of dimensions $120 \times 180 \times 180$ mm^3 centered on the PTV, with isotropic voxels of $5 \times 5 \times 5$ mm^3. This box size was chosen to accommodate the PTV and the relevant OARs, namely the rectum and bladder, while maintaining a balance between computational feasibility and model accuracy. A larger bounding box would have increased model complexity and computational time without substantial benefit.

Dataset and Patient Cohort The dataset used for model training comprised 168 patients from the Institut régional du Cancer de Montpellier radiotherapy department. These patients were selected based on their anatomical conformity to the $120 \times 180 \times 180$ mm^3 bounding box. These patients received either $62\,\mathrm{Gy}$ or $78\,Gy$ prescribed doses to the PTV, with OARs including the bladder and rectum. The dataset was split into training, validation, and test subsets, with 80% used for training, 10% for validation, and 10% for testing.

Base Architecture The model architecture is based on a 3D U-net, a well-established neural network architecture for volumetric data. The input to the network consisted of four elements: the patient's CT scan, the contour of the PTV, the rectum contour, and the bladder contour. The model output was the predicted three-dimensional dose distribution. The encoder part of the U-net consisted of four convolutional layers with residual connections to improve gradient flow during training, while the decoder section included five convolutional layers. Skip connections were implemented between the corresponding encoder and decoder layers to preserve spatial information across the model.

Incorporation of DVHs Dose-volume histograms represent one-dimensional curves, whereas the CT images, anatomical contours, and predicted dose distributions are inherently three-dimensional data. We employed the Direct Affine Feature Transforms (DAFT) technique to integrate these disparate data types within the neural network [**?**]. DAFT dynamically scales latent feature maps within the network, enabling the combination of imaging data with DVH information.

For this study, we incorporated the DVHs for the primary structures of interest: the PTV, rectum, and bladder. Not all points along a DVH curve hold equal clinical significance. Dosimetrists typically focus on regions at the beginning and end of the curve, where the volume approaches 0% or 100%. To better capture these critical areas, we employed a non-uniform sampling strategy based on the Chebyshev distribution, which provides a higher density of points near the curve's extremities. The Chebyshev points, defined in the range $[-1, 1]$, were remapped to the interval $[0, 1]$ for this purpose. Given their critical importance in clinical decision-making, this sampling technique allows us to prioritize accurate sampling at the curve's extremities. The sampled points were subsequently processed by a two-layer perceptron, responsible for predicting the scaling parameters, α and β, used by the DAFT mechanism to modulate the feature maps.

Three models comparison We evaluated three model configurations with varying levels of DVH incorporation, the architectures of which are described in figure 6.1.

The first model referred to as "C" or the *classic* model (figure 6.1a), consists of a standard 3D U-net architecture without any incorporation of DVH information. The second model denoted as "B" or the *bottleneck* model (figure 6.1b), integrates target DVH data using the DAFT technique, as described previously, at the bottleneck layer of the U-net. In the third model, termed "A" or the *all connections* model (figure 6.1c), DVH information is incorporated via the DAFT technique both at the bottleneck layer and across all skip connections between the encoder and decoder of the U-net. During the model training process, the clinical DVHs corresponding to the real delivered doses were used as target DVHs for the optimization.

6.1.3 Results

Our results indicate that incorporating DVH data improves dose prediction's quantitative and qualitative aspects.

Quantitative Performance We used the Mean Absolute Error (MAE) between the predicted and ground-truth dose distributions to evaluate model performance. The incorporation of dose-volume histogram data into the networks resulted in improved quantitative performance. The MAE measured on the test dataset was 2.42 Gy for model A, 2.58 Gy for model B, and 3.18 Gy for model C.

Prescription Adaptation In addition to the quantitative improvements, a qualitative analysis of the DVHs associated with the predicted dose distributions confirmed the benefit of including DVH information. A key finding from our study was that models A and B could adapt their deep dose predictions based on the prescribed dose, with model A showing a slight advantage over model B regarding accuracy (see figure 6.2). The dataset comprised patients with two distinct prescription doses: 62 Gy and 78 Gy to the PTV. Model C consistently predicted dose distributions resembling a 65 Gy prescription, demonstrating a lack of adaptability to the varying prescription levels (see figure 6.2). In contrast, models A and B displayed greater flexibility, successfully adjusting their dose predictions following the prescribed doses for each patient. This adaptive behavior highlights the effectiveness of

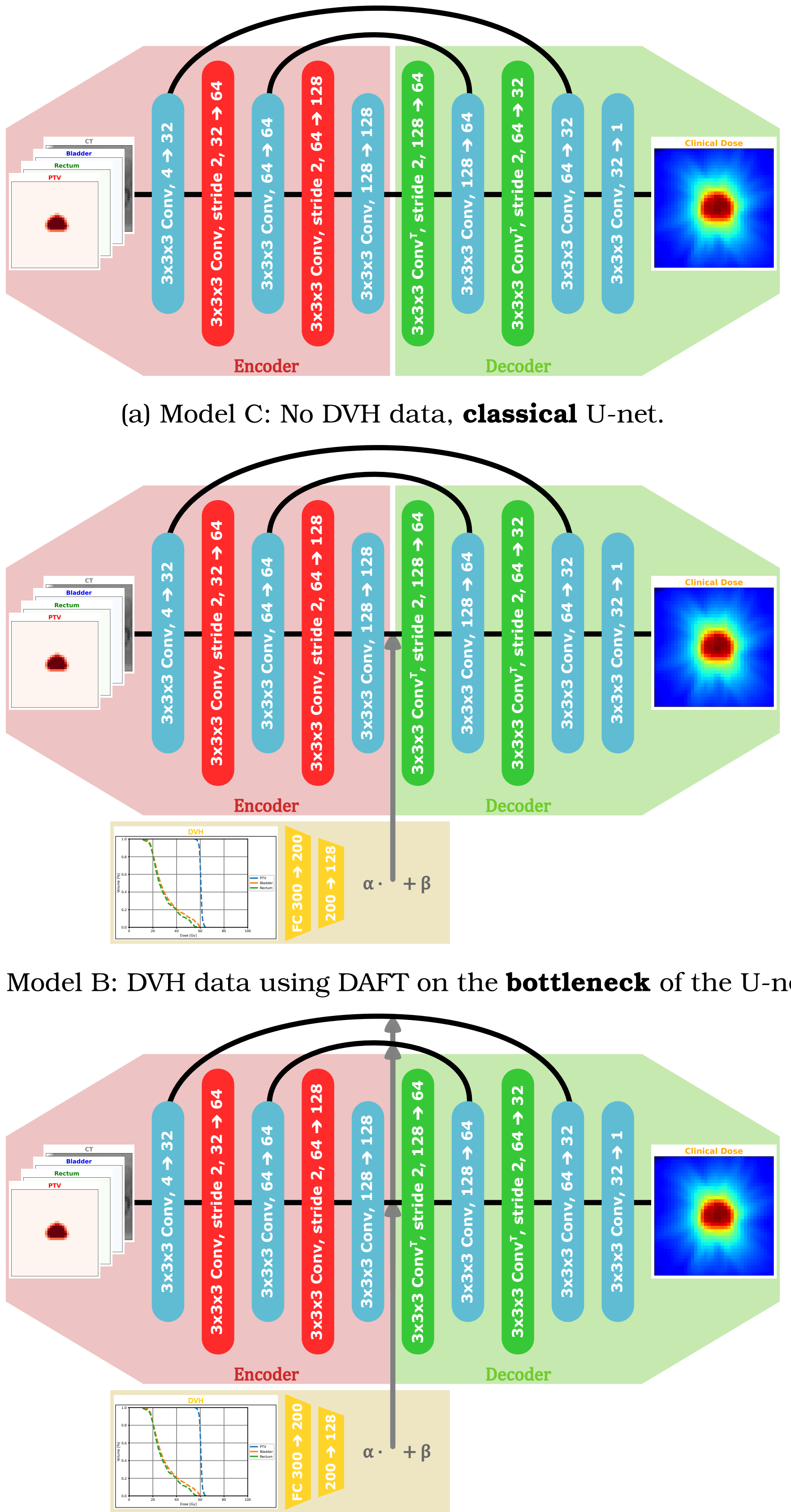

(a) Model C: No DVH data, **classical** U-net.

(b) Model B: DVH data using DAFT on the **bottleneck** of the U-net.

(c) Model A: DVH data using DAFT on all connections between the encoder and the decoder part of the U-net.

Figure 6.1: Architecture diagram of models A, B and C.

(Solid line is predicted dose DVH, dotted line is target dose DVH.)

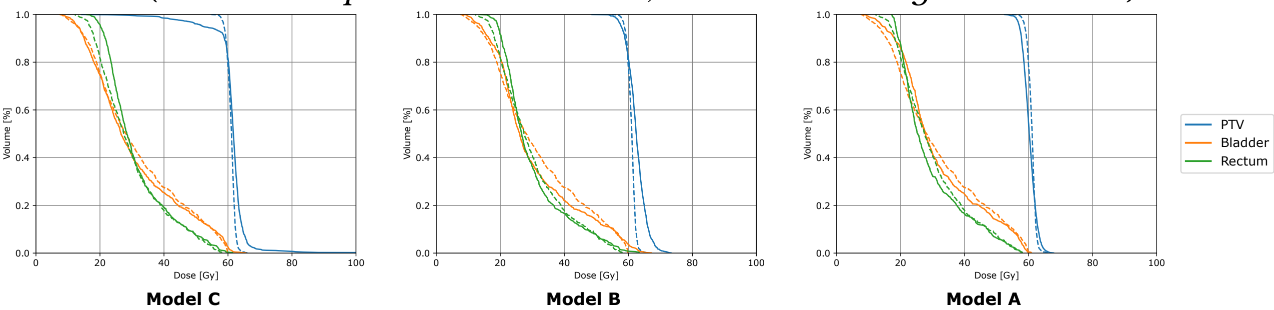

(a) Patient 1, prescribed $62\,$Gy.

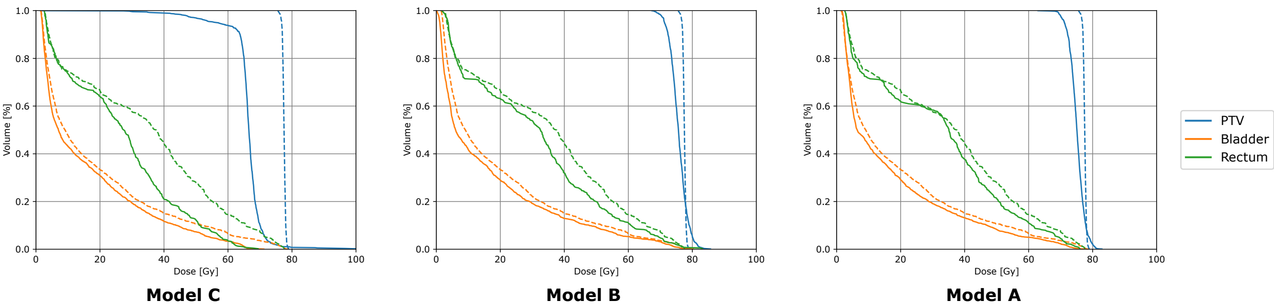

(b) Patient 2, prescribed $78\,$Gy

Figure 6.2: DVHs of the dose predicted by each model on two test set patients.

incorporating DVH information, allowing the models to tailor dose predictions to specific prescription requirements.

Clinical Relevance The ability to adjust dose predictions based on DVH data demonstrates a significant advantage of our approach. The prescription dose can vary in clinical practice depending on the tumor type, stage, and patient characteristics. By incorporating DVH data, our models provide a more flexible and personalized approach to dose prediction, allowing the TPS to generate a plan that aligns with clinical objectives and dosimetrist input.

6.1.4 Conclusions

Our study shows the importance of incorporating DVH information into deep learning-based dose prediction models. In this study, the target DVH links the clinical objectives defined by the dosimetrist and the predicted dose distribution. We create a system allowing center-dependent adjustments by embedding this information into the model. This system also allows interactive adjustment of the dose distribution when the proposed treatment plan is close to clinically acceptable. The comparison of models A, B, and C highlights the advantages of integrating DVH data in the network. The comparison also shows that integrating the information once at the bottleneck is sufficient.

An additional advantage of the proposed method is the capacity to generate standardized target DVH templates for treatment planning. While averaging 3D dose distributions across multiple patients is not feasible, it is possible to compute average DVHs. These average DVHs can be stratified by anatomical site, prescription dose, and clinical practice, providing a target for dose prediction with no effort. Dosimetrists and doctors can further modify these templates to meet specific clinical requirements in case of non-standard patients. Once an optimal set of DVHs is established for a given center's protocols, it can be reused for future patients with only minor adjustments. Furthermore, sharing dose templates and treatment protocols from leading centers will allow knowledge transfer and elevate the quality of care in less-resourced hospitals. This framework could enhance the efficiency and consistency of the treatment planning process.

Our proposed approach demonstrates the feasibility and benefits of incorporating DVH data into deep learning-based dose prediction models for radiotherapy treatment planning. By embedding DVH information, we improve dose prediction accuracy and allow for interactive fine-tuning based on clinical objectives. This technique opens the door to a new workflow where dosimetrists can design target DVHs, and the TPS generates the deliverable treatment plan that best matches these targets. Further studies will explore the generalizability of our model across different cancer types and radiotherapy modalities. Additionally, clinical validation studies will be crucial to assess the real-world impact of our proposed method on treatment outcomes and workflow efficiency.

6.2 Attention Mechanism on Dose-Volume Histograms for Deep Dose Predictions[2]

6.2.1 Introduction

This study builds on work from the previous section We explore using attention mechanisms to improve the incorporation of target Dose-Volume Histogram information into deep-learning models for radiotherapy dose prediction. In traditional radiotherapy planning, DVHs are essential for assessing and optimizing dose distributions for the Principal Target Volume and Organs at Risk. However, existing deep learning models for dose prediction, while capable of generating accurate 3D dose distributions, often fail to integrate DVH constraints fully [**?**]. This limitation reduces their utility in real-time treatment planning.

In previous work, deep learning approaches primarily focused on predicting dose distributions directly from patient imaging data, such as CT scans and anatomical contours of the PTV and OARs. These methods typically rely on convolutional neural networks (CNNs), like the Unet, trained with voxel-wise loss functions [**?**]. While successful in producing accurate 3D dose maps, they generally treat DVH-related information as secondary, with little attention given to adapting predictions based on these critical clinical metrics.

In the last section, we proposed integrating target DVH into the deep dose model to address this gap. In this section, we extend prior approaches by proposing attention mechanisms to integrate target DVH information more effectively into the dose prediction process. Attention mechanisms, widely adopted in domains such as natural language processing and image recognition, enable models to focus on relevant features within the input data selectively [**?**]. By leveraging attention, we aim to enhance the model's capacity to dynamically adapt its dose predictions following specified DVH constraints, providing a more precise and clinically responsive framework for radiotherapy treatment planning.

This work evaluates three U-net-based architectures, including a novel model using a cross-attention mechanism to incorporate DVH information into the dose prediction process directly. Our goal is to enhance the accuracy and adaptability of deep learning models for dose prediction, ultimately enabling dosimetrists to have greater control over the treatment planning process through DVH-guided model interactions.

Related work Previous studies have explored the application of attention mechanism for dose prediction in radiotherapy planning. Osman et al., for example, developed an attention-gated 3D U-Net architecture model to predict full 3D dose distribution [**?**]. Cros et al. investigated the combination of dense elements with attention mechanisms for 3D radiotherapy dose prediction [**?**]. In contrast, our research uses the attention mechanism for its power in mixing different data types. We used cross attention between DVH features and bottle neck

[2] Presented at SFRO 2024.

compressed 3D data to predict clinically acceptable dose distributions. To our knowledge, this innovative paradigm has not been previously explored in the literature.

6.2.2 Material and Methods

Patient Data and Preprocessing We again used the cohort of 168 patients from the previous section who had undergone radiotherapy treatment. The dataset included patients prescribed 62 Gy or 78 Gy on the PTV. The dataset was randomly split into 80% for training, 10% for validation, and 10% for testing. We collected the CT scans, PTV contours, and OAR contours for each patient. The CT data was resampled to a voxel size of $0.5 \times 0.5 \times 0.5 mm^3$ to standardize inputs across patients. As in the last section, we used the same box $120 \times 180 \times 180$ mm^3 centered on the PTV.

Model Architecture and Training The backbone architecture for all models in this study is a 3D-convolutional Unet, a commonly used CNN for image-to-image translation tasks, such as segmentation and dose prediction. Our U-net is of depth two, meaning it performs two levels of down-sampling and up-sampling. The U-net outputs a 3D dose prediction for each voxel within the patient's anatomy. Details architecture diagrams can be found in figure 6.3.

U-net 0 (Baseline) The first model, U-net 0 (architecture diagram can be found on figure 6.3a), serves as a baseline and does not incorporate target DVH information. It receives the CT scan, PTV, and OAR contours as input and predicts the 3D dose distribution purely from this spatial data.

U-net 1 (DVH with DAFT) The second model, U-net 1 (architecture diagram can be found on figure 6.3b), incorporates DVH data using the DAFT approach, like in the previous section. In this model, the target DVHs are provided as additional inputs, and the model is trained to predict 3D dose distributions that match these target DVHs.

U-net 2 (DVH with Cross-Attention) Our novel contribution, U-net 2 (architecture diagram can be found on figure 6.3c), integrates DVH data using a cross-attention mechanism. In this architecture, the model takes queries from the 3D dose prediction and keys and values from the target DVHs. The result of the 4-head attention mechanism is the same shape as that of the 3D input. The cross-attention mechanism allows the model to adjust its dose predictions dynamically based on the desired DVH information. The output of the attention mechanism is re-injected into the U-net during the decoding process, modifying the predicted dose map to match the target DVHs better.

Loss Function and Optimization The models were trained using a loss function that combines voxel-wise MAE with an L1 loss on the DVH, designed to penalize deviations be-

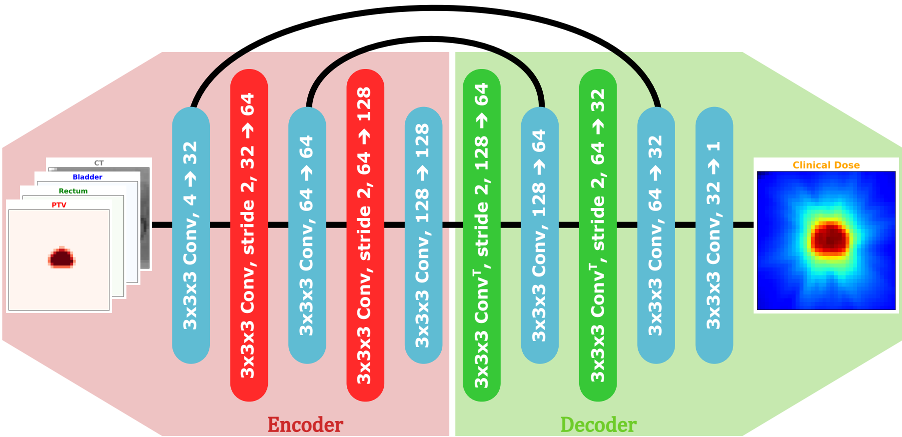

(a) U-net 0: no DVH information.

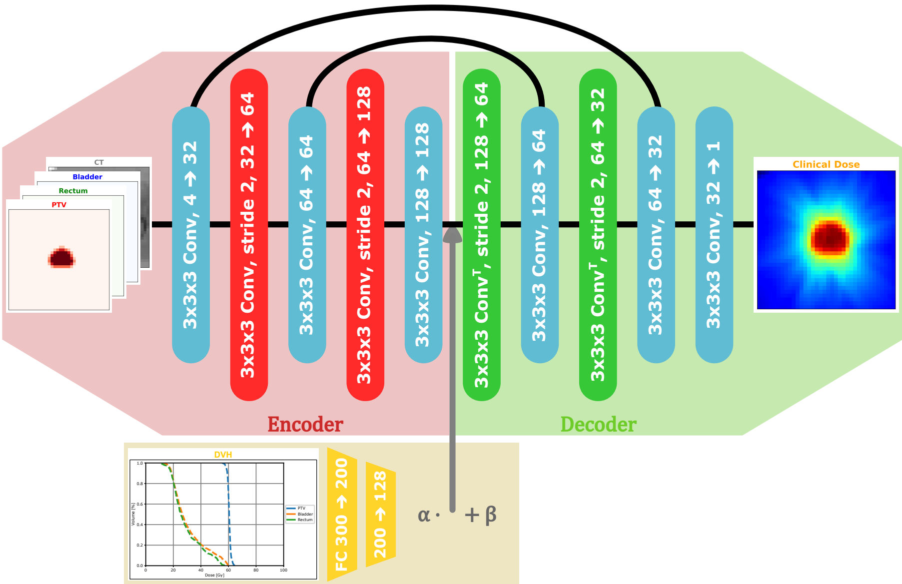

(b) U-net 1: DVH with DAFT.

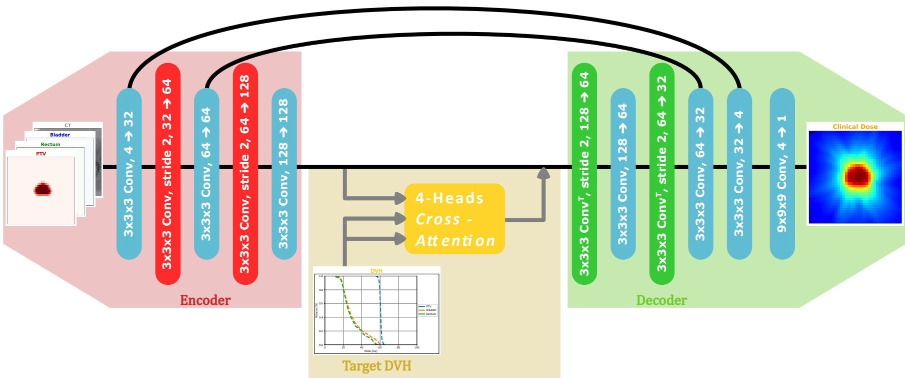

(c) U-net 2: DVHs with cross-attention.

Figure 6.3: Architecture diagrams of U-nets 0, 1 and 2.

Metric	Unet-0	Unet-1	Unet-2
3D Dose MAE (Gy)	3.093	2.254	2.210
Mean DVH Deviation (Gy)	1.942	1.051	0.930

Table 6.1: Models performances comparison.

tween the predicted and target DVHs. Incorporating the L1 loss on DVH significantly improved the model's convergence. The total loss function is expressed as:

$$\text{Total Loss} = \alpha \cdot \text{MAE}_{\text{voxel}} + \beta \cdot \text{L1}_{\text{DVH}}$$

where α and β are hyper-parameters that control the relative contribution of the two terms. For this study, we set both α and β to 1, based on performance observed on the validation set. However, future work could further optimize these parameters to enhance model performance.

The models were trained using the Adam optimizer with a 10^{-4} learning rate. Using the validation loss criterion, early stopping was applied to prevent overfitting and ensure robust generalization.

6.2.3 Results

Evaluation Metrics The performance of the models was assessed using two primary metrics. The first metric was the 3D Dose MAE, which measures the voxel-wise MAE between the predicted dose distributions and the corresponding ground truth values. The second metric was the DVH deviation, calculated as the mean L1 deviation between the predicted and target DVHs for both the Principal Target Volume (PTV) and Organs at Risk (OARs). These metrics provide a comprehensive evaluation of the models' accuracy in predicting dose distributions and adherence to clinical DVH constraints.

Models Performances The performance of the three models is summarized in Table 6.1. Both U-net 1 and U-net 2, which incorporated DVH information, outperformed the baseline U-net 0 across all metrics.

As shown, the inclusion of DVH data significantly reduced the MAE in the predicted dose distributions. Unet-2, which used a cross-attention mechanism, showed the best overall performance, with a minor error reduction compared to U-net 1.

Prescription Adaptability The ability of the models to adapt to varying prescriptions was also evaluated. Similarly to the last section, U-net 0 struggled to predict the correct dose when the prescription varied from its training distribution. Regardless of the actual prescription, the model consistently predicted doses around 65 *Gy*. In contrast, U-net 1 and U-net 2 adapted their dose predictions to the provided DVHs, making them more versatile in clinical scenarios where the prescription may differ across patients. There were only a few differences between the performances of U-net 1 and U-net 2.

6.2.4 Conclusions

This study re-demonstrates the feasibility of incorporating DVH data into deep-learning models for radiotherapy dose prediction. We have marginally improved model performances and adaptability by using an attention mechanism to integrate target DVHs. The cross-attention mechanism, in particular, offers a novel way to align predicted dose distributions with clinical goals flexibly.

Our findings indicate that this approach could facilitate the development of a more efficient radiotherapy treatment planning workflow. In this proposed framework, dosimetrists would focus primarily on creating standardized target DVH templates rather than manually adjusting dose distributions for each patient. These templates would serve as a foundation, requiring minimal adjustments to accommodate individual patient-specific characteristics, thereby streamlining the treatment planning process.

Designing a template for 3D dose distributions is not feasible, as 3D doses are highly patient-specific and cannot be transferred between patients. In contrast, DVHs are more generalizable and can be applied across different patients. This generalizability makes them suitable for the proposed workflow, where template DVHs can be established and used with deep learning-based dose prediction models guided by target DVH. This workflow could reduce planning time and improve consistency across patients. Future work will explore incorporating more complex DVH structures and refining the attention mechanism to enhance model interpretability and clinical usability.

Conclusion and Perspectives

Abstract

This dissertation explores the automation of radiotherapy dosimetry, focusing on optimization techniques to improve treatment planning. Dosimetry, a crucial step in radiotherapy, directly impacts both the efficacy and safety of cancer treatments. We investigated various optimization methods and proposed three automation frameworks: a partially automated approach that allows clinicians to make adjustments, a fully automated reinforcement learning system that eliminates manual intervention, and a deep dose-based framework that uses deep learning while providing flexibility for manual adjustments through target dose-volume histograms.

This concluding chapter summarizes the main findings and limitations of the present manuscript. We end in a prospective assessment of the long-term implications for the field of radiotherapy. This chapter aims to provide a comprehensive overview of the potential impact of our findings on the advancement of radiotherapy practices in the future.

7.1 Main findings

This manuscript has explored critical advancements in radiotherapy, particularly in dose optimization. Dosimetry remains a crucial step in RT as it directly determines the treatment plan delivered to patients. Dosimetry optimization ensures the delivery of the prescribed radiation dose to cancerous tissues while sparing healthy structures. However, it is also the stage where the efficacy and safety of the treatment are defined. Thus, improvements in this step have profound clinical importance.

Through this dissertation, we have investigated various optimization techniques. First, we focused on constructing loss functions and comparing optimization algorithms. We have further proposed multiple avenues for automating the dosimetry process to enhance treatment efficiency and reduce manual workloads.

Partially Automated Clustering-based Framework The partially automated clustering-based framework proposes a partially automated system for dosimetry, where human intervention remains integral to the process. The model automates most of the dose calculation but leaves room for manual adjustments by clinicians and dosimetrists. This half-automated approach allows dosimetrists to refine or modify the treatment plan based on their expertise, maintaining the traditional workflow while benefiting from automation to save time and improve efficiency. The clustering strategy facilitated a more profound comprehension of the interrelationships between doses.

Fully Automated Reinforcement Learning with Classical Optimization Approach The fully automated reinforcement learning combined with the classical optimization approach takes the automation further. Within this paradigm, dosimetrists are entirely superseded, obviating the need for their input. The system calculates and generates the optimal treatment plan based on predefined clinical constraints and objectives without requiring post-calculation adjustments by the dosimetrist. Our innovative approach is distinguished by its direct learning from historical dose distributions. This system eliminates the reliance on ill-defined metrics that often fail to represent the clinical acceptability of treatment plans accurately. We have empirically demonstrated the adaptability of this framework to diverse clinical settings, only requiring retraining to work with new institutions. This paradigm entirely obviates the need for dosimetrist intervention, streamlining the treatment planning process.

Fully Automated Deep Dose Based Scheme It is also essential to recognize that automating the dosimetry process does not mean replicating every step a human would take. Instead, a more strategic approach involves re-engineering the workflow to optimize its suitability for machine learning or artificial intelligence models. Automation can streamline workflows by eliminating unnecessary complexity and standardizing treatment protocols, thus making them more efficient and reliable.

The fully automated target-DVH-guided deep dose scheme approaches offer a more balanced solution by integrating deep learning models into the fully automated dosimetry process. These systems generate dose distributions and include the flexibility for post-calculation manual adjustments via the modification of target DVHs. The deep learning models are trained on large datasets of treatment plans and dose distributions, learning the relationships between anatomical structures, dose distribution, and dose-volume histograms. This knowledge enables the models to make accurate dose predictions while still allowing clinically adapted dose predictions via modification of the target DVH. Moreover, a single model is needed, and the DVH prompt can be adapted for each center instead of creating a new model from scratch, as in the fully automated scheme.

One of the key advantages of these frameworks is that they offer both full automation and clinician control. Dosimetrists can adjust the automated dose plan when needed, providing oversight absent from the previous approaches. We anticipate that clinicians will make frequent adjustments during the early stages of adoption. Later, the need for manual intervention should gradually decrease, as confidence in the deep learning models grows, and dosimetrists get better prompt the model with target DVH. Over time, clinicians may find the model's initial dose recommendations sufficiently accurate, requiring manual optimization only in exceptional cases, significantly different to the training data.

This gradual adoption mirrors the process observed with auto-contouring systems in radiotherapy. Initially, clinicians made numerous adjustments to the auto-generated contours, but as the technology matured, they began accepting the contours with fewer and fewer modifications. We expect a similar trajectory with automated dosimetry systems, leading to higher acceptance in the clinical community.

7.2 Limitations

Partially Automated Clustering-based Framework The partially automated clustering-based framework, while innovative, comes with a significant hurdle: It would require a change in the current clinical workflow. Clinicians and dosimetrists have well-established practices; altering these routines may face resistance. Even with partial automation, shifting habits could be difficult, as it demands additional time and training. Since radiotherapy professionals often rely on established methods they trust, adopting this hybrid model on a broad scale might be unlikely.

Fully Automated Reinforcement Learning with Classical Optimization Approach While this full automation represents a significant leap in efficiency, it also presents challenges. The system's rigidity can become a source of frustration for clinicians, as it does not allow for minor manual adjustments to the dose distribution, which are often necessary in practice. When clinicians encounter situations where the automated plan requires slight modifications, they must start the entire process from scratch. This lack of flexibility could lead to dissatisfaction and reluctance to adopt the framework, as dosimetrists may

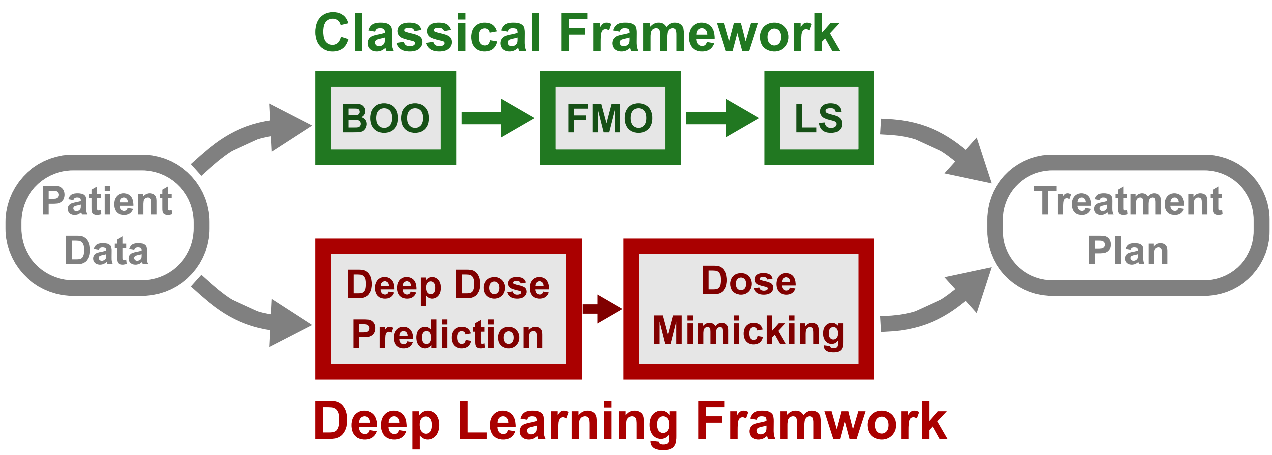

BOO: *Beam Orientation Optimization*
FMO: *Fluence maps Optimization*
LS: *Leaf Sequencing*

Figure 7.1: Comparison of classical versus deep dose frameworks for the creation of treatment plans.

value the ability to fine-tune treatment plans. Therefore, this approach may face significant resistance in clinical practice despite its theoretical appeal.

Fully Automated Deep Dose Based Scheme The fully automated deep dose-based scheme represents a more ambitious approach, aiming at enabling full automation and human fine-tuned plan creation. The clinical implementation and acceptance of the target DVH framework by healthcare professionals remain to be established. Further evaluation and validation in real-world settings are necessary to ensure its effectiveness and integration into routine clinical practice.

From Research to Product While our research has introduced several promising methodologies, there are inherent limitations. One key challenge is transitioning from prof of concept models to real-world clinical applications. Models developed in this research, particularly those based on deep learning, are designed with a research-oriented focus and are relatively small in scale. To realize the full potential of the target DVH deep dose frameworks, there is a clear need to transition from the current research-oriented models to high-resolution, clinically viable products. This transformation will require collaboration between researchers, software developers, and clinical practitioners to ensure the models are scalable, robust, and compatible with existing clinical infrastructures.

Future work The target dose-volume histogram represents the most promising avenue. Prioritizing the development and refinement of target DVH-based approaches is our recommendation for future research.

7.3 Long-Term Impact on Radiotherapy

Treatments Standardization The widespread adoption of automated dosimetry will benefit patients and clinicians in the long term. By standardizing treatment planning across centers, these systems will ensure that all patients, regardless of location, have access to high-quality treatments based on the best clinical practices. This standardization is particularly important for isolated clinics or those with limited specialist availability, where clinicians may lack experience dealing with rare or complex cases. Ultimately, this standardization will lead to more equitable access to advanced radiotherapy treatments, improving patient outcomes on a global scale.

Conclusion The research presented in this thesis has demonstrated the importance and feasibility of automating the dosimetry process in radiotherapy. While there are challenges in clinical adoption and model scalability, the future of radiotherapy will undoubtedly move toward more automated systems. Among the various frameworks explored, the deep dose approach provides the most promising pathway for effective automation, offering a blend of full automation and manual adjustment flexibility. This balance will likely encourage gradual adoption, leading to a new era in radiotherapy where treatment planning is faster, more precise, and universally accessible.